R-07-06

Mechanical modelling of the Singö deformation zone

Site descriptive modelling Forsmark stage 2.1

Rune Glamheden, Lars Maersk Hansen, Anders Fredriksson,
Lars Bergkvist, Ingemar Markström, Mats Elfström

Golder Associates AB

February 2007

Svensk Kärnbränslehantering AB
Swedish Nuclear Fuel
and Waste Management Co
Box 5864
SE-102 40 Stockholm Sweden
Tel 08-459 84 00
+46 8 459 84 00
Fax 08-661 57 19
+46 8 661 57 19

ISSN 1402-3091
SKB Rapport R-07-06

Mechanical modelling of the Singö deformation zone

Site descriptive modelling Forsmark stage 2.1

Rune Glamheden, Lars Maersk Hansen, Anders Fredriksson,
Lars Bergkvist, Ingemar Markström, Mats Elfström

Golder Associates AB

February 2007

Abstract

This project aims at demonstrating the theoretical approach developed by SKB for determination of mechanical properties of large deformation zones, in particular the Singö deformation zone. Up to now, only bedrock and minor deformation zones have been characterized by means of this methodology, which has been modified for this project.

The Singö deformation zone is taken as a reference object to get a more comprehensive picture of the structure, which could be incorporated in a future version of the SDM of Forsmark. Furthermore, the Singö Zone has been chosen because of available data from four tunnels.

Scope of work has included compilation and analysis of geological information from site investigations and documentation of existing tunnels. Results have been analyzed and demonstrated by means of RVS-visualization. Numerical modelling has been used to obtain mechanical properties. Numerical modelling has also been carried out in order to verify the results by comparison of calculated and measured deformations.

Compilation of various structures in the four tunnels coincides largely with a magnetic anomaly and also with the estimated width. Based on the study it is clear that the Singö deformation zone has a heterogeneous nature. The number of fracture zones associated with the deformation zone varies on either side of the zone, as does the transition zone between host rock and the Singö zone.

The overall impression from the study is that the results demonstrate that the methodology used for simulating of equivalent mechanical properties is an applicable and adequate method, also in case of large deformation zones. Typical rock mechanical parameters of the Singö deformations that can be used in the regional stress model considering the zone to be a single fracture are: 200 MPa/m in normal stiffness, 10–15 MPa/m in shear stiffness, 0.4 MPa in cohesion and 31.5 degrees in friction angle.

Sammanfattning

Föreliggande projekt har som syfte att visa att den av SKB:s utvecklade teoretiska metoden är applicerbar för att fastställa stora deformationszoners mekaniska egenskaper. Fram till nu har endast kompetent bergmassa och mindre deformationszoner karaktäriserats med denna metod, som har modifierats för föreliggande projekt.

Singözonen har valts som referensobjekt för att erhålla en mera omfattande bild av strukturen, som kan användas i en framtida version av SDM för Forsmark. Dessutom är Singözonen väl dokumenterad från fyra korsande tunnlar.

Arbetet har omfattat sammanställning och analys av geologisk information från platsundersökningar och befintliga tunnlar. Resultaten har analyserats och åskådliggjorts med hjälp av RVS modellering. Numeriska modeller har använts för att erhålla mekaniska egenskaper. Numeriska modeller har också använts för att verifiera resultaten genom jämförelser mellan beräknad och observerad deformation.

Sammanställning av strukturer i de fyra tunnlarna sammanfaller i stort med ett geomagnetiskt lineament och zonens tolkade vidd. Baserat på studien står det klart att Singözonen är heterogen till sin natur. Antalet sprickzoner på båda sidor varierar liksom bredden på övergångszonen mellan sidoberget och Singözonen.

Det generella intrycket är att resultaten visar att den använda metoden för att simulera ekvivalenta mekaniska egenskaper är användbar och adekvat också när det gäller större deformationszoner. Typiska bergmekaniska parametrar i Singözonen, som kan användas i den regionala spänningsmodellen, där zonen betraktas som en spricka är: 200 MPa/m som normal styvhet, 10–15 MPa/m som skjuvstyvhet, 0,4 MPa för kohesion och en friktionsvinkel på 31,5°.

Contents

1 Introduction

This project aims to demonstrate the application the theoretical approach developed within SKB's site investigation project for determination of mechanical properties of large deformation zones, in particular the Singö deformation zone (Singö DZ, Singö Fault, Singö Zone). Up to now, only bedrock and minor deformation zones have been characterized by this methodology. Application of the theoretical approach to large deformation zones requires some modifications of the current methodology, principally concerning sectors of highly fractured and deeply altered rock. The Singö deformation zone was chosen as an object of study to verify the strategy of modelling.

1.1 Objective of the study

The study has the following threefold objective:

- To develop and verify a methodology for theoretical modelling of large deformation zones.
- To obtain a deeper understanding of the geology and structure of the Singö deformation zone by compiling available documentation from existing tunnels.
- To determine typical rock mechanical parameters of the Singö deformation zone that can be used in regional stress modelling.

The Singö deformation zone is taken as a reference object to get a more comprehensive picture of the structure, which could be incorporated in a future version of the SDM of Forsmark. In addition, observations from tunnel passages through this zone are available to verify the modelling strategy.

1.2 Scope of work

The scope of work includes the following parts:

- Compilation and analysis of geological information available from site investigation and construction phases of existing tunnels through the Singö deformation zone.
- Visualization of geological information using the RVS tool which has been developed by SKB to be used in conjunction with Microstation.
- Numerical modelling to obtain equivalent mechanical properties of the bedrock and typical parts of the deformation zone.
- Numerical modelling of convergence and deformation in monitored sections of the SFR-tunnel passage.
- Verification of the numerical results by comparison with measured deformations in the SFR-tunnel passage.
- Back analysis of mechanical properties to fit the measured deformations in the SFR-tunnel passage.
- Numerical modelling using strength and deformation properties that are valid for the Singö Zone as a whole.

2 Definitions and terminology

In rock engineering, the present state and engineering properties of a rock type is the most important issue. Of lesser importance is the rock type, in a strict lithological sense, and of even less importance is its geological history. Therefore, terms used in mapping for rock engineering purpose often do not have the same meanings as used in general geology. The most important terms for the rock engineering description of the zone used in this report are explained in Table 2-1. The "geological" subdivision of the deformation zone into core and transition zone which is used in Section 4.5 follows the definitions used by SKB as shown in Figure 2-1. /Munier et al. 2003/.

Table 2-1. List of terms commonly used in tunnel mapping at Forsmark /Carlsson and Olsson 1976, Hansen 1982a, Christiansson and Bolvede 1985/.

Term	Explanation	Typical fractures/m
Fractured zone	Zone with a considerably higher fracture frequency than the surrounding rock mass. Commonly, two grades are used: block size 20–50 cm and block size 10—20 cm (shotcrete required). Block shape is also an important issue, and can be described as cubic, tabular or columnar, depending on joint sets and spacing.	2–5, and 5–10, respectively
Crushed zone	Zone where rock is crushed to cubic ("sugar cube rock") or irregular pieces, generally less than 10 cm in size, and often with a fine grained, earth like matrix between the rock pieces. Important is that the crushed zone is still in a state of disintegration, and never sealed, as can be the case for a fault breccia.	10 and over
Gouge	Soft fracture infilling material, such as mica, chlorite, hydro mica and other clay minerals. Also used for chlorite schist.	Not applicable
Fault gouge	Soft fracture infilling material as above, caused by faulting.	Not applicable
Clay	Used as a general term for fine grained clay-silt sized formable fracture infillings, not necessarily including clay minerals.	Not applicable
Gneissic granite, Orthogneiss	Used for undifferentiated metamorphic granite like rocks. May in Tunnel 2 also cover red metavolcanics.	Not applicable
Paragneiss, sedimentary gneiss	Used for undifferentiated foliated supracrustal rocks, including metavolcanics.	Not applicable

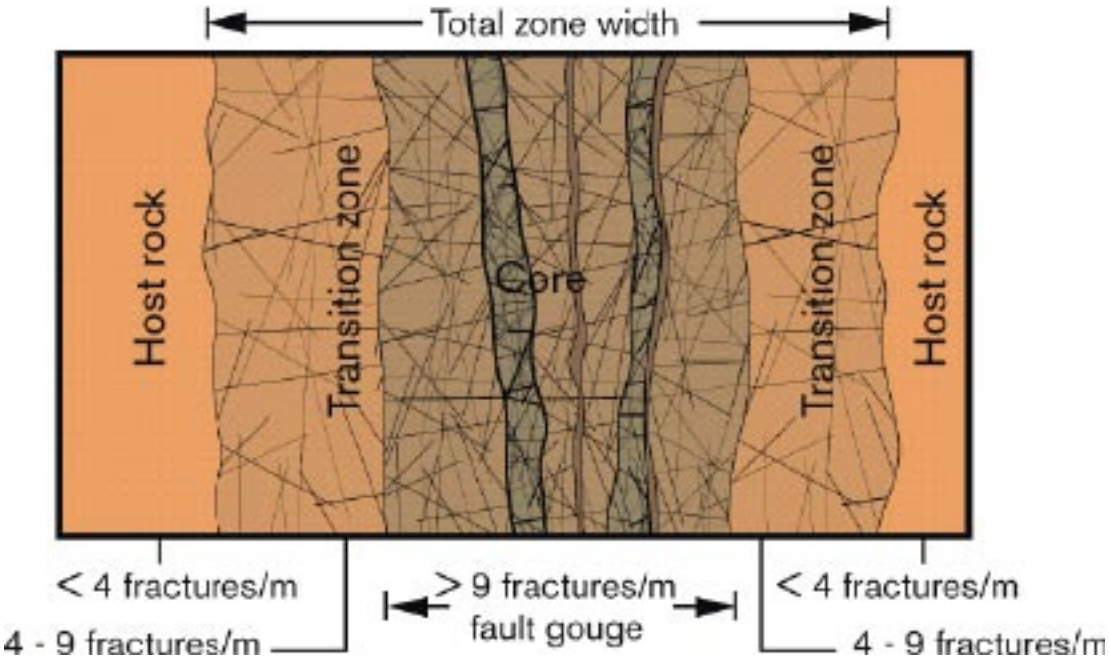

Figure 2-1. *Principles for subdivision of a brittle deformation zone, commonly used by SKB, in particular for logging of drill cores. /Munier et al. 2003/. It is somewhat uncertain what elements in the figure are meant to be fault gouge. A strict interpretation of the figure identifies fault gouge as > 9 fractures/m, which is not in agreement with common terminology. The darker grey and dark reddish grey structures in the core are not explained, and some of them may have been meant to be fault gouge.*

3 Overview of the Forsmark site

The Forsmark Nuclear Power Station site, located in Northern Uppland some 100 km to the north of Stockholm, is one of the areas where the Swedish Nuclear Fuel and Waste Management Company (SKB) is undertaking investigations with the objectives of siting a repository for spent nuclear fuel.

Based on a feasibility study and site investigations, SKB has defined a candidate area as being suitable for the location of the repository, located to the south-east of the nuclear power plant site. The candidate area, which is approximately 6 km long and 2 km wide, is shown in Figure 3-1.

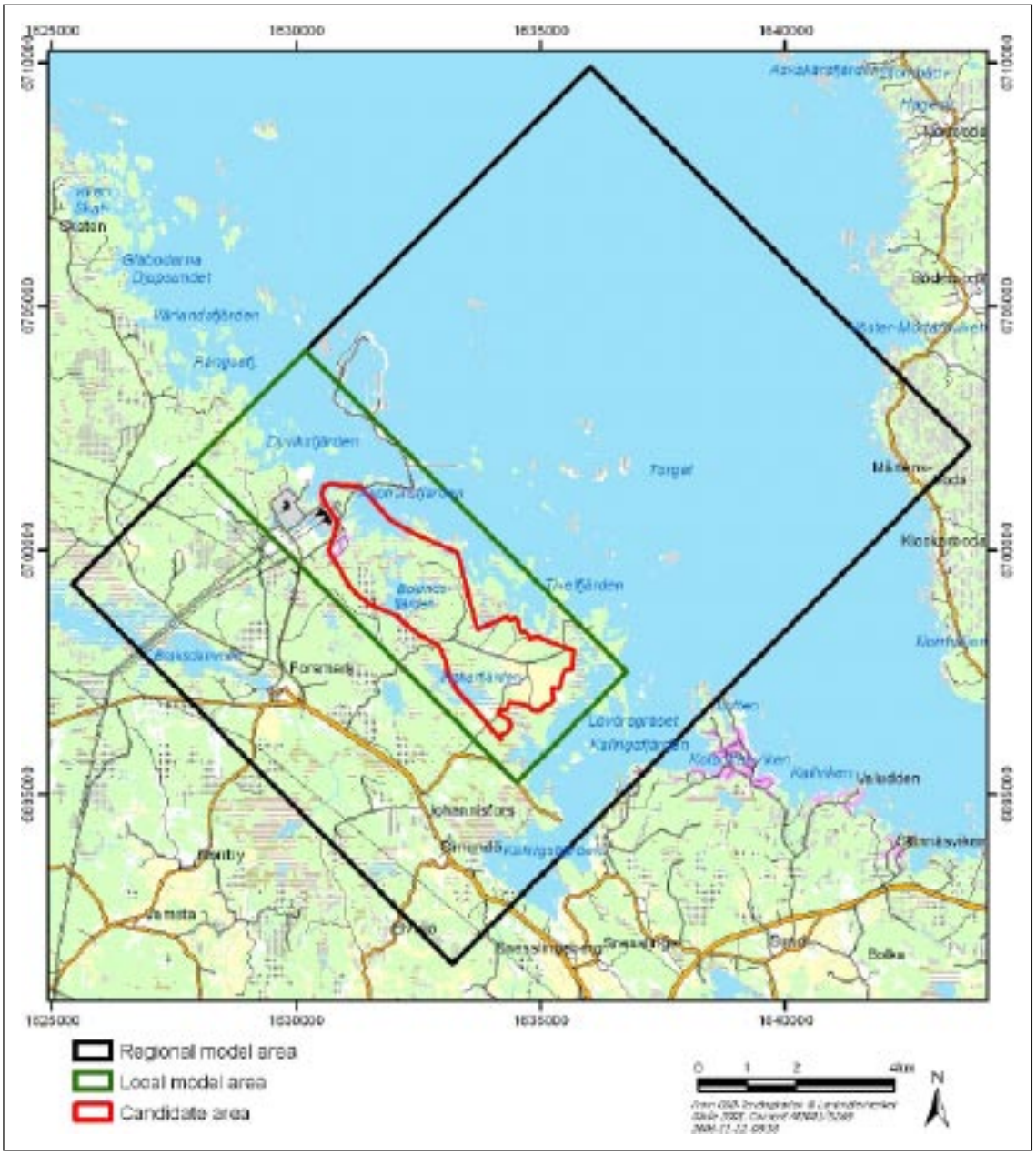

Figure 3-1. *An overview of the Forsmark site showing the regional (black line) and local (green line) model areas in conjunction with the candidate area (red line) /SKB 2005/.*

The Singö fault, which is the subject of this study, is located beneath the bottom of the Sound of Öregrundsgrepen, outside the candidate area close to the north-eastern boundary of the local model volume. The local model volume comprises the volume within which the repository is expected to be sited, while the regional model defines the boundary conditions for the local model. In other words, it is not likely that the fault will be encountered in any part of a repository for spent nuclear fuel or any of its appurtenant facilities, such as access tunnels. However, since the fault provides boundary conditions in a local stress model and also may affect the hydraulic conditions of a repository, its properties are still of interest for the description of the site.

3.1 Engineered facilities at Forsmark

At Forsmark, a number of engineered facilities exist, the most important of which are listed in Table 3-1 and also illustrated in Figure 3-2. All of these are commonly labeled in text with a short ID. In addition, the corresponding SKB official IDs, used in the SICADA database are shown in the table. Design data of the four tunnels which are excavated in the Forsmark area are shown in Table 3-2.

The SFR twin tunnels were excavated full face eastward, along the chainage direction, starting from the islet Stora Asphällan. Tunnel 1-2 and Tunnel 3 were both excavated from two faces, one face starting from the mainland side, proceeding northward along the chainage direction, the other from the islet Loven proceeding against the chainage direction. Tunnel 1-2 was excavated in two phases: a top heading of 50 m^2 followed by bench blasting of the remaining 30 m^2, whereas Tunnel 3 was excavated full face. Rock support in the tunnels is further treated in Section 4.6.1.

Table 3-1. Nomenclature of engineered facilities at the Forsmark site.

Engineered structure	Short ID	SICADA ID	Year of completion
Forsmark Nuclear Power station, Units 1 and 2	Unit 1-2		
Forsmark Nuclear Power station, Unit 3	Unit 3		
Storage for low and medium radioactive waste	SFR		
Discharge tunnel for cooling water from Units 1 and 2	Tunnel 1-2	TFKB12	1976
Discharge tunnel for cooling water from Unit 3	Tunnel 3	TFKB3	1982
Construction tunnel for SFR	SFR-B	TFRBT	1985
Operational tunnel for SFR	SFR-D	TFRDT	1985

Table 3-2. Tunnel design data /Carlsson et al. 1985a/.

Tunnel ID	Rock cover, m	Length, m	Span, m	Cross section area, m^2	Inclination
Tunnel 1-2	55–60	2,300	11	80	0. except for in-and outlet
Tunnel 3	50–55	3,000	10	55	0. except for in-and outlet
SFR-B	50	1,000	7.5	49	1:10
SFR-D	50	1,000	8.5	65	1:10

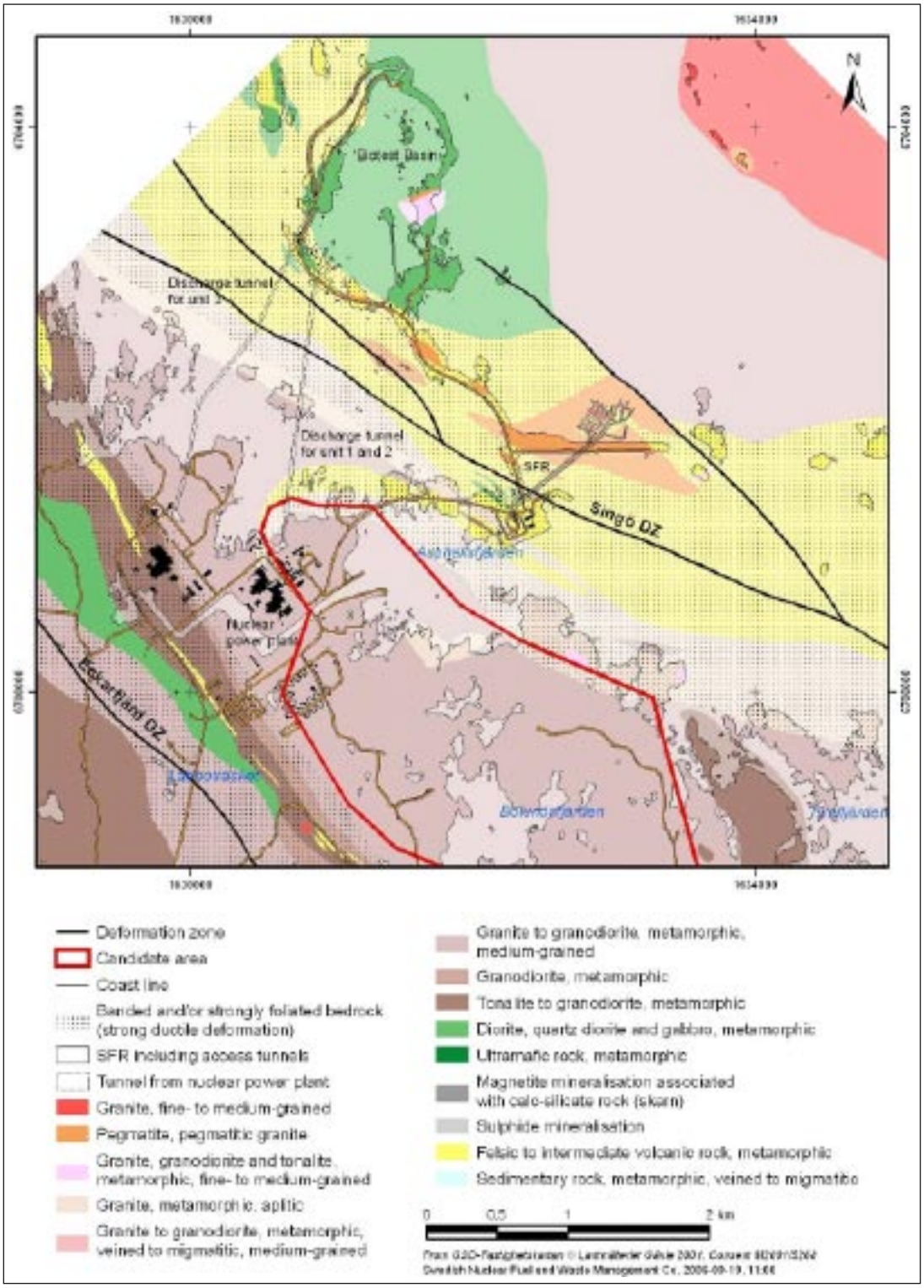

Figure 3-2. *Bedrock map of the Singö deformation zone and its surroundings at the Forsmark site, including part of the Candidate Area for spent nuclear fuel storage /SKB 2005/. The map also shows the engineered facilities, as listed in Table 3-1. (File received from SKB: forsmark_bedrock_defzone_20060919_1100.jpg.)*

3.2 General geology and tectonics

The bedrock in the Forsmark area is of Precambrian age and consists of metaintrusive and metasupracrustal rocks. The metaintrusive rocks are dominated by granitic to tonalitic rocks while the supracrustals are dominated by volcanogenic rocks, cf Figure 3-2.

The dominant rock type on the mainland, at the candidate area is a metamorphic medium grained granite to granodiorite /SKB 2005/. North to northeast of the candidate area aplitic metamorphic granite dominates in a belt about 1 km wide which has a NNW to SSE trend. Further north this aplitic granite borders to a felsic to intermediate metavolcanic rock. Most of the Singö deformation zone in the model area is situated in this volcanic rock. In this suite of metavolcanic rocks there is also an intrusion of a pegmatitic granite at the North-east side. This pegmatitic granite occurs at the vicinity of the SFR area.

3.3 The Singö deformation zone

In the area around Forsmark several deformation zones have been identified, which strike WNW to NW with a vertical or steep SW dip /SKB 2005/. The Singö deformation zone, the subject of this study, is the most well-known of these structures and is found to the north of the north-eastern border of the candidate area, see Figure 3-2.

The Singö deformation zone is described in the Preliminary site description as a 200 m thick vertical or steeply dipping zone that exists over a length of at least 30 km /SKB 2005/. The span for the thickness is ± 50 m. The general strike and dip of the zone is 120/90. The Singö deformation zone is considered to be a regional fault line which may extend at least as far as Gävle to the north and Singö at the south.

3.4 Tunnels through the Singö deformation zone

The Singö deformation zone is intersected by all of the four tunnels previously described, as shown in Figure 3-2.

In the discharge tunnel for units 1 and 2, the width of the Singö deformation zone has been estimated to be about 200 m. About 350 m to the north-west, where the discharge tunnel for unit 3 intersects the fault, its width has been estimated to 175 m. In the SFR tunnels, about 1,500 m to the south-east, the width has been reported to be about 120 m /Carlsson et al. 1985a/.

4 Compilation and analysis of geological information

Geological data from the investigation and the construction phases of the two discharge tunnels for spent cooling water and from the two access tunnels to SFR have been compiled in order to describe the heterogeneity and variability of the Singö fault. This is been done in order to obtain a more comprehensive picture of the fault. The Singö deformation zone is composed of several sectors that exhibit different geological characteristics and different mechanical properties. Each sector has been characterized with respect to conditions of matrix and fractures in order to determine proper mechanical properties of each zone sector. A compilation of primary data and their sources are shown in Table 4-1.

4.1 Site investigations

Site investigations were carried out in 1970's /Larsson 1973, Moberg 1973/ and early 1980's /Moberg 1980/ prior to the construction works for the discharge tunnels for cooling water from the Nuclear power plant at Forsmark, and for the SFR. Investigations for a Candidate Area for spent fuel storage have been carried out since 2002. Investigation results of relevance for this study comprise:

- Geomagnetic survey.
- Seismic refraction survey.
- Core drillings along the tunnel alignments.
- Mapping of bedrock exposures.

Most of the results from the early investigations are unpublished. Some of the core drillings intersect the Singö deformation zone. Characteristics of zone passage in the drill cores are:

- Increased fracturing of drill cores.
- Alteration of the rock mass.
- Decomposition of the rock mass.
- Core losses.

Table 4-1. Primary data used for the conceptual model.

Data	Source	Comment
Rock types, zones and fracture data in the SFR tunnels	/Christiansson and Bolvede 1985/ (unpublished report, core logs, field notes, and drawings)	Large amount of detailed data. Lithology partly differentiated. 1 m fracture cut off
Rock types, zones and fracture data in Tunnel 1-2	/Carlsson and Olsson 1976/. /Lundström and Tenne 1976/ (unpublished drawings)	Lithology differentiated. 3 m fracture cut off
Rock types, zones and fracture data in Tunnel 3	/Hansen 1982ab/ (unpublished report, core logs, field notes, and sketch drawings)	Lithology very coarse subdivision. 3 m fracture cut off
Core drillings for Tunnel 1-2 (D63) and Tunnel 3 (D381, D392)	/Moberg 1973 and 1980/ (unpublished core logs and drawings)	Physical core description and fractures/m
Geomagnetic lineament	The site investigation model PFM_DZ_Local_v.2.1.rvs	See /SKB 2005/ for context
Seismic refraction lines across the Singö DZ	SICADA files (listed in Appendix A). Original source are site investigations for Tunnel 1-2, Tunnel 3, and SFR	Anomalies over Tunnel 3 do not coincide with tunnel observations and also not with seismic anomalies in drawing 970802
Water leakage in Tunnel 1-2	/Carlsson and Olsson 1977/	

4.2 Mapping of the tunnels

The Singö deformation zone has been encountered in four tunnels: the SFR construction tunnel, the SFR operational tunnel (SFR twin tunnels), Tunnel 1-2, and Tunnel 3. To some extent, Tunnel 1-2 and Tunnel 3 were mapped after the roof had been covered by shotcrete. In these cases, geological information comes from the lower parts of the walls. Fracture cut off is reported to be 1 metre in the SFR twin tunnels and 3 m in the two discharge tunnels.

4.2.1 Mapping in Tunnel 1-2

The tunnel was mapped during the excavation of the top heading /Carlsson and Olsson 1976/. Little attention was paid to lithology which, therefore, is generalized. Stretches with adverse structures (zones with crushed rock and clay) subject to particular support measures, such as reinforced shotcrete arches, were further mapped after bench excavation /Lundström and Tenne 1976/.

Figure 4-1 shows the tunnel passage through the central 75 metres of the Singö deformation zone with a compilation of the results of these two mapping events. The most important structures are the wide fractures filled with "clay" and totally weathered and crushed rock.

4.2.2 Mapping and core drilling in Tunnel 3

Tunnel 3 was also mapped during construction, once to twice a month. A zone with fractures filled with clay altered material and crushed rock caused comprehensive rock falls and was supported by means of cast concrete arches after each round. Due to this, geological mapping in the Singö zone was only done on 3 excavation rounds (each 5 metres), chainages 2/525–2/530 and 2/535–2/545. Core drilling in Tunnel 3 was commenced from the face at chainage 2/535 and continued to 2/485. The appearance of the mapped tunnel sections correspond well to the core. Figure 4-2 shows a core box comprising the first eight metres of drilling (corresponding to chainage 2/535–2/527) with crushed and disintegrated rock and also multiple core losses. Another core drilling started at chainage 2/475 and terminated at 2/425. In all 100 metres were subject to core drilling.

Samples of clay were taken in Tunnel 3, at chainages 2/535, 2/540, and 2/545. The samples were analyzed at Swedish Geological Survey, by means of X-ray diffraction, which showed the presences of the minerals hydro-mica, chlorite, hematite-stained plagioclase feldspar, and quartz, but no swelling clay minerals.

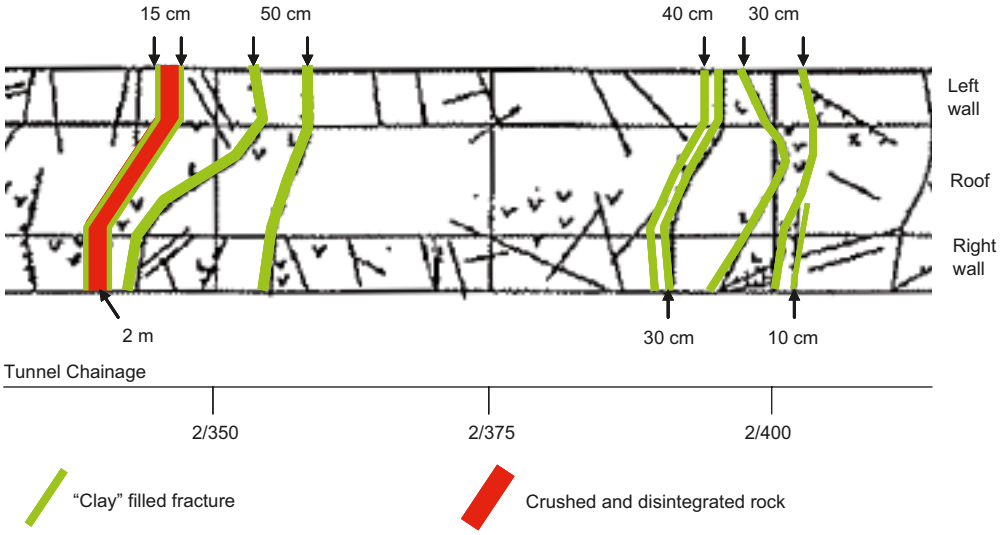

Figure 4-1. *Mapping of unit 1-2 discharge tunnel at its crossing with the central part of the Singö deformation zone. Thicknesses are indicated for each discontinuity (compiled from mapping by /Carlsson and Olsson 1976, Lundström and Tenne 1976/).*

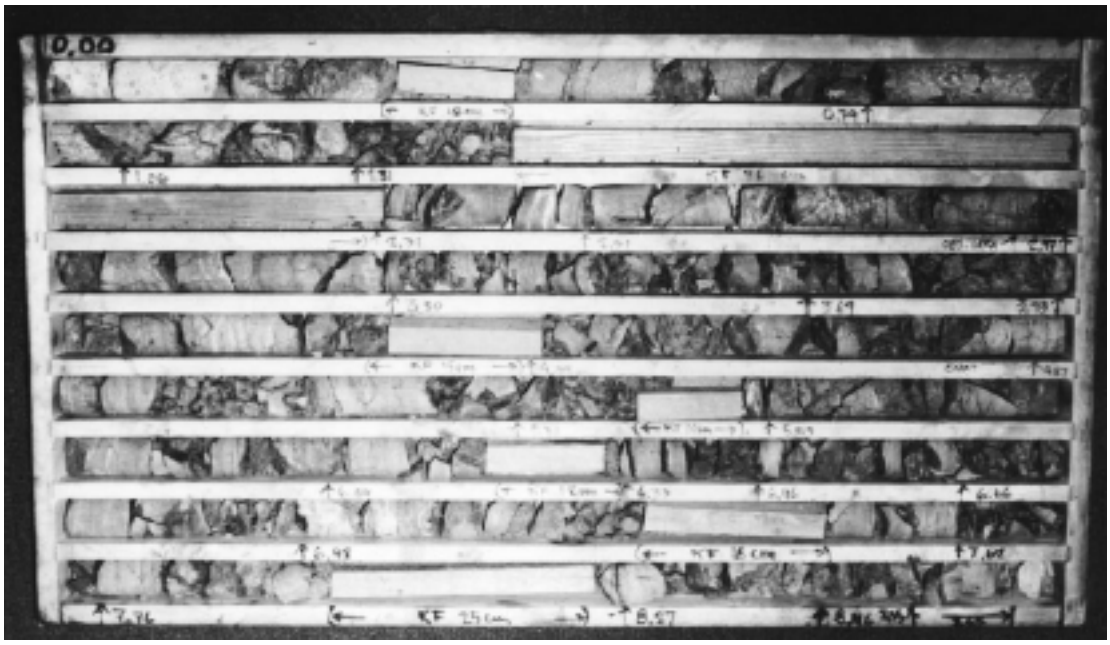

Figure 4-2. *Eight metres of drill core from drilling in Tunnel 3 starting at chainage 2/535 (in core 0.00). The unrecovered parts of the core, replaced by wooden fillets, are interpreted as fault breccia and gouge, and clay and small rock fragments having been washed away by flush water.*

4.2.3 Mapping of the SFR tunnels

For mapping of the SFR tunnels, two engineers worked in shifts. As a result, almost the entire tunnel length could be mapped before being covered with shotcrete. Thus these two tunnel mappings give rise to the most comprehensive and detailed data.

4.3 Rock type distribution

4.3.1 Overall conditions

Bedrock of the Forsmark area has been treated in previous publications /SKB 2005/ and a map of the bedrock is shown in Figure 3-2, which, however, extends further north than does the corresponding map in that work.

Bedrock distribution of the entire tunnel lengths is shown in Figure 4-3. A comparison with the bedrock map shows that the four tunnels pass most of the rock units of the area, roughly in proportion to the occurrence of rock units in the area. Not unexpectedly, Tunnel 3, being the longest of the tunnels, features a rock type distribution being most similar to the overall pattern, covering metamorphic granite to granodiorite, aplitic fine grained metagranite, metavolcanics deformed to a greater or lesser extent (the deformed varieties mapped in the tunnels as "metasediments" or "paragneiss"), pegmatite, amphibolite, and also diorite. The SFR tunnels are the shortest and show a distribution not typical for the overall pattern. Massive granite and "metasediment" (or metavolcanics) predominate, and some of the rocks feature a strongly foliated structure (usually mapped as "mylonitic").

On the general map, minor occurrences of metasediments are not specified, but instead they are included in the area of metavolcanics. The rock types are difficult to distinguish, and part of the tunnel stretches mapped as metasediments, are actually mica-altered and foliated metavolcanics. In addition, it may be difficult to distinguish aplitic granite from reddish metavolcanics, in particular the strongly foliated varieties.

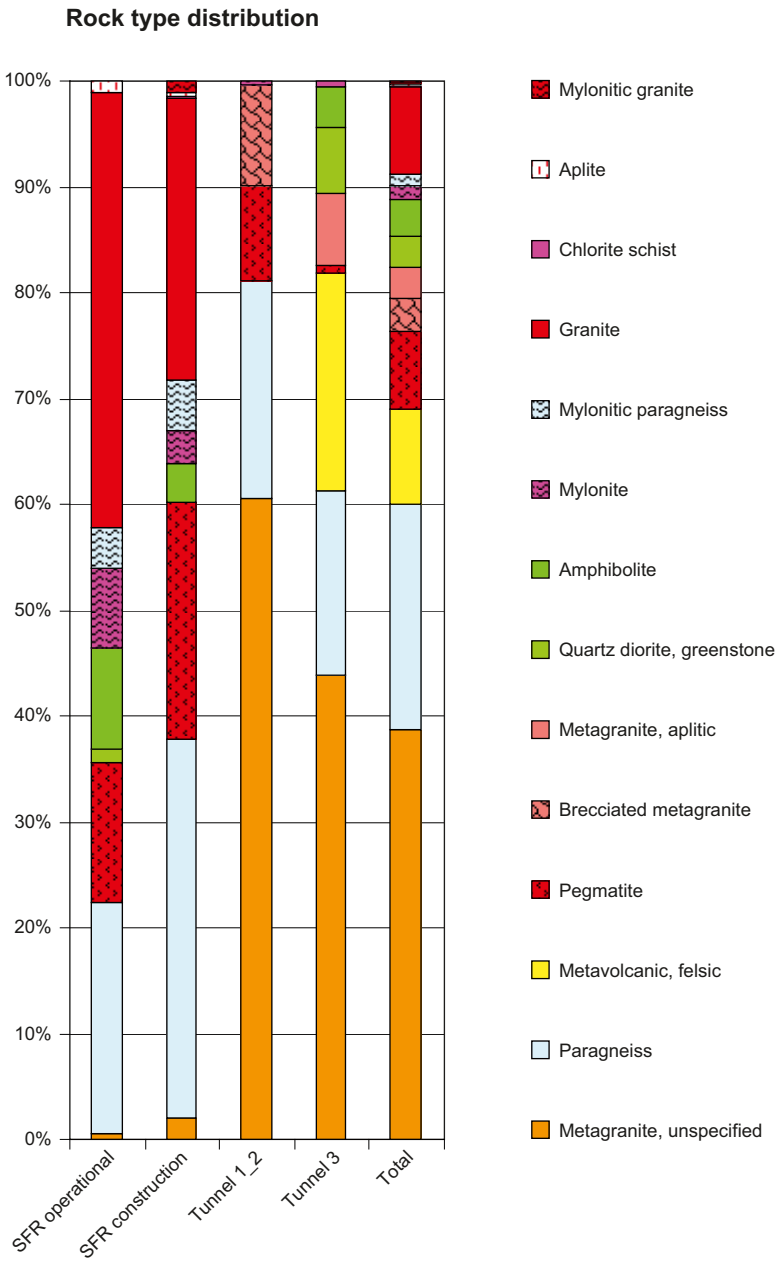

Figure 4-3. *Rock type distribution in four tunnels at Forsmark. Tunnel lengths: SFR 2×800 m, Tunnel 1-2 1,900 m, and Tunnel 3 2,500 m.*

4.3.2 Rock types in the Singö deformation zone

Rock type distribution at the tunnel passages through the Singö zone are shown in Figure 4-4. The pattern differs between the tunnels. At SFR, foliated /metavolcanics (labeled “metasediments”) with pegmatite predominate. Mylonitic structure is common. In Tunnel 3, the rock type is mainly aplitic metagranite, partly foliated from chainage 2/320 to ca 2/430, where this rock type terminates at an amphibolite dyke, beyond which the rock consists of alternating layers of aplitic metagranite, amphibolite, and red metavolcanic (field notes /Hansen 1981–82/). Thereafter, the rock was mapped as a red metavolcanic for the remaining part of the zone. In Tunnel 1-2, all rock in the zone has been mapped as brecciated metagranite, of the aplitic type.

In one core drilling during the site investigations for Tunnel 1-2, the rock was characterized as “aplitic to leptitic”, the latter a term commonly used for metavolcanics in Swedish Precambrian. As mentioned above, the aplitic metagranite appear to grade into a foliated structure and may be difficult to distinguish from red metavolcanics. Thus, it is difficult to exactly establish the boundary between these two rock types in Tunnel 1-2, so the distribution in the two discharge tunnels may actually be more similar than appears from the diagrams.

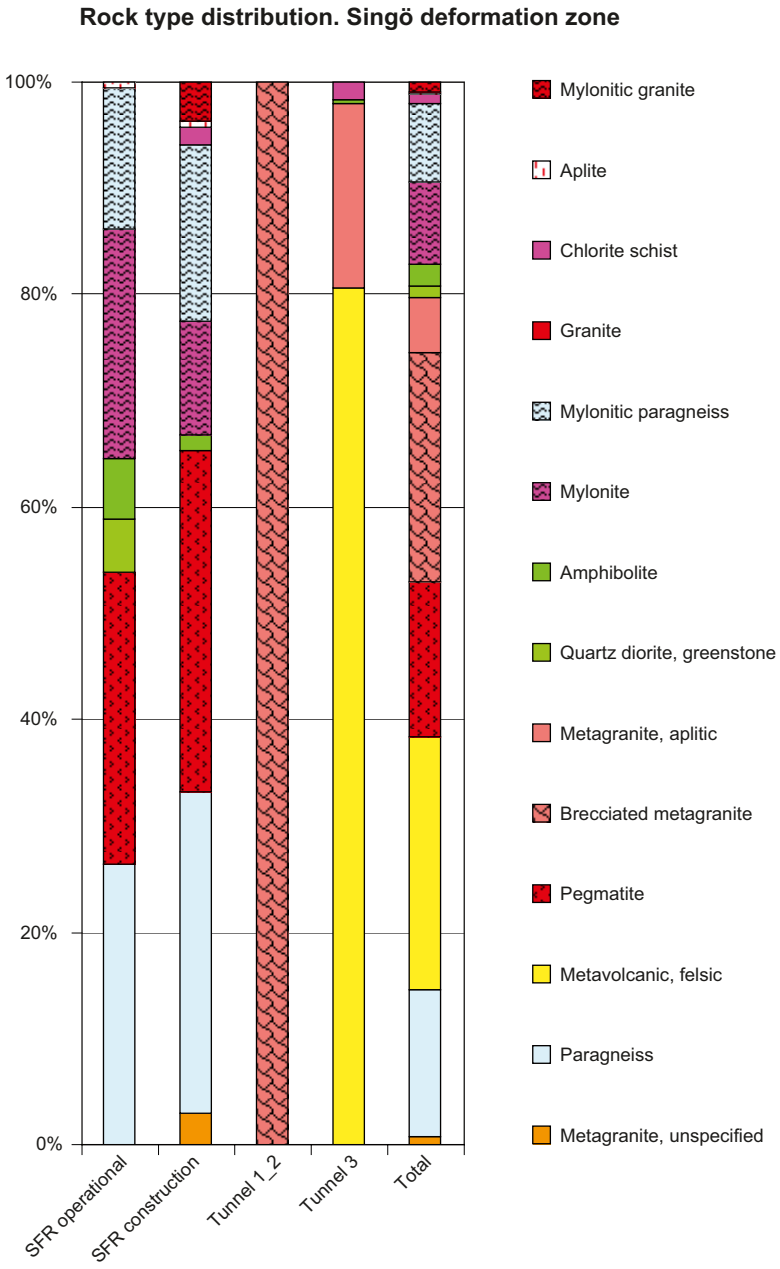

Figure 4-4. *Rock type distribution within and close to the Singö deformation zone in four tunnels at Forsmark: SFR: 2×200 m, Tunnel 1-2: 176 m, and Tunnel 3: 242 m.*

4.4 Fracture statistics

4.4.1 Fracture orientation

Figure 4-5 and Figure 4-6 show pole contour plots of fractures for the SFR and unit 3 tunnels, respectively. Largely, the fracture systems are similar, with two sub-vertical sets, striking approximately NW and NE, respectively, and one set of sub-horizontal fractures. However in Tunnel 3 the fracture system is rotated clockwise relative to SFR. The figures also show that the fracture system does not change considerably across the Singö deformation zone.

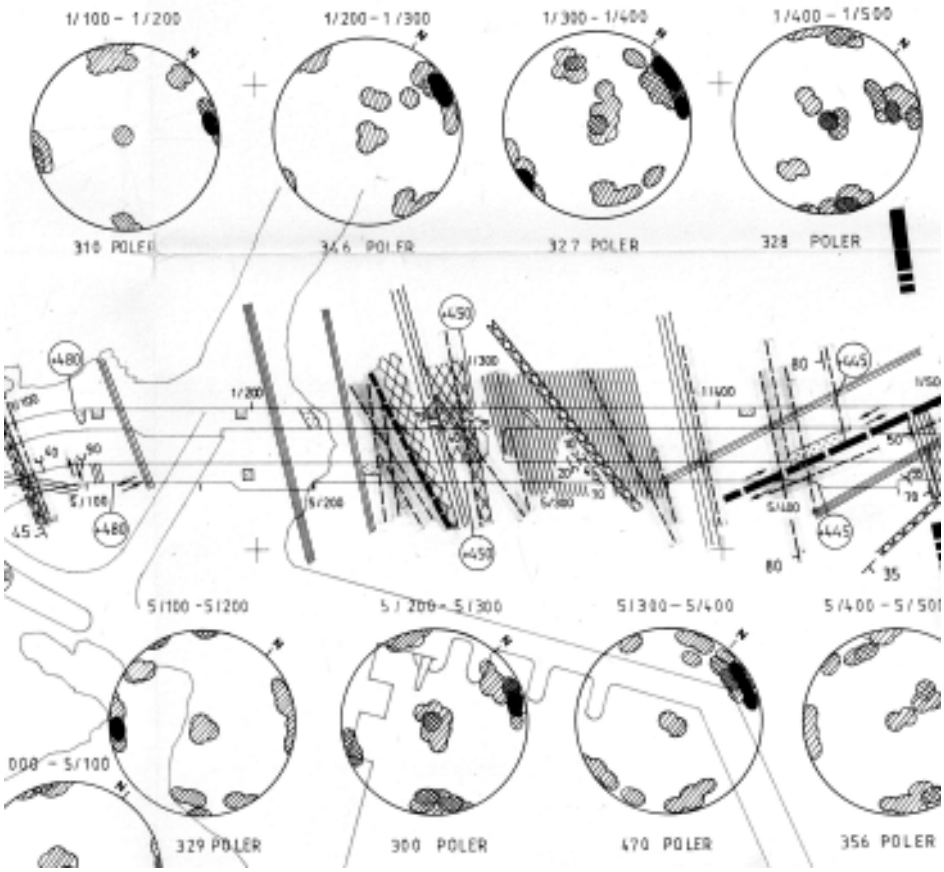

Figure 4-5. *Poles to fracture planes in the SFR operational (above) and construction (below) tunnels in the area of intersection with the Singö deformation zone chainage scale is in metres. Pole concentrations in %: black ≥12; grid 6-12; lines 3-6; no fill >3. /Christiansson and Bolvede 1985/.*

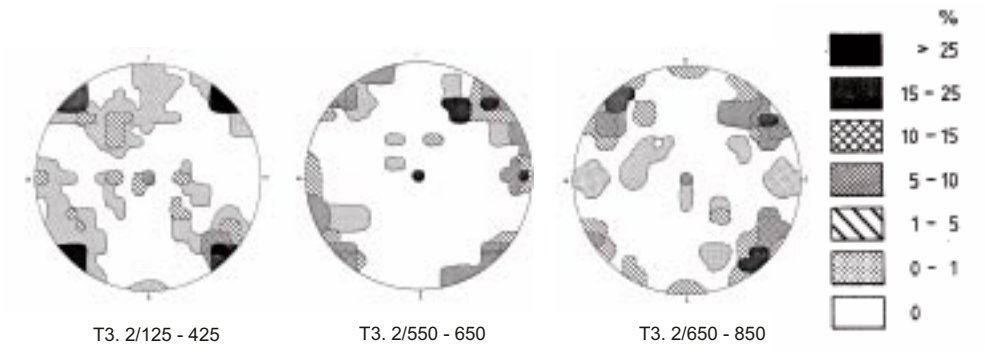

Figure 4-6. *Contour plot of poles to fracture planes in the unit 3 discharge tunnel. Chainages from left to right: 2/125–425, 556 poles; 2/550–650, 511 poles;2/650–850, 183 poles /Hansen 1982bc/.*

4.4.2 Fracture length

For the identified filled fractures, trace lengths have been recorded in the SFR tunnels and Tunnel 1-2. Trace lengths have been divided into 2 groups: greater than 10 m, crossing the entire tunnel and less than 10 m, terminating within the tunnel envelope surface. The distribution is shown in Figure 4-7.

4.4.3 Fracture infilling materials

The mapping of the two discharge tunnels is not accurate enough to produce any relevant statistics. For Tunnel 1-2, and for the SFR tunnels, selected material filled fractures are shown in the RVS model. According to field notes for Tunnel 3, the following fracture materials occur in the Singö zone in order of abundance as shown in Table 4-2.

4.4.4 Fracture intensity

In Figure 4-8 and Figure 4-9, fracture intensity is shown as P_{10} (fractures per metre along a scan line) and P_{20} (fractures per square metre on a surface) for Tunnel 3 /Hansen 1982/ and the SFR operational tunnel /Christiansson and Bolvede 1985/, respectively. The peaks correspond in both tunnels to the intersection with the Singö deformation zone. In the tunnels, the total number of single fracture traces longer than 3 m was counted by hand from the tunnel map, while fracture frequency for zones was determined from estimates of mean spacing for each fracture set. In Tunnel 3, average fracture frequency (P_{20}) in host rock is 0.16 per m^2, distributed on 0.22 in the rock mass to the SW of the Singö deformation zone, and 0.06 m to the NE of it. The SW side of the Singö Zone features many fracture zones, while the rock on the NE side of the zone has very few. In the SFR tunnel the situation is just the reverse.

Table 4-2. Fracture infilling materials in Tunnel 3.

From chainage	To chainage	length, m	Material 1	Material 2	Material 3	Material 4
2,390	2,430	40	calcite	laumontite	chlorite	
2,511	2,545	34	crushed angular rock material, 2–20 cm in size	crushed rock material, 0–2 cm in size	plastic clay	chloritic gouge
2,545	2,625	105	chlorite	calcite		

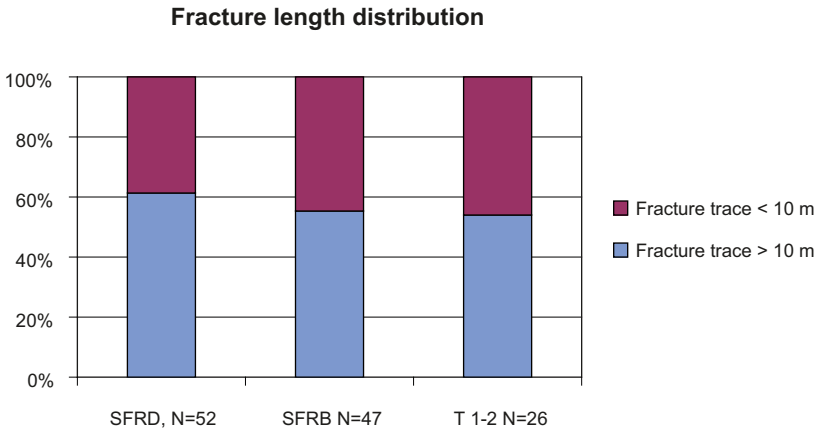

Figure 4-7. *Fracture trace length distribution for fractures with material infillings in three tunnels. SFR operational tunnel (SFRD) chainage 1/162–1/433, SFR construction tunnel (SFRB) chainage 5/150–5/416), and the unit 1-2 discharge tunnel (T 1-2) chainage 2/228–2/620.*

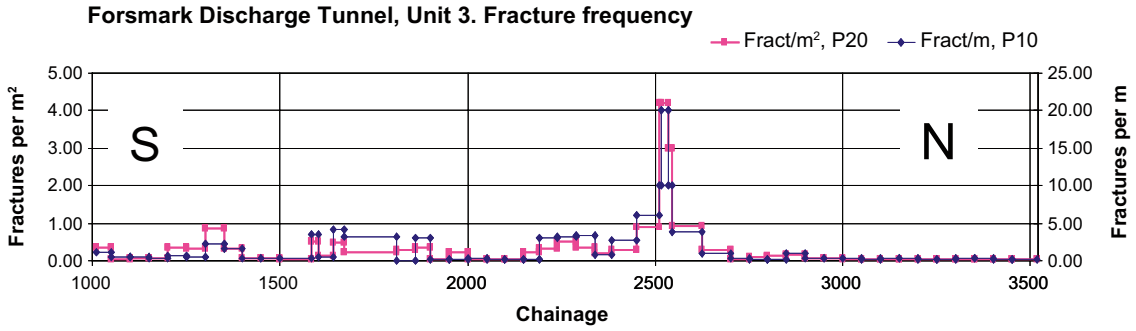

Figure 4-8. *Observed fracture intensity in the discharge tunnel for unit 3. P_{10} is the amount of fractures per metre crossing the right-hand spring-line. P_{20} is the amount of fractures per square metre within the tunnel envelope surface. Fractures with a trace length from 3 m were recorded.*

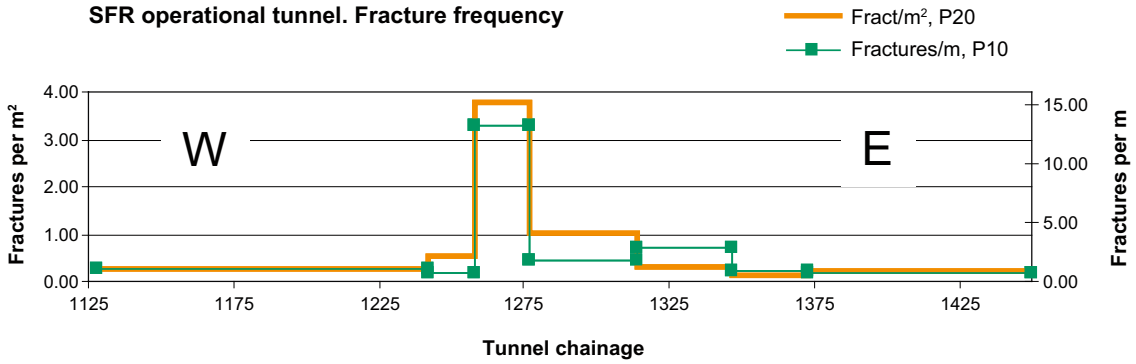

Figure 4-9. *Observed fracture intensity in the SFR operational tunnel. P_{10} is the amount of fractures per metre crossing the right-hand spring-line. P_{20} is the amount of fractures per square metre within the tunnel envelope surface. Cut-off length: 3 m.*

The frequencies can be compared to what has been mapped during the site investigation program at five outcrops located inside the candidate area /Hansen et al. 2004/. The P_{20} of these outcrops is within the range of 0.14–0.19 fractures per m², unevenly distributed between the locations. While outcrops at Drill sites 2, 3, and 4 have 10% fracture traces longer than 3 m, the other two have only 3%. Nevertheless, the average P_{20} fracture frequency in host rock appears to be of the same order of magnitude in the tunnel as on surface (Table 4-3).

Fracture frequency (P_{10}) in the SFR operational tunnel compared to that of drill cores along the tunnel is shown in Figure 4-10. On the northeast side, the rock is strongly foliated, which may be the reason for the high fracture frequency in the drill core compared to that of the tunnel.

Table 4-3. Fracture frequencies in host rock in Tunnel 3 /data from Hansen 1982/ compared to those of mapped drill sites in the area. Cut off length is 3 m /data from Hansen et al. 2004/.

Host Rock fracture frequency	Length	Envelope area	Fractures	Fractures per m²
Tunnel 3, SW of Singö DZ	1,375	27,500	6,135	0.22
Tunnel 3, NE of Singö DZ	817	16,340	906	0.06
Total Tunnel 3	2,192	43,840	7,041	0.16
		Mapped outcrop area	Fractures	Fractures per m²
Drill sites 2, 3, 4, 5, and Klubbudden		2,501	349	0.14
Drill sites 2, 3, and 4		1,675	322	0.19
Drill site 5, and Klubbudden		826	69	0.08

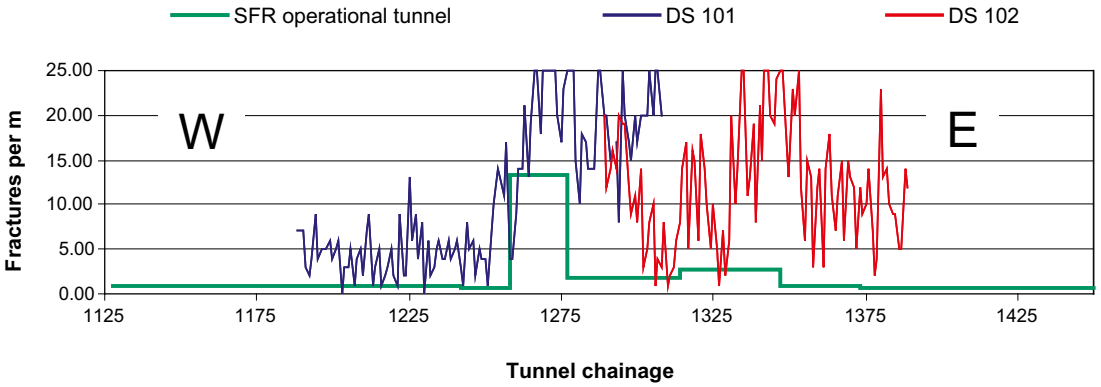

Figure 4-10. *Observed fracture intensity, P_{10}, in the operational tunnel for SFR, compared to P_{10} for 2 core drillings (DS 101 and DS 102) along and close to the tunnel.*

4.4.5 Water bearing structures

Figure 4-11 shows stereographic projections of poles to water bearing fractures recorded in the SFR operational tunnel, and Figure 4-12 shows the same for Tunnel 1-2 at the Singö Zone. As can be seen from the figures, steeply dipping, WNW to NW striking fractures are the predominant set of water bearing fractures.

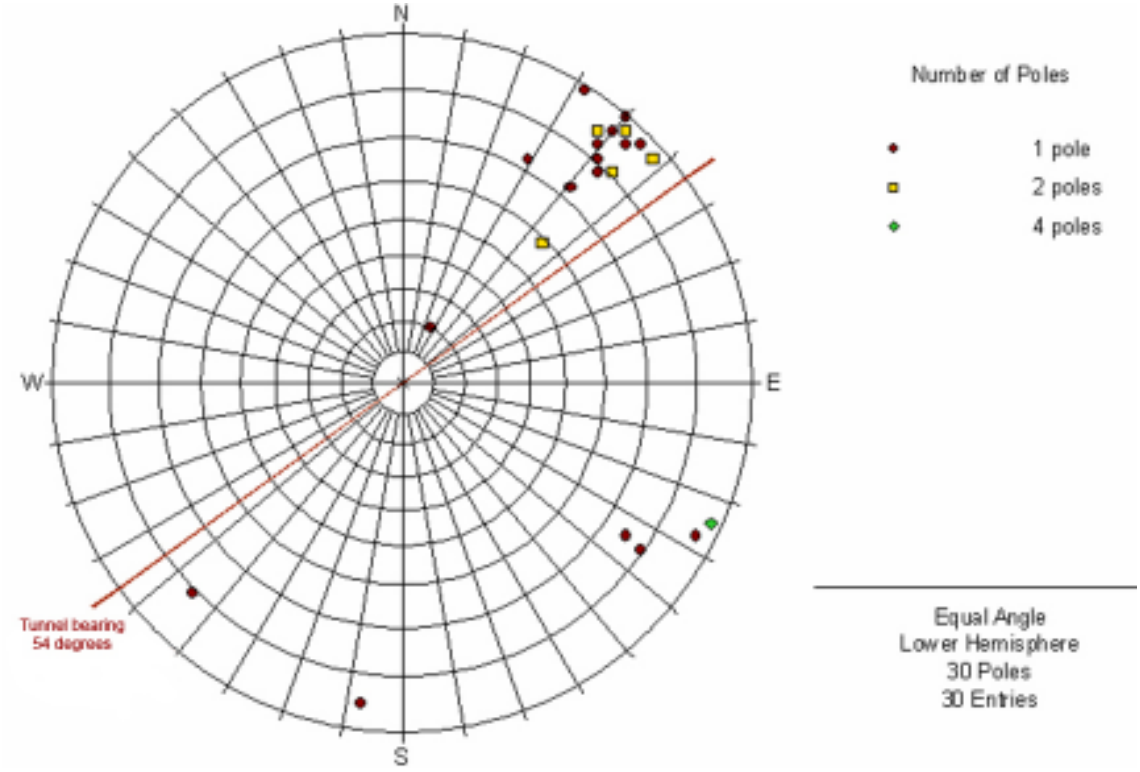

Figure 4-11. *Poles to water-bearing fractures in the SFR operational tunnel. Chainage 1/180–440.*

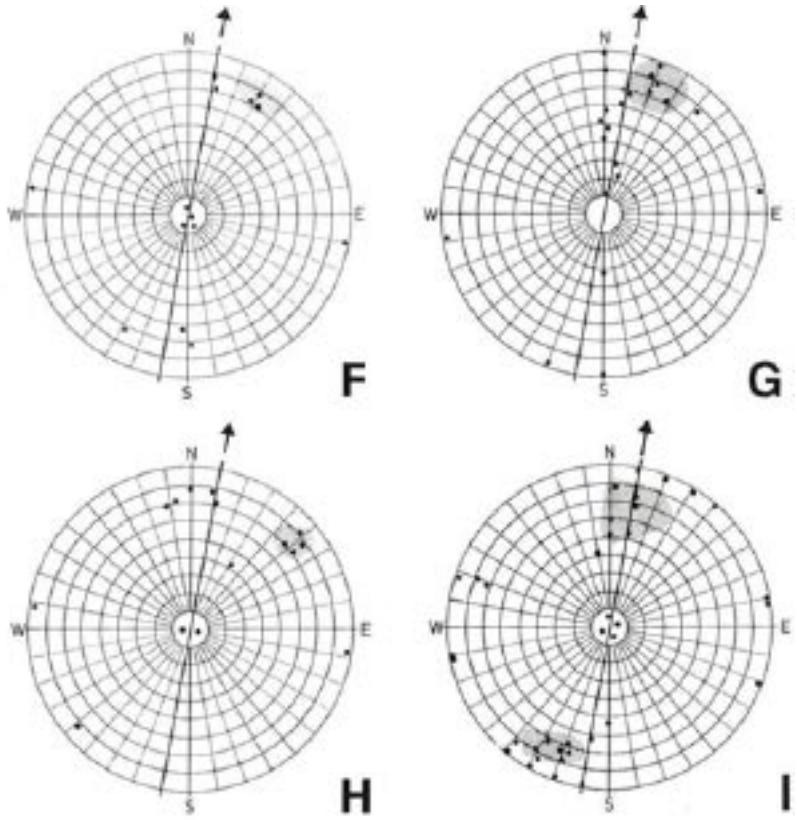

Figure 4-12. *Poles to fractures in the unit 1-2 discharge tunnel. Shaded areas indicate water-bearing fracture sets. Arrow shows tunnel direction. Chainages F: 2/150–300, G (Singö zone): 2/300–500, H: 2/500–570, and I: 2/570–680 /Carlsson and Olsson 1977/.*

4.5 Zone interpretation and subdivision

The appearance of the Singö deformation zone differs somewhat between the tunnels, but transition zones and core zone, similar to what has been defined by SKB (Figure 2-1) occur in all four tunnels. The core is characterized by clay alteration and crushed rock, with cubic blocks, 2–20 cm in size, and has been encountered in all four tunnels. Strictly following the SKB division based on fracture frequency (Figure 2-1), the core zone in tunnel 3 is 34 m wide. If also wide clay filled fractures are required, the width is only 25 m. Table 4-4 to Table 4-7 show the chainages for the various zones in three of the four tunnels.

Table 4-4. Mapped position of the Singö deformation zone in the SFR operational tunnel.

ID	Zone sector	Chainage Start	stop	stretch, m	Zone stretch
TFRDT_Z_001	Host rock	1,100	1,242	142	
TFRDT_Z_002	Transition	1,242	1,258	16	16
TFRDT_Z_003	Zone core	1,258	1,277	19	19
TFRDT_Z_004	Transition	1,277	1,373	96	96
TFRDT_Z_005	Host rock	1,373	1,800	427	
	Total			700	131

Table 4-5. Mapped position of the Singö deformation zone in Tunnel 1-2.

ID	Zone sector	Chainage Start	stop	stretch, m	Zone stretch
TFKB12_Z_001	Host rock	1,000	2,290	1,290	
TFKB12_Z_002	Transition	2,290	2,340	50	50
TFKB12_Z_003	Zone core	2,340	2,360	20	20
TFKB12_Z_004	Transition	2,360	2,390	30	30
TFKB12_Z_005	Zone core	2,390	2,405	15	15
TFKB12_Z_006	Transition	2,405	2,475	70	70
TFKB12_Z_007	Host rock	2,475	2,925	450	
	Total			1,925	185

Table 4-6. Mapped position of a splay to the Singö deformation zone in Tunnel 1-2.

Sector	Tunnel chainage Start	Stop	stretch (m)
Transition zone	2,570	2,655	85

Table 4-7. Mapped position of the Singö deformation zone in Tunnel 3.

ID	Zone sector	Chainage Start	stop	stretch, m	Zone stretch
TFKB3_Z_001	Host rock	1,010	2,340	1,375	
TFKB3_Z_002	Transition	2,340	2,511	126	126
TFKB3_Z_003	Zone core	2,511	2,545	34	34
TFKB3_Z_004	Transition	2,545	2,625	80	80
TFKB3_Z_005	Host rock	2,625	3,517	892	
	Total			2,507	240

4.5.1 Core zone

The core zone is the most consistent part, common for all of the tunnels, with a total width of 15–35 metres.

It is characterized by a 2–12 m wide zone of crushed rock, showing a high degree of alteration and disintegration, with a block size of 2–20 cm, and a fracture frequency (P_{10}) of well over 10 fractures per metre. Matrix consists of silty, sandy and gravelly material. On one or both sides of the crushed rock, several clay filled fractures are found, with a thickness of a few cm to circa 1 metre. The clay is assessed to be a result of rock alteration. The number, order of occurrence, thickness and appearance of these elements vary between the tunnels, as has been further detailed in Table 4-8. In Tunnel 1-2, the core zone can be observed as split into 2 branches separated by ca 30 m of fractured rock (transition zone) with no observations of zones with crushed rock or clay.

Given the general appearance of tunnel observations and geophysical anomalies, the core of the Singö zone may be generalized as a system of more or less planar structures, branching and anastomosing, usually with small angles, 10–45 degrees, between them (Figure 4-1 and Figure 4-5). However, the tunnel observations are too far from each other to be related with a reasonable degree of confidence.

Table 4-8. Characteristics of the core zone in the SFR operational tunnel, the discharge tunnel for units 1-2, and the discharge tunnel for unit 3.

Zone elements from SE to NW as observed in tunnels	Width (m) SFR tunnel	Tunnel 1-2	Tunnel 3	Remarks
Rock with fractures filled with clay (possibly altered rock). Most fractures less than 5 cm, a few 10–30 cm. Tabular blocks, thickness 5–20 cm. certain parts with crushed blocky rock, cubic block size 2–20 cm.		17	15	In Tunnel 3 only two rounds were mapped. Core drilling through part of zone.
Crushed rock, cubic block size 2–20 cm.		2	7	In Tunnel 1-2, the zone of weathered and crushed rock is flanked by clay-filled fractures, each 15 cm.
Totally clay altered rock.	1	1	1	In Tunnel 2, there are two fractures each 50 cm of width, spaced 6 m.
Crushed rock, block size 0–20 cm.	12		1	
Rock with fractures filled with clay (possibly altered rock). Most fractures less than 5 cm, a few 10–30 cm. Tabular blocks, thickness 5–20 cm. Certain parts with crushed blocky rock, cubic block size 2–20 cm.	6	15	10	In Tunnel 1-2, there are two actually two core zones, this one being separated from the first zone by some 30 m of fractured rock mass, i.e. transition zone (cf Figure 4-1).
Total core.	19	35	34	

4.5.2 Transition zones

These are defined as zones with between two and ten fractures per metre. The transition zones in the SFR tunnels have been subdivided into three sectors: A, B, and C, as described in Table 4-9.

In all, the core zone with boundaries, being quite distinct, is more straight-forward to identify and correlate between the four tunnels than are the other elements of the Singö deformation zone. The boundaries of the transition zones appear to be more difficult to define and establish in the two discharge tunnels.

Table 4-9. Sector division of the northeast transition zone in the SFR tunnels.

A	Fractured sector	This sector is closest to core, and characterized by cubic fracturing with a block size of 10–50 cm, corresponding to ca 2–10 fractures per metre.
B	Tabular sector	This sector is characterized by a tabular block shape striking across the tunnels, with a joint spacing of 5–50 cm. This is possibly due to that the passage of these tunnels through the Singö deformation zone occur in a mica rich sequence of the supracrustal rocks, which in the two discharge tunnels are found further to the North-east, far from the Singö DZ.
C	Altered sector	This sector is closest to host rock and is characterized by a gradual increase in rock alteration and fracture frequency.

4.6 Construction experience

4.6.1 Rock support

The Singö deformation zone was encountered during construction of all four tunnels. The tunnel for unit 1-2 was constructed using shotcrete, rock bolts and reinforced shotcrete arches for temporary support. The construction was thereafter supplemented with grouted dowels, supplementary shotcrete and shotcrete arches for permanent support.

During construction of the unit 3 tunnel, in addition to the above mentioned support, steel sets and cast concrete arches were required during the passage of the core of the zone. Figure 4-13 shows the tunnel front after having advanced into the core of the Singö deformation zone. Repeated rockfalls from the face and roof resulted in the need for rapid constructions of steel sets, which were also used as formwork for a 35 m long cast concrete arch.

Based on the experience from these two tunnels, spiling and pre-grouting were implemented for the construction of the SFR twin tunnels.

A comparison of implemented rock support methods for the four tunnels is shown in Table 4-10.

Table 4-10. Rock support methods in percentage of fault passage and their implementation in the SFR twin tunnels and also the discharge tunnels for units 1-2 and unit 3 modified after /Carlsson et al. 1985b/.

Tunnel	Singö DZ in tunnel, metres	Grouted dowels	Shotcrete 30–50 mm	Shotcrete 100–200 mm	Reinforced shotcrete 80–100 mm	Fiber shotcrete 50–80 mm	Shotcrete arches	Cast concrete arches	Grouting	Pre-grouting	Spiling
Units 1-2	200	67	0	65	4	0	16	0	10	0	0
Unit 3	200	66	0	36	24	0	17	17	13	0	0
SFR operational	120	100	0	0	33	68	28	0	0	30	82
SFR construction	120	100	10	0	20	67	26	0	0	21	86

Figure 4-13. *Rockfall in Tunnel 3 at the intersection with the Singö deformation zone. Steel sets were used for temporary support and for formwork for a cast concrete arch from /Carlsson et al. 1985a/.*

4.6.2 Water inflow to the tunnels

Water inflow in Tunnel 1-2, is shown in Figure 4-14, and in two boreholes (DS101 and DS102) along the SFR tunnels together with data from probing and pre grouting in Figure 4-15.
A comparison shows that while the peak in the SFR tunnel coincides with the core of the Singö zone, and the crushed and disintegrated rock therein, there is no high flow associated with the core encounter in Tunnel 1-2, but instead in what may be a branch of the zone. In Tunnel 1-2, the abundance of clay filled fractures may have given rise to a low hydraulic conductivity. This may also be the case for Tunnel 3, from which no extreme flow has been reported from the core of the zone.

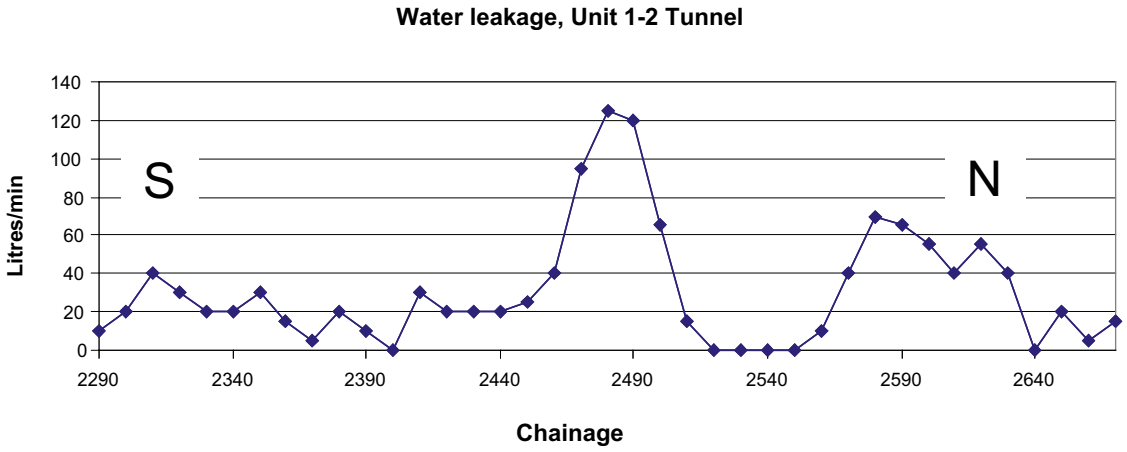

Figure 4-14. *Water flow into the unit 1-2 discharge tunnel. The split core of the Singö zone crosses at Chainage 2340–2405.The peak is related to what may be a splay of the Singö zone /Carlsson and Olsson 1977/. The source does not indicate whether the leakage was before or after grouting.*

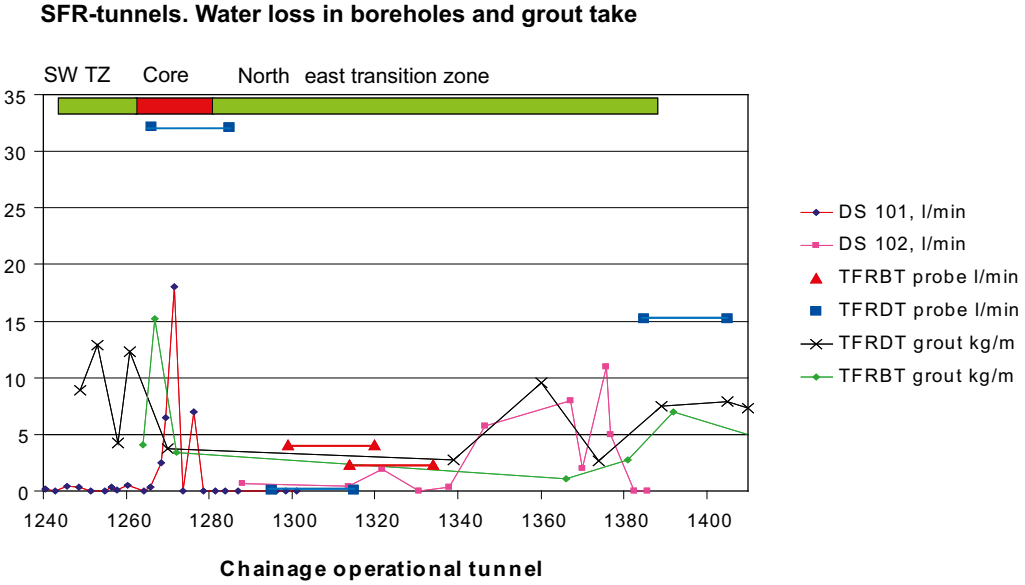

Figure 4-15. *Water flow in liters per minute in the SFR tunnels during excavation through the Singö zone, as measured in two long drill holes (DS 101 and DS 102) and in probe holes for grouting, compared to grout take in kg cement per drill metre.*

5 Modelling the Singö deformation zone in RVS

The geology of the fault is visualized in an RVS model based on the geology compiled in each tunnel passage plus geomagnetic and seismic refraction data. A summary of data files used for the model is given in Appendix A. Figure 5-1 and Figure 5-2 show an overview of the model area and volume with mapped elements, and SICADA data files developed during the present work are presented in Table 5-1.

Table 5-1. Tables of data developed for this study[1].

File name	Type of data	Section of the report
Filled_fractures_061031.xls	Material filled fractures mapped in the Forsmark tunnels	4.4
Frac_freq_061031.xls	Fracture frequencies mapped in the Forsmark tunnels	4.4
Structures_tunnels_061031.xls	Structures such as fracture zones and zones of crushed rock mapped in the Forsmark tunnels	4.5
Water_structures_tunnels_061031.xls	Water bearing structures mapped in the Forsmark tunnels	4.4
Zones_061123.xls	Singö DZ subdivision mapped in the Forsmark tunnels	4.5

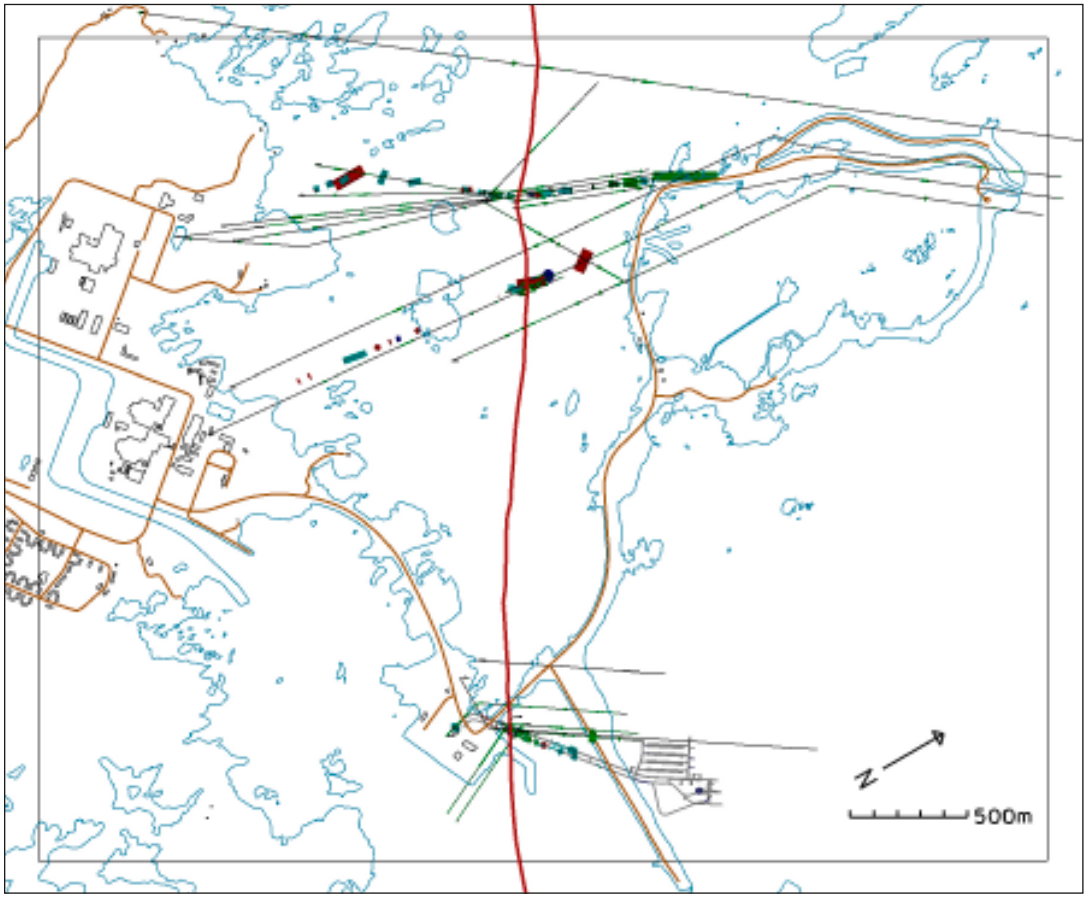

Figure 5-1. *RVS model boundaries and elements. Plan view. Red line is center of magnetic anomaly.*

[1] Final file names may deviate from the temporary file names in the table.

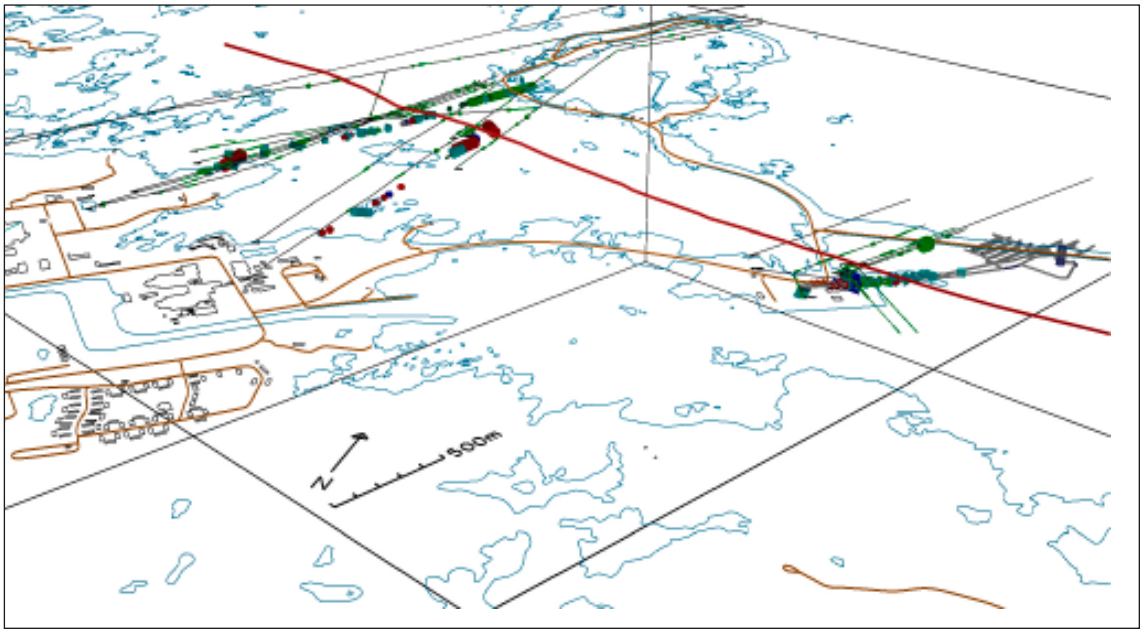

Figure 5-2. *RVS model boundaries and elements. Perspective view.*

5.1 Rock types

For Tunnel 1-2 and Tunnel 3 the rock types in the model are based on the bedrock model developed for the Site Model Forsmark version 1.2 /SKB 2005/. For the SFR tunnel detail model, bedrock details are based on the geological mapping of the two SFR tunnels (Figure 5-3). Rock type distribution in the tunnels and rock name deviations from the regional model have been treated in Section 4.3, as well as other uncertainties regarding rock terminology.

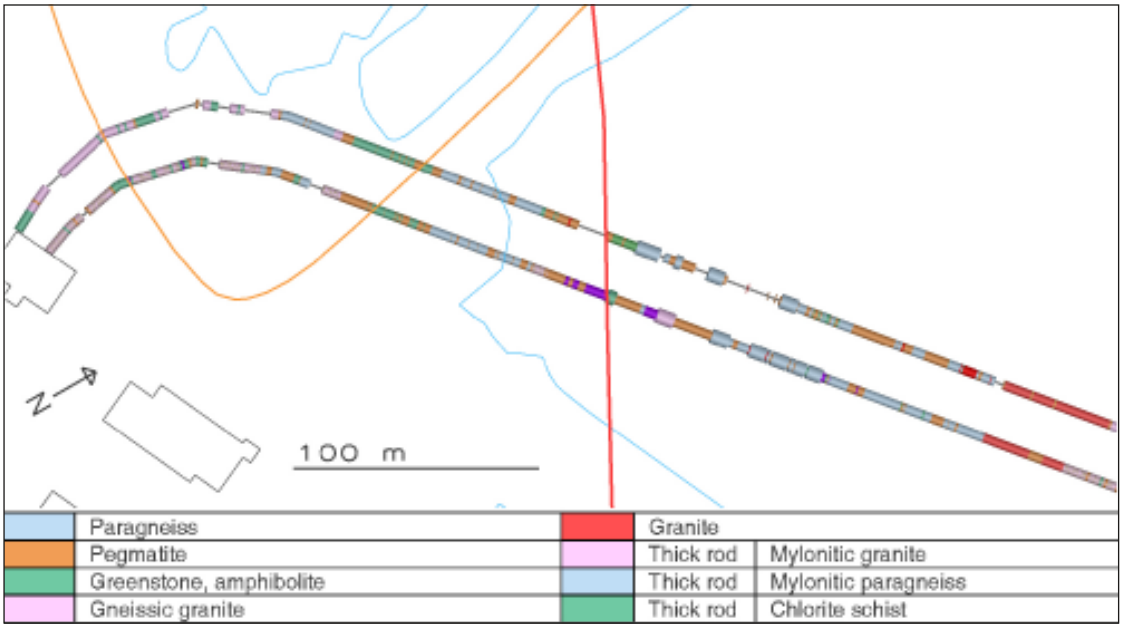

Figure 5-3. *RVS model of rock types in the SFR twin tunnels. Orange curve is the access road to the discharge tunnel outlets. Red curve in the middle is the centre of the magnetic anomaly indicating the Singö deformation zone.*

5.2 Structures and geophysical anomalies

The RVS model is based on:

- Structural elements such as clay filled fractures, crush zones, and fracture zones mapped in the tunnels.
- Geomagnetic lineament interpretation.
- Seismic refraction low velocity zones.

Figure 5-4 shows part of the RVS model near the SFR tunnels with the different structural elements.

5.3 Subdivision of the Singö deformation zone

Following the usually implied terminology of SKB (cf Figure 2-1) and in accordance with the definition given in Section 4.5, the Singö deformation zone has been divided into three subzones from southwest to northeast:

- SW Transition zone.
- Core zone.
- NE Transition zone.

The characteristics of the zones have been treated in Section 4.5. A summary of the elements and their evidence is shown in Table 5-2.

Visualization of subzone occurrences in the tunnels is shown in Figure 5-5, and details are shown in Figure 5-6, Figure 5-7, and Figure 5-8. The core zone model is based on observations in all of the four tunnels, and thus eight points have been used to model the boundaries as connected planes. The modeled planes have been given a vertical dip as most of the associated structures with crushed rock and clay feature such dip. A few of the clay filled structures dip steeply towards either the NE or SW, but do not verify any inclination of the zone as a whole. In Tunnel 1-2, the core zone is split into 2 branches separated by about 30 m of fractured rock (cf Figure 4-1).

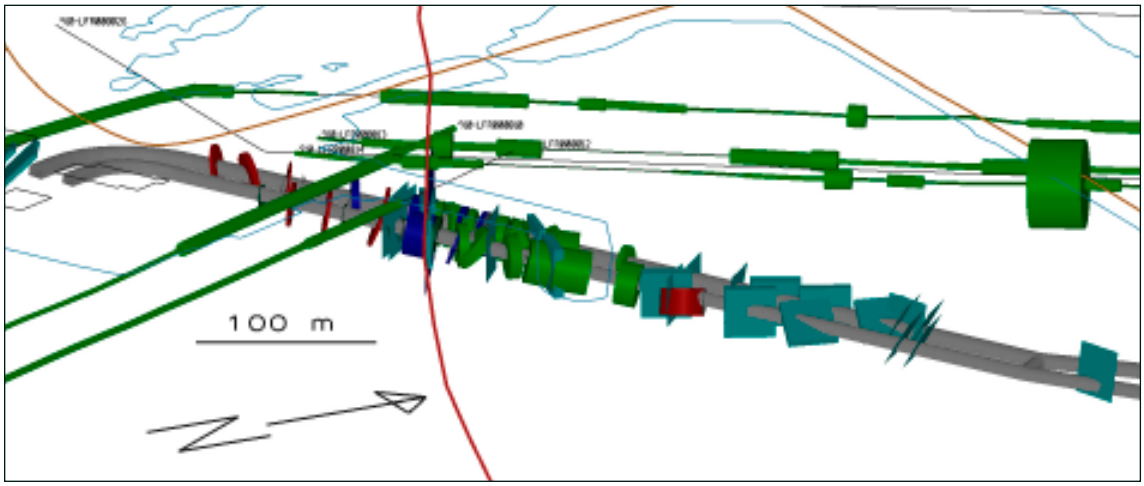

Figure 5-4. *RVS model of the SFR tunnels with geomagnetic lineament (reddish curve left of centre), seismic refraction low-velocity zones (green cylinders above tunnel, at about elevation –10 m), tunnel observations of crushed zones (blue cylinders), fracture zones (red cylinders) and water bearing structures (greenish-blue rectangles).*

Table 5-2. Summary of elements of the Singö deformation zone and their evidence in tunnels and geophysics.

Element	Evidence SFR tunnels	Tunnel 1-2	Tunnel 3	Core drillings	Magnetic anomaly	Seismic refraction
SW boundary of SW transition zone	Mapping	Mapping	Mapping	Not identified	Not identified	Not identified
Core zone	Mapping	Mapping	Mapping core drilling in tunnel 2/535–2/486	D381, D63, D65. core drilling in tunnel 2/535–2/486	From SKB 2005	Over Tunnel 3 4 consistent anomalies are found, but not corresponding with the tunnel mapping
NE boundary of NE transition zone	Mapping	Mapping	Mapping	Not identified	Not identified	Not identified
Splay of Singö Fault	Not identified	Mapping	Mapping		From SKB 2005	

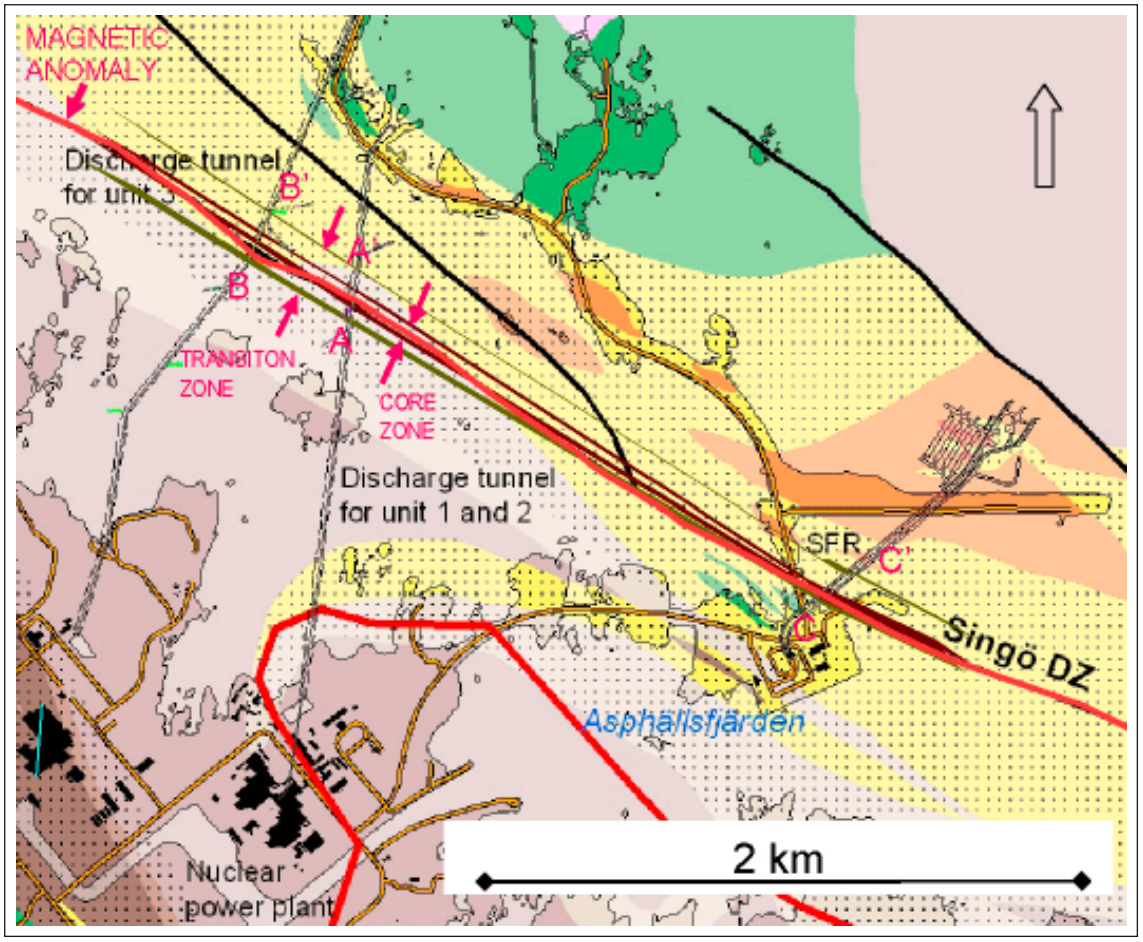

Figure 5-5. *Map of the model of the Singö deformation zone in the area of SFR and the Forsmark Nuclear power station compared to the model centre line (red) derived from the geomagnetic anomaly map (SKB). The core and transition zone boundaries are indicated with arrows, respectively. AA', BB', and CC' correspond to the detail maps and sections in Figures 5-6, 5-7 and 5-8.*

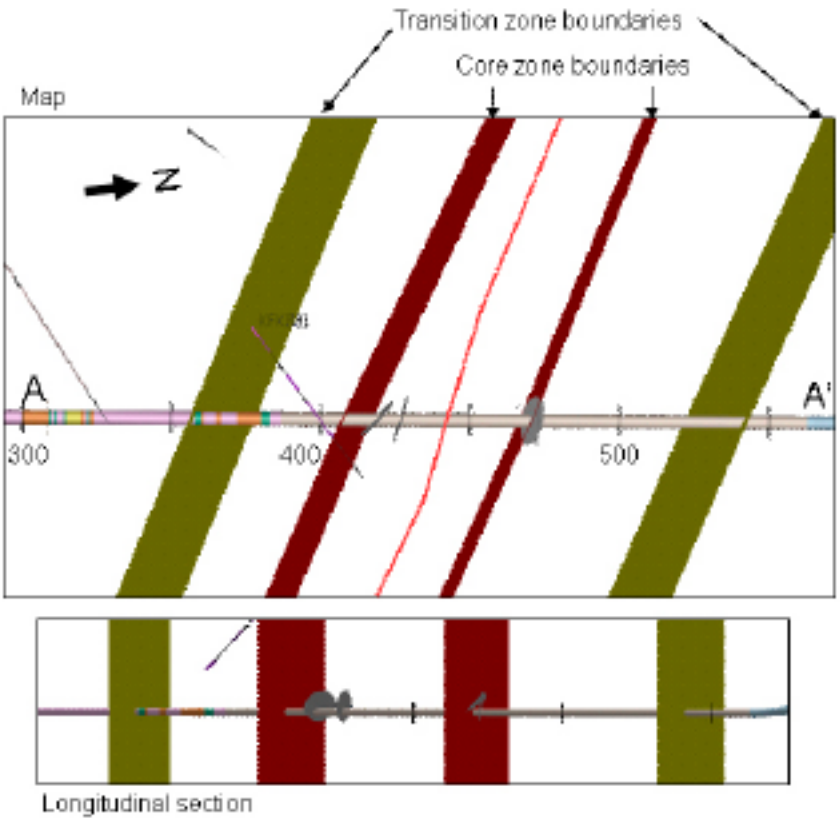

Figure 5-6. *Map and longitudinal section showing zoning of the Singö deformation zone at the intersection with discharge Tunnel 1-2. Numbers indicate SICADA/RVS sections. Red line indicates the centre line of the magnetic anomaly. Gray discs are major clay filled fractures.*

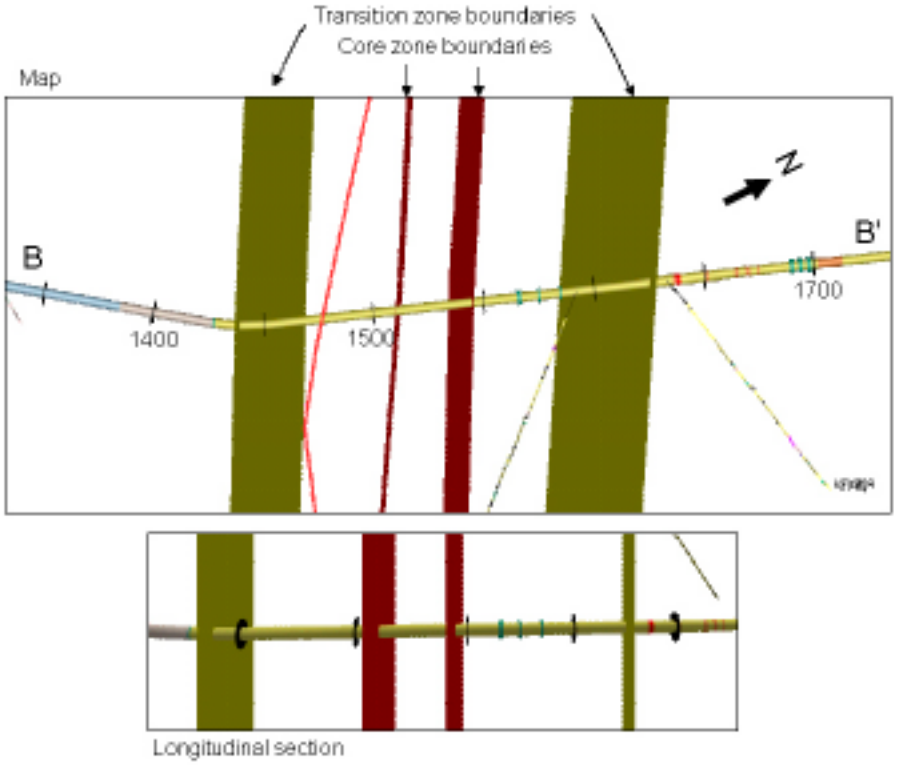

Figure 5-7. *Map and longitudinal section showing zoning of the Singö deformation zone at the intersection with discharge Tunnel 3. Numbers indicate SICADA/RVS sections. Red line indicates the centre line of the magnetic anomaly.*

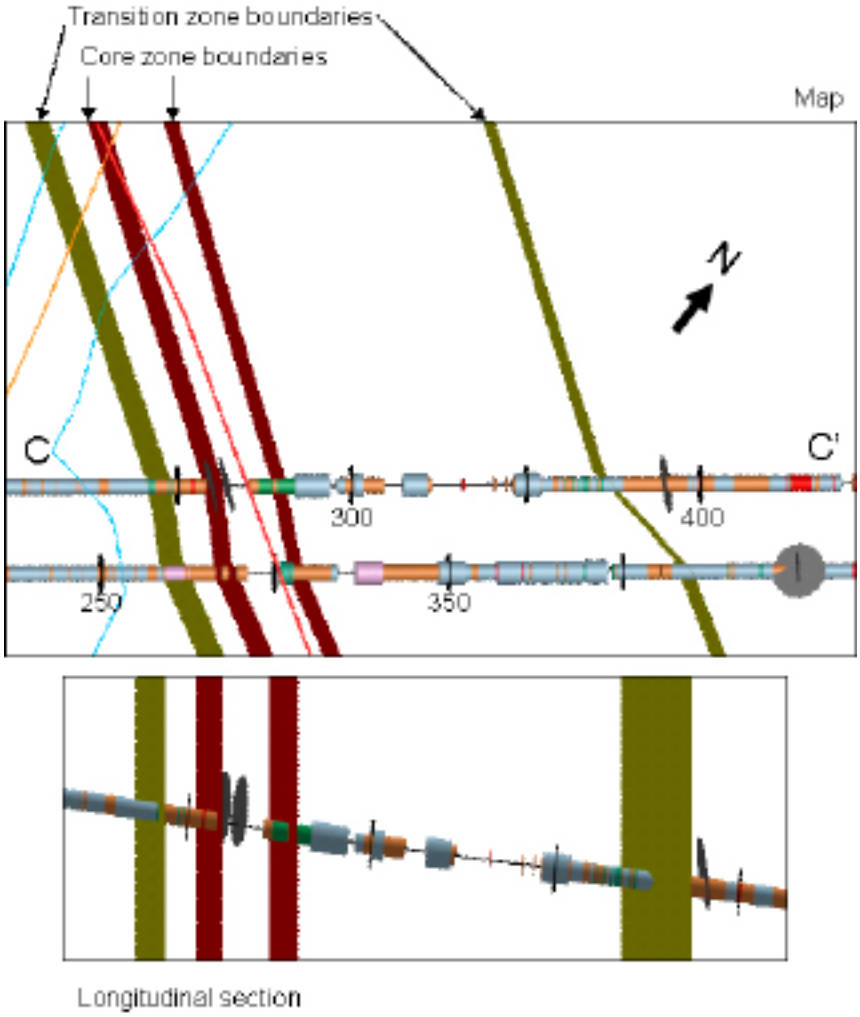

Figure 5-8. *Map and longitudinal section showing zoning of the Singö deformation zone at the intersection with the SFR twin tunnels. Numbers indicate SICADA/RVS sections. Red line indicates the centre line of the magnetic anomaly. Gray discs are major clay filled fractures.*

The strongest and most consistent seismic refraction low velocity zones over Tunnel 3 occur some 40 m NE of the core observation in the tunnel. Over Tunnel 1-2 and the SFR tunnels, the seismic low velocity zones are not consistent. For this reason, seismic low velocity zones have not been used as points in the RVS model.

The magnetic anomaly centre lineament fits fairly well with the modeled core centre, except for a SW bend when crossing Tunnel 3. At the model boundaries the modeled zone boundaries follow the strike of this lineament.

The SW and NE boundaries of the fractured and transition zones on either side of the core zone are modeled as vertical planes in the same way as the core.

6 Measured rock mass response in the Singö fault

6.1 Monitoring program

The monitoring program during excavation of the SFR tunnels included convergence measurements and extensometer measurements in three sections within the Singö fault /Carlsson et al. 1985/. Two monitoring sections were installed in the zone core, one in the operation tunnel (1/262)[2] and one in the construction tunnel (5/250). The third section (1/317) was located in the operation tunnel in the tabular sector. The locations of the monitoring sections in relation to the interpreted subdivision of the deformation zone are shown in Figure 6-1. The positions of convergence measurements and extensometers within the monitoring sections are presented in Figure 6-2.

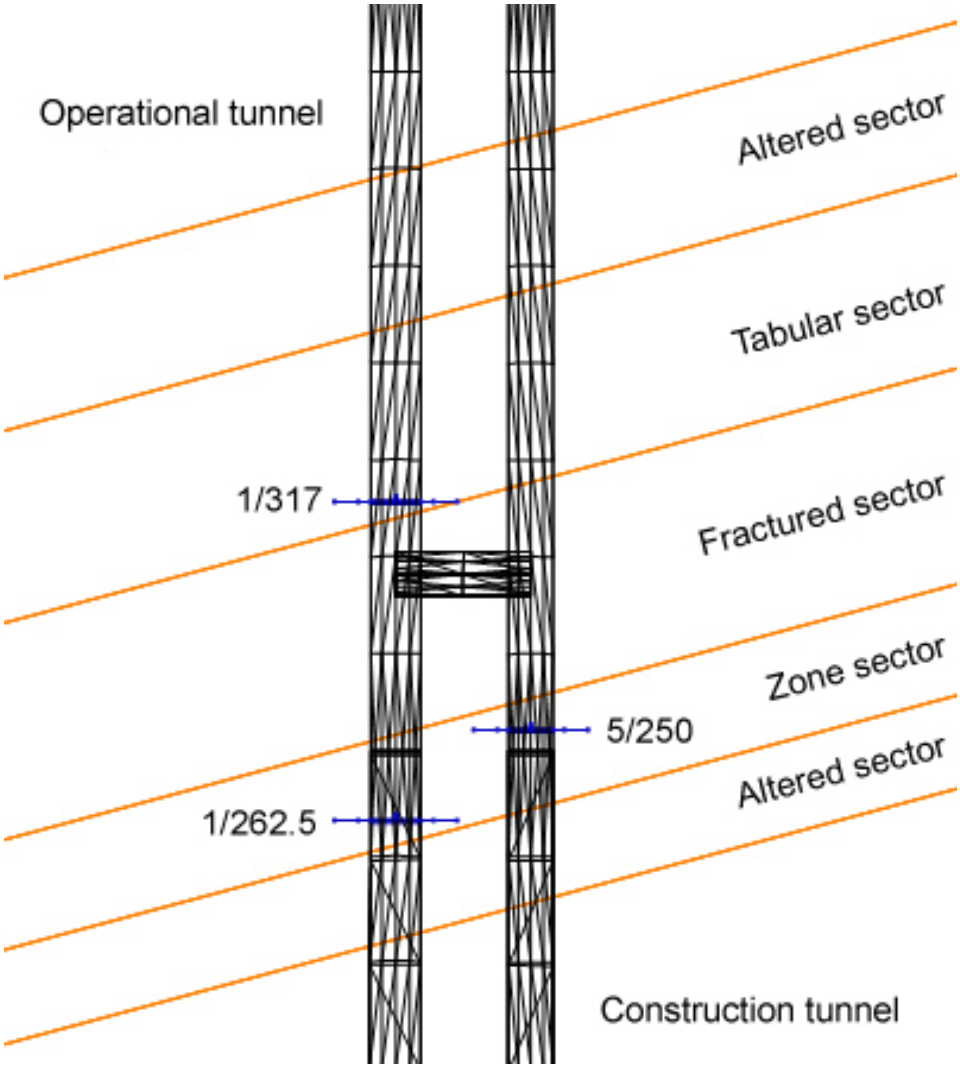

Figure 6-1. *Locations of the monitoring sections in relation to the adopted subdivision of the deformation zone.*

[2] The position of this monitoring section is differing somewhat between available sources, i.e. between 1/261.5 and 1/263. The section 1/262.5 is assumed to be the true position based on specified anchor coordinates on a hand drawing.

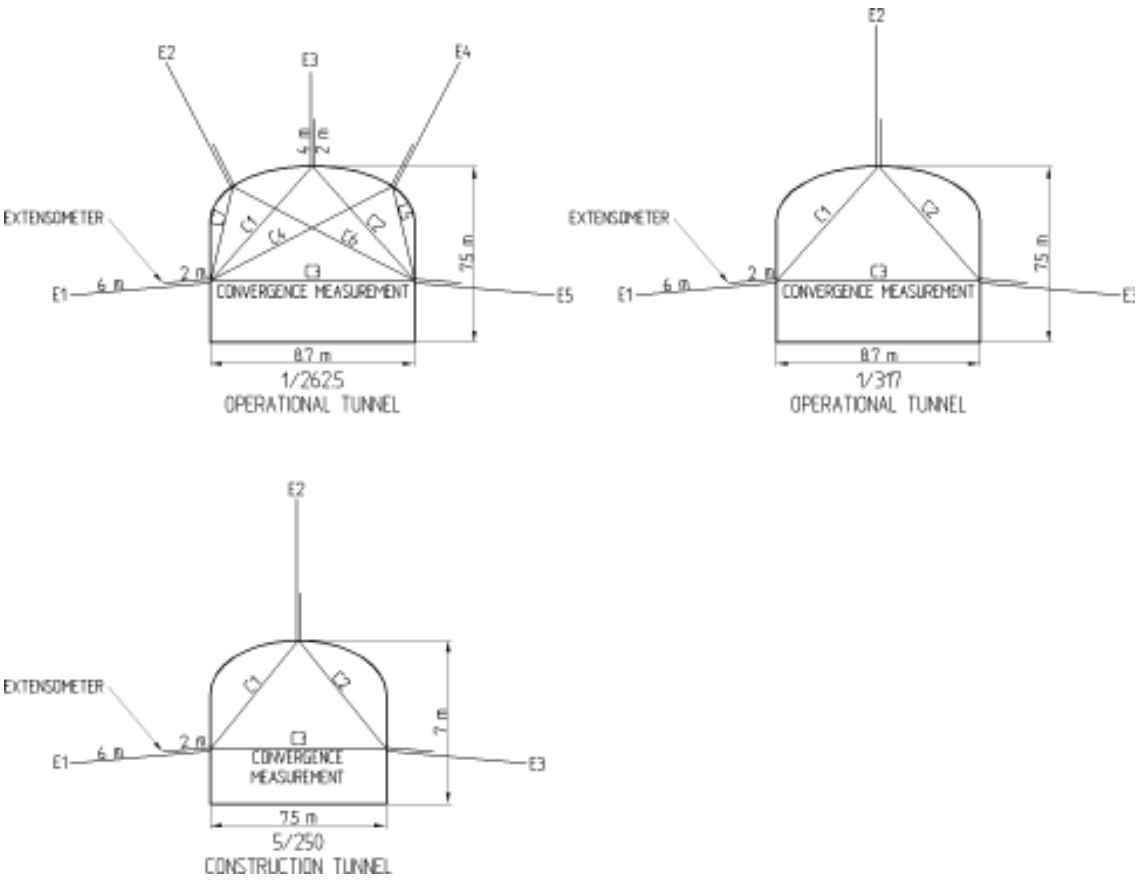

Figure 6-2. *Positioning of the convergence measurements and extensometers in the monitoring sections.*

Monitoring at section 1/262.5 in the operational tunnel comprised convergence measurements between five anchors, and deformation measurements with 2 m, 4 m and 6 m long extensometers installed at the same positions as the anchors. Monitoring at section 5/250 in the construction tunnel and at section 1/317 in the operational tunnel comprised convergence measurements between three anchors, and extensometer measurements at the same positions as the anchors.

The measurements were carried out manually. Readings were taken on daily basis following installation, and the monitoring frequency was later decreased to weekly and monthly as the response decreased. The monitoring was carried out for approximately two years at section 5/250, about one and half year at section 1/262.5, and approximately one year at section 1/317.

The convergence measurements were performed with a distometer and the extensometer measurements with a dial gauge. According to the instrument manufacturer the accuracy of the distometer is 1×10^{-6} of the recorded distance. This gives a value of approximately ± 0.01 mm for readings across the tunnels. The accuracy of the dial gauge is estimated to be within ± 0.05 mm.

The recorded response in the monitoring section is dependent on the location of the tunnel face when the initial reading is performed. Table 6-1 presents an estimation of the displacement that already had occurred in the tunnel at initial reading, based on a work by /Hanafy 1980/ and notes of the tunnel face position in the logbook of mapped geology. As shown in the table the displacement that has occurred at the time of the initial reading at section 1/262.5 and 5/250 is estimated to be 60% and at section 1/317 to 95% of the total movement. Thus, the recorded rock mass response independent of the rock quality is expected to be much less at section 1/317 than at the two other monitoring sections.

Table 6-1. Estimates of the displacements that had occurred prior to the initial readings, based on a work by /Hanafy 1980/ and notes of the tunnel face position in the logbook of mapped geology.

Monitoring Section	Position of face at initial reading	Distance between face and monitoring section (m)	Displacement prior to initial reading (%)
Operational tunnel			
Section 1/262.5	1/265	2.5	60
Section 1/317	1/329	12.0	95
Construction tunnel			
Section 5/250	5/252	2.0	60

6.2 Measured response at section 1/262.5

Measured convergence and deformation versus distance to tunnel face at section 1/262.5 is presented in Figure 6-3 and Figure 6-4. The results consistently display much smaller deformation of the roof than of the walls. The vertical deformation of the roof is less than 1 mm, while the horizontal deformation of the walls is 4–6 mm. The measured convergence horizontally across the tunnel reaches 8 mm. The total deformation in the 6 m long extensometers in the walls indicates approximately 2 mm larger convergence of the tunnel walls, than the convergence measurements.

The 2 m long extensometers indicate larger deformation in the outer wall (E1) than in the pillar wall (E5), while the 6 m long extensometer show contrary conditions. Furthermore, the relative deformation between the 2 m and 6 m long extensometers are small in the outer wall compared to the pillar wall.

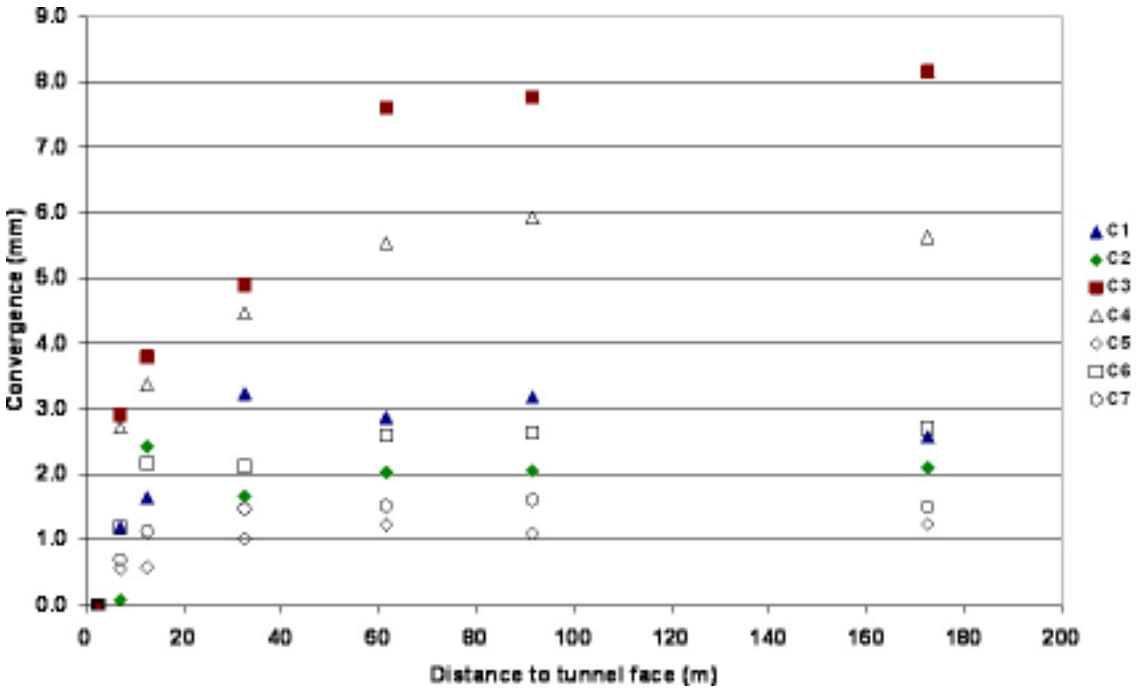

Figure 6-3. *Measured convergence versus distance to tunnel face at section 1/262.5 in the operational tunnel. It should be noted that the measured response is a function of the excavation of the construction tunnel as well.*

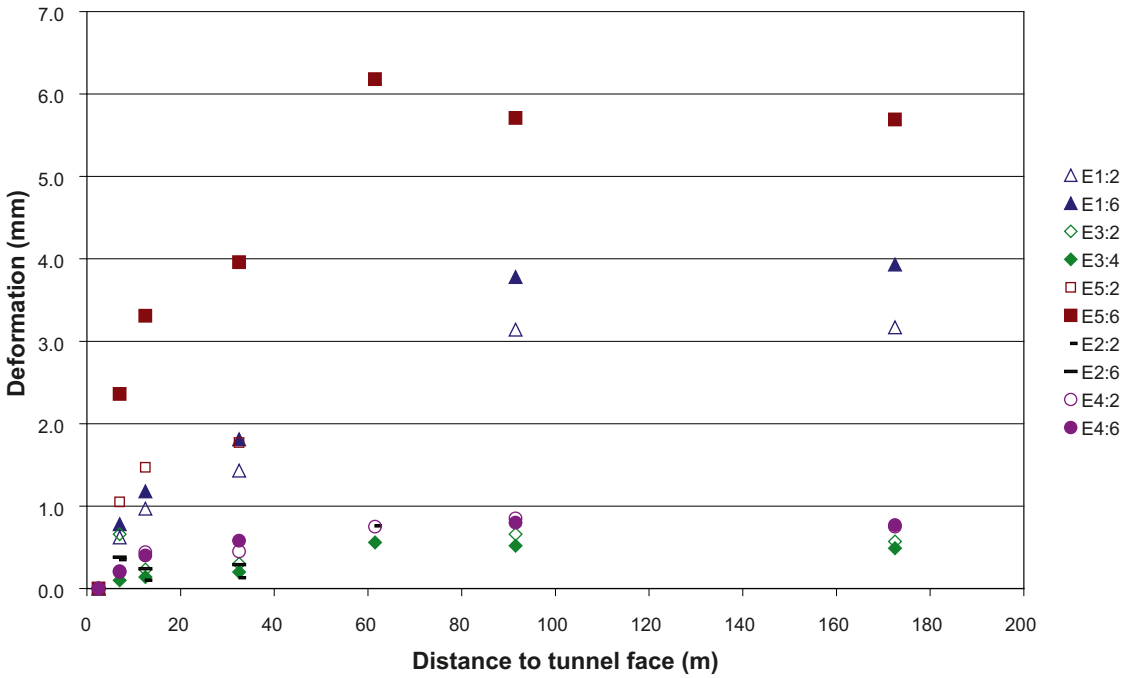

Figure 6-4. *Measured deformation in extensometers versus distance to tunnel face at section 1/262.5 in the operational tunnel. It should be noted that the measured response is a function of the excavation of the construction tunnel as well.*

6.3 Measured response at section 5/250

Measured convergence and deformation versus distance to tunnel face at section 5/250 is presented in Figure 6-5 and Figure 6-6. In this section, the recorded deformation of the roof is negligible compared to the deformation of the tunnel walls. Early in the monitoring period the convergence horizontally across the tunnel reaches approximately 7 mm after which it decreases to approximately 6 mm. The total deformation in the 6 m long extensometers in the walls corresponds well with the final convergence of the walls.

The extensometer measurements show larger deformation in the pillar wall than in the outer wall. Moreover, the relative deformation between the 2 m and 6 m long extensometers demonstrate that the deformation of the walls is mainly superficial.

6.4 Measured response at section 1/317

The measured convergence and deformation is much smaller in this section compared to the two previous sections, see Figure 6-7 and 6-8. This is also what one expects, independent of rock mass quality, since the initial reading was performed after the tunnel face had passed far ahead of the monitoring section, see Section 6.1. Due to the long distance to the tunnel face at the time when the monitoring was initiated, the results in this section also have less resolution than the results in the two previous sections.

The measured deformation in the roof, as in former sections, is small and insignificant. The convergence horizontally across the tunnel reaches a final value of 0.6 mm. This value agrees well with the total deformation recorded in the 6 m long extensometers in the walls.

The extensometer measurements show somewhat larger deformation in the outer wall than in the pillar wall.

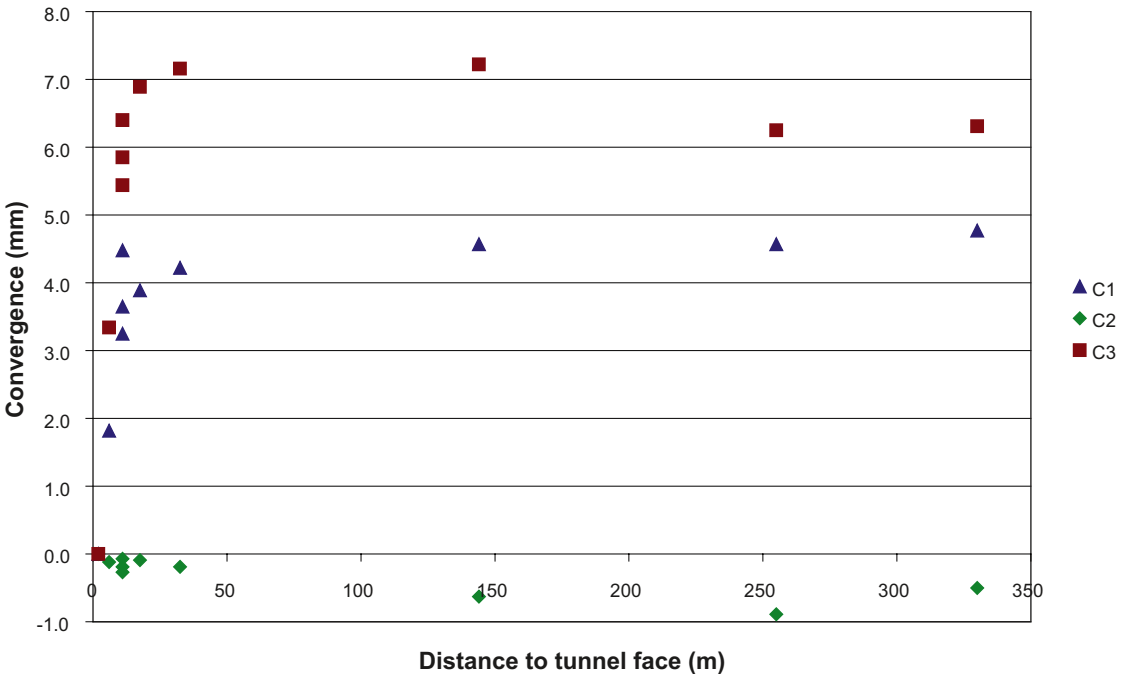

Figure 6-5. *Measured convergence versus distance to tunnel face at section 5/250 in the construction tunnel. It should be noted that the measured response is a function of the excavation of the operational tunnel as well.*

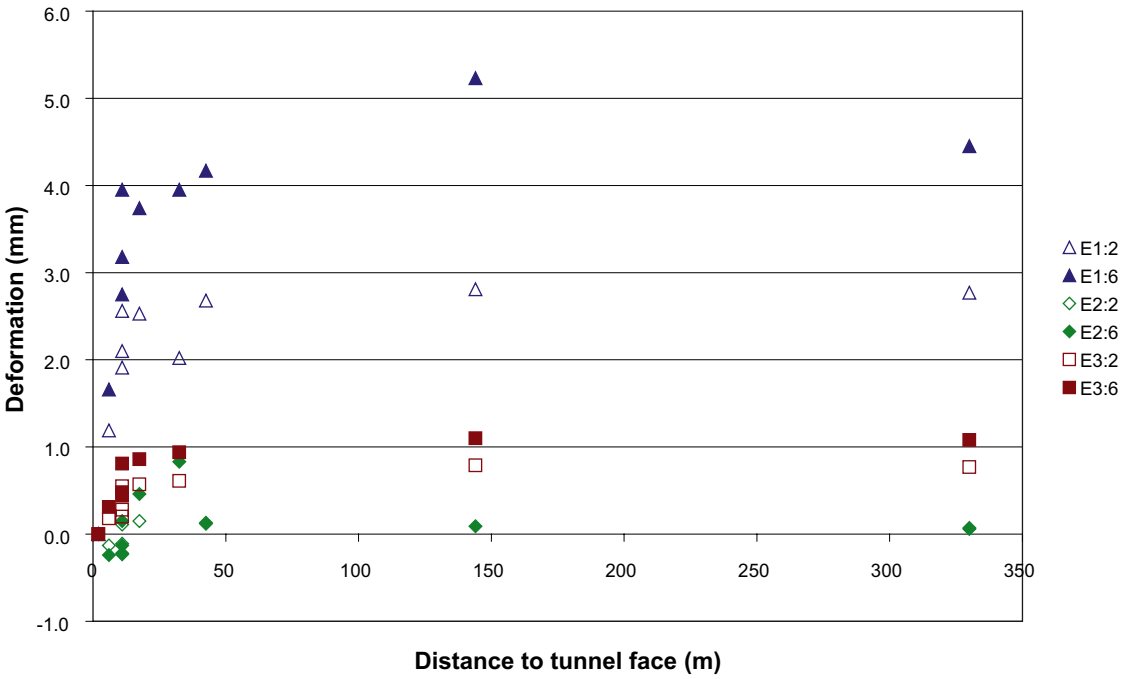

Figure 6-6. *Measured deformation in extensometers versus distance to tunnel face at section 5/250 in the construction tunnel. It should be noted that the measured response is a function of the excavation of the operational tunnel as well.*

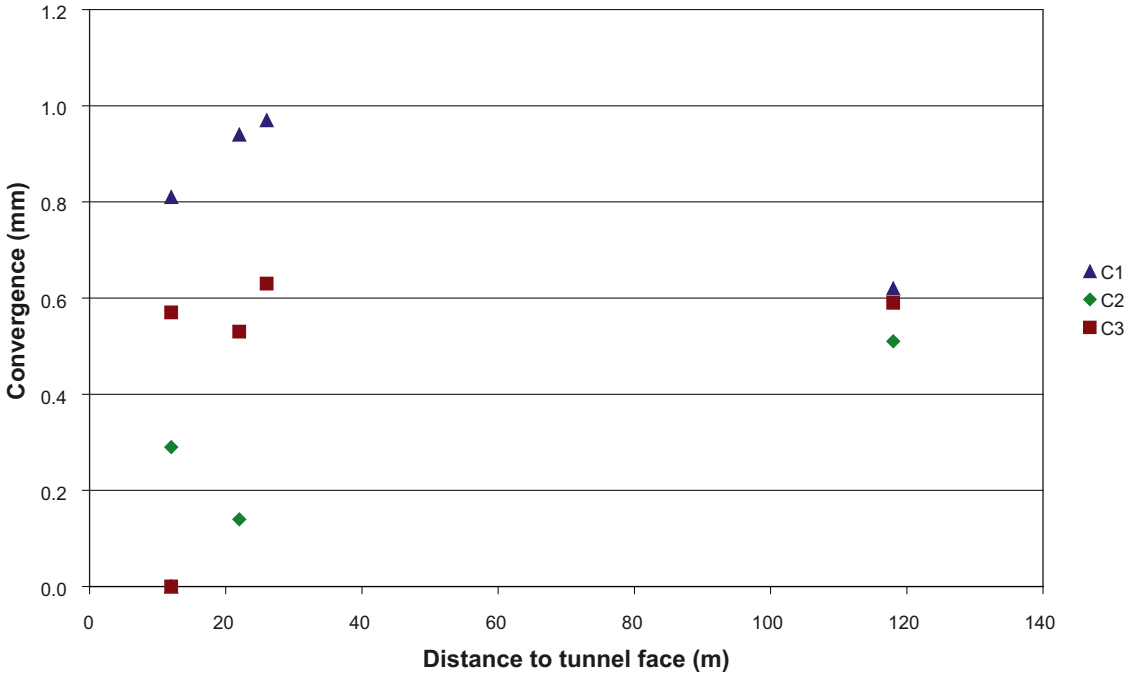

Figure 6-7. *Measured convergence versus distance to tunnel face at section 1/317 in the operational tunnel. It should be noted that the measured response is a function of the excavation of the construction tunnel as well.*

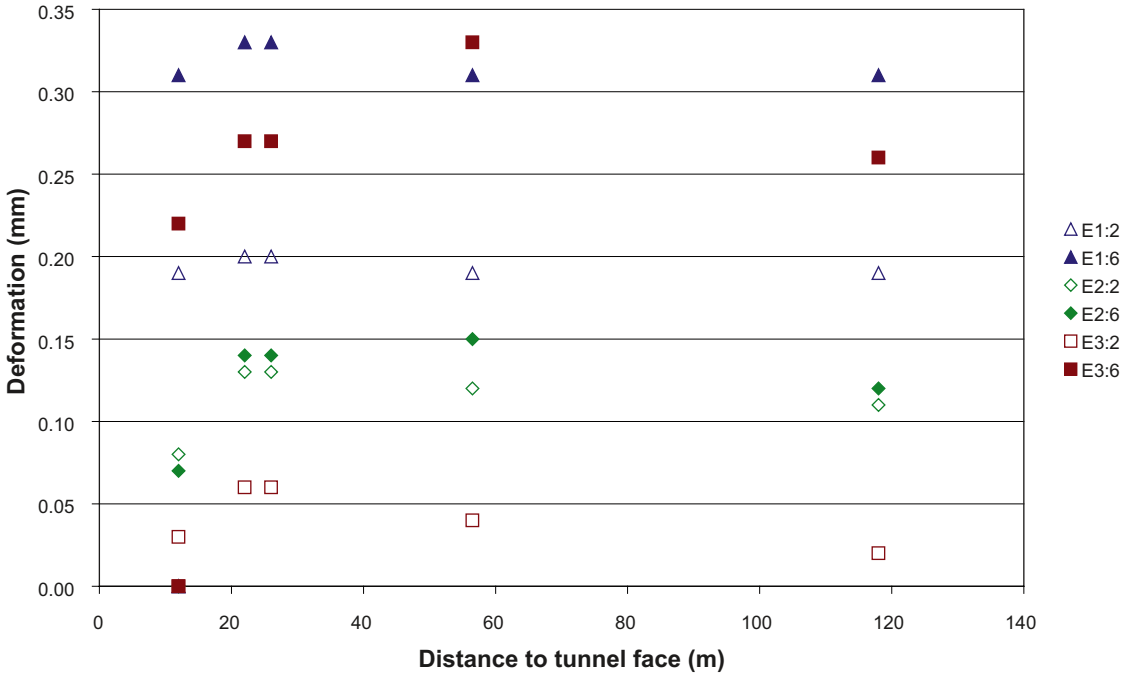

Figure 6-8. *Measured deformation in extensometers versus distance to tunnel face at section 1/317 in the operational tunnel. It should be noted that the measured response is a function of the excavation of the construction tunnel as well.*

7 Numerical modelling of equivalent properties for the different sub sectors of the deformation zone

7.1 Model description

The procedure used for the numerical simulation is the same as described in /Olofsson and Fredriksson 2005/, but has in this case been applied to large deformation zones. The approach is based on a discrete fracture network (DFN) description of the fractured rock mass system and on the results of mechanical testing of intact rock and on rock fractures. The 3D DFN representative of the site is simulated and 2D fracture trace planes are extracted to be used as input for 3DEC. In this project only vertical fracture trace planes perpendicular to the tunnels were simulated.

To estimate the mechanical properties of the rock mass a load test on a rock block with fractures was simulated with the numerical code 3DEC. Fracture network realizations were first generated with the numerical software FracMan, which were then transferred into the mechanical model. The rock block was loaded in plain strain condition. From the calculated relationship between stresses and deformations the mechanical properties of the rock mass were determined.

The model was loaded at three different confining stress levels, first to give an estimation of the rock mass parameters at different depths, and secondly to interpret the rock mass strength properties according to Hoek and Brown. The parameters are evaluated with the software RocData (Rocscience) using the results of the numerical tests at the three different levels of confining stress. The best fit for the rupture envelope is calculated and the Hoek and Brown parameters of the rock mass for a given uniaxial compressive strength are produced, see Figure 7-1.

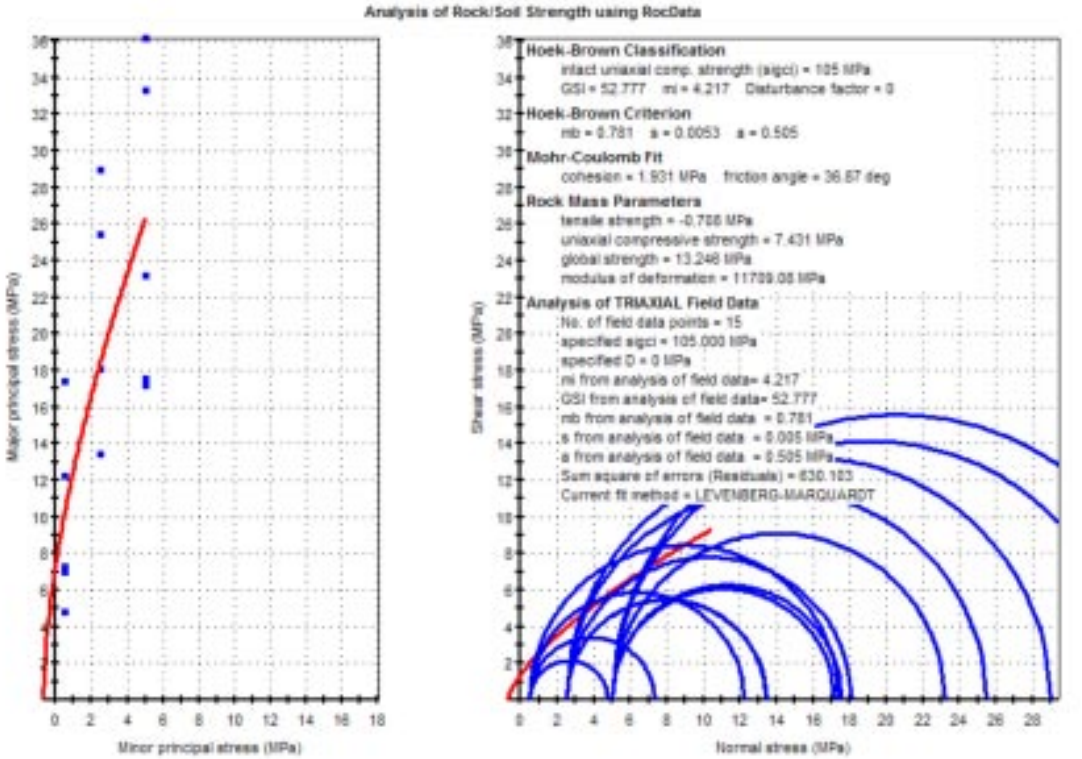

Figure 7-1. *Evaluation of the rock mass parameters within the zone core according to Hoek and Brown and using the software Rocdata /RocData User's Guide 2004/.*

The rock in and around the deformation zone was divided into three sub sectors, see Section 5.3, namely: host rock, transition zone and rock in the core of the zone. The impact of the fracture pattern has been studied in each sub sector by simulating and testing 5 realizations of the same DFN. Based on data given in Section 4 the fracture intensity, P_{10}, in the three sub sectors is estimated according to Table 7-1. The fractures in borehole DS101 and DS102 are not oriented therefore it is not possible to separate the fracture intensity, P_{10}, on fracture sets.

There are three main fracture sets in and around the zone, see Section 4.4.1. Two sets are sub-vertical striking NS and EW, and one sub-horizontal.

In the report entitled "Preliminary site description Forsmark area – version 1.2" /SKB 2005/ the parameters for the DFN model are given. The general DFN model for the Forsmark area consists of four sub-vertical sets and one sub horizontal set of fractures. The two sub-vertical sets around and in the Singö deformation zone are assumed to have the same properties as the NS-set and the EW-set in the general DFN model. The sub-horizontal set is assumed to have the same properties as the sub-horizontal set in the general DFN-model. The parameters for orientation and size distribution are summarized in Table 7-2 and Table 7-3.

Fracture networks with varying fracture intensity were generated and explored by simulated exploration boreholes parallel to the tunnels through Singö deformation zone. The volumetric fracture intensity, P_{32}, was varied until the P_{10} in the boreholes agreed with the values in Table 7-1. The variation of P_{32} for fracture set no. 3 did not influence the recorded P_{10} in the exploration boreholes parallel to the tunnels. The P_{32} for this fracture set was therefore set equal for all sub sectors. The final P_{32} values for the different fracture sets are given in Table 7-4.

Table 7-1. Fracture intensity, P_{10}.

Parameter	Host rock	Transition zone	Core of the zone
P10	5	14	25

Table 7-2. Input parameters for orientation /SKB 2005/.

Set nr	Probability distribution model	Mean Pole Trend/Plunge	Dispersion
Set no. 1	Bivariate Fisher	92.4/5.9	19.3, 19.7
Set no. 2	Fisher	190.4/0.7	30.6
Set no. 3	Fisher	342.9/80.3	8.2

Table 7-3. Input parameters for size distribution, median values /SKB 2005/.

Set nr	Probability distribution model	Exponent	Minimum radius (m)
Set no. 1	Power Law	2.88	0.28
Set no. 2	Power Law	2.95	0.15
Set no. 3	Power Law	2.92	0.25

Table 7-4. Input parameters for volumetric fracture intensity P_{32}.

Set nr	Host rock	Transition zone	Core of the zone
Set no. 1	3.0	8.0	17.2
Set no. 2	3.5	9.0	18.0
Set no. 3	3.5	3.5	3.5

7.2 Evaluated mechanical properties

Due to time and cost constraints only five DFN realizations were simulated for each sub sectors from the DFN properties defined in Table 7-2 (orientation sets), Table 7-3 (size distributions) and Table 7-4 (P_{32}). For the host rock the mechanical properties were evaluated for twenty DFN realizations as comparison.

Three different sets of input material parameters were applied to the three different sub sectors, see Table 7-5. The characteristics of the host rock refers to the mean values of the mechanical properties evaluated for intact rock and fractures in version 2.1 /SKB 2006/. There are no tests available from the intact rock, nor from the fractures in the sub sectors in the zone. The properties for these sub sectors have been estimated from values given in the literature and empirical experiences.

For the rock in the core of the zone the input properties of the intact rock were reduced. The Young's modulus, Ei, was estimated to 30 GPa and the uniaxial strength to 105 MPa /Jahanshahi and Vasseghi 1991/.

The properties of the fractures were estimated from /Boutard and Groth 1975/ and from /Barton 1974/ for clay filled discontinuities.

For the transition zone the properties are estimated to be between those for the host rock and the core of the zone.

The five DFN realizations for each of the sub sectors were analyzed at three different stress levels: 5 MPa (equivalent to the maximum principal stress σ_1), 2.5 and 0.5 MPa. The mechanical models were loaded with a constant velocity in the vertical direction while the horizontal stresses were constant during the loading test. The deformation modulus, E_m, the Poisson's ratio, ν_m, and the vertical stress of failure, σ_{vf}, were evaluated at the three stress levels to provide an estimation of cm and ϕ_m. The stress at failure is defined as the maximum vertical stress or the vertical stress at 0.010 vertical strain if the vertical stress-vertical strain curve does not show a marked maximum.

A summary of the distributions obtained for the rock mass deformation parameters, E_m and ν_m at the three stress levels is given in Table 7-6, Table 7-8 and Table 7-10 for the respective sub sectors. For the host rock the deformation parameters, E_m and ν_m were also evaluated for twenty DFN realizations as comparison. For the lower confining stress (0.5 MPa) twenty DFN-realizations gives a slightly lower mean value, see Table 7-6. For the numerical modelling of the deformations in the SFR tunnel passage (Section 8) therefore a deformation modulus of 45 GPa for the host rock was used.

The distributions obtained for the rock mass strength properties are presented in Table 7-7, Table 7-9 and Table 7-11. The variability of the parameters for one sub sector account only for the influence of the fracture pattern, the material input parameters are constant for each sub sector.

Table 7-5. Input parameters for intact rock and fracture properties.

	Parameter	Host rock	Transition zone	Core of the zone
Intact rock	Ei (GPa)	76	60	30
	vi	0.23	0.23	0.23
	ϕi (°)	60.5	40.0	40.0
	Ci (MPa)	27.7	23.3	23.3
	Ti (MPa)	13.5	6.8	6.8
Fractures	Kn (MPa/mm)	837.4	80.0	8.0
	Ks (MPa/mm)	30.6	2.0	0.2
	ϕf (°)	34.3	25.0	25.0
	Cf (MPa)	0.7	0.05	0.05

Table 7-6. Rock mass deformation properties of host rock.

Parameter	Mean	Std dev.	Min	Max
Em 5 MPa (GPa)	51.6	5.9	40.6	58.0
Em 5 MPa (GPa)*	51.9	6.3	40.6	61.9
vm 5 MPa	0.31	0.02	0.28	0.33
vm 5 MPa*	0.32	0.03	0.28	0.37
Em 2.5 MPa (GPa)	46.7	6.2	37.6	53.8
Em 2.5 MPa (GPa)*	46.7	6.8	35.6	64.0
vm 2.5 MPa	0.35	0.03	0.31	0.39
vm 2.5 MPa*	0.36	0.03	0.31	0.43
Em 0.5 MPa (GPa)	49.6	10.9	28.7	59.9
Em 0.5 MPa (GPa)*	43.5	11.3	22.3	59.9
vm 0.5 MPa	0.34	0.05	0.29	0.43
vm 0.5 MPa*	0.40	0.10	0.29	0.64

* Based on 20 realizations.

Table 7-7. Rock mass strength properties of host rock (interval 0.5–5 MPa).

Parameter		Mean
cm (MPa)	Mohr-Coulomb	4.0
ϕm (°)		65
σt (MPa)		–0.3

Table 7-8. Rock mass deformation properties of the transition zone.

Parameter	Mean	Std dev.	Min	Max
Em 5 MPa (GPa)	16.1	4.5	11.3	21.5
vm 5 MPa	0.43	0.01	0.41	0.45
Em 2.5 MPa (GPa)	17.1	4.5	12.5	22.0
vm 2.5 MPa	0.41	0.02	0.39	0.43
Em 0.5 MPa (GPa)	13.0	4.4	9.3	19.4
vm 0.5 MPa	0.49	0.03	0.47	0.55

Table 7-9. Rock mass strength properties of the transition zone (interval 0.5–5 MPa).

Parameter		Mean
cm (MPa)	Mohr-Coulomb	2.0
ϕm (°)		51
σt (MPa)		–0.1

Table 7-10. Rock mass deformation properties of the rock in the core of the zone.

Parameter	Mean	Std dev.	Min	Max
Em 5 MPa (GPa)	2.7	1.2	1.5	4.0
vm 5 MPa	0.43	0.01	0.42	0.45
Em 2.5 MPa (GPa)	2.5	1.1	1.5	3.7
vm 2.5 MPa	0.45	0.01	0.44	0.46
Em 0.5 MPa (GPa)	2.6	1.1	1.4	4.0
vm 0.5 MPa	0.46	0.01	0.46	0.48

Table 7-11. Rock mass strength properties of the rock in the core of the zone (interval 0.5–5 MPa).

Parameter		Mean
cm (MPa)	Mohr-Coulomb	2.0
ϕm (°)		37
σt (MPa)		–1.0

7.3 Verification of the numerical results

7.3.1 Comparison with the empirical model

The results from the rock block model were verified by comparison of the calculated equivalent properties with properties evaluated by the empirical model. The procedure outlined by /Hoek et al. 1995/ has been followed. The deformation modulus and the strength of the rock mass are estimated from the Geological Strength Index, GSI. /Bieniawski's 1976/ Rock Mass Rating, RMR_{76}, can be used to estimate the value of GSI. In Table 7-12 the estimation of GSI is presented for the sub sectors in the Singö deformation zone.

The rock mass properties have been estimated from GSI and by using the program RocLab version 1.021 from Rocscience Inc /RocLab User's Guide 2002/. The estimated values are shown in Table 7-13. The cohesion and friction angle are determined in the stress range 0–5 MPa.

In Figure 7-2 the deformation modulus estimated from GSI is compared with the values estimated from the numerical simulations. The estimations from GSI give a higher deformation modulus for the host rock and the transition zone than the numerical simulations. For the rock in the core of the zone they give comparable results.

In Figure 7-3 the strength properties estimated from GSI are compared with the values estimated from the numerical simulations. The strength is expressed as uniaxial strength, σ_m, for the rock mass calculated from the cohesion, c_m, and the friction angle, ϕ_m using the equation:

$$\sigma_m = 2 \cdot c_m \cdot \cos(\phi_m) / (1 - \sin(\phi_m))$$

The values estimated by the two methods compare rather well, see Figure 7-3.

Table 7-12. Estimating GSI from Bieniawski's Rock Mass Rating system.

	Rating 1 Strength	Rating 2 RQD	Rating 3 Spacing	Rating 4 Joint conditions	Rating 5 and 6	RMR76 or GSI
Host rock	15	15	20	25	10	85
Transition zone	7	8	10	6	10	41
Core of the zone	7	3	5	0	10	25

Table 7-13. Rock mass properties estimated from GSI.

	GSI	Deformation modulus, (GPa)	Cohesion, (MPa)	Friction angle, (degrees)	Tensile strength, (MPa)
Host rock	85	71.3	5.6	60.1	–1.15
Transition zone	41	43.4	2.0	49.9	–0.04
Core of the zone	25	1.05	1.5	48.7	–0.01

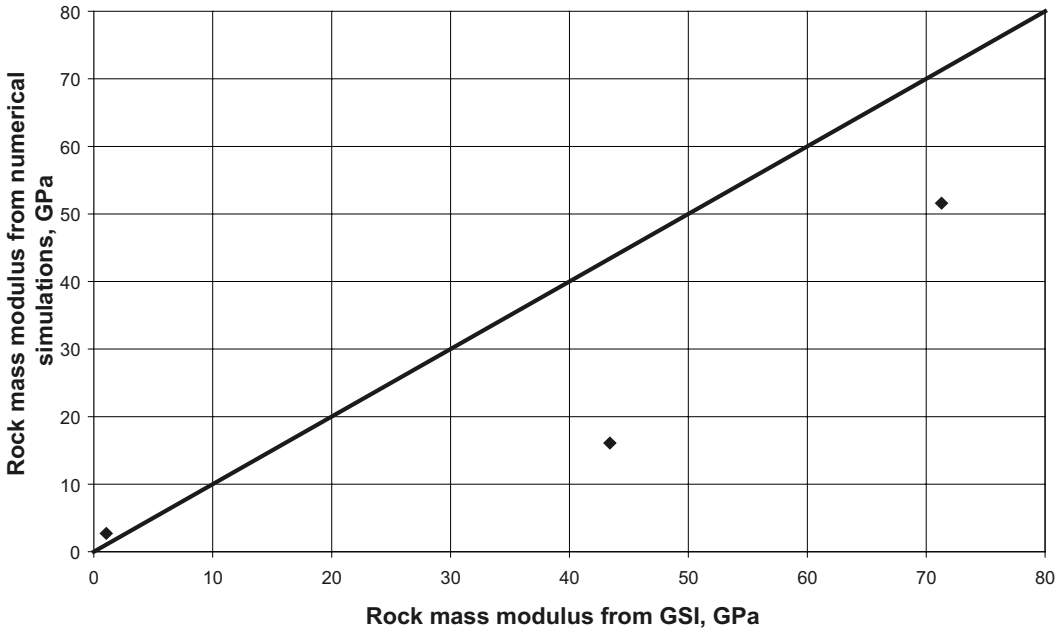

Figure 7-2. *Comparison between rock mass modulus estimated from GSI (line) and from numerical simulations (dots).*

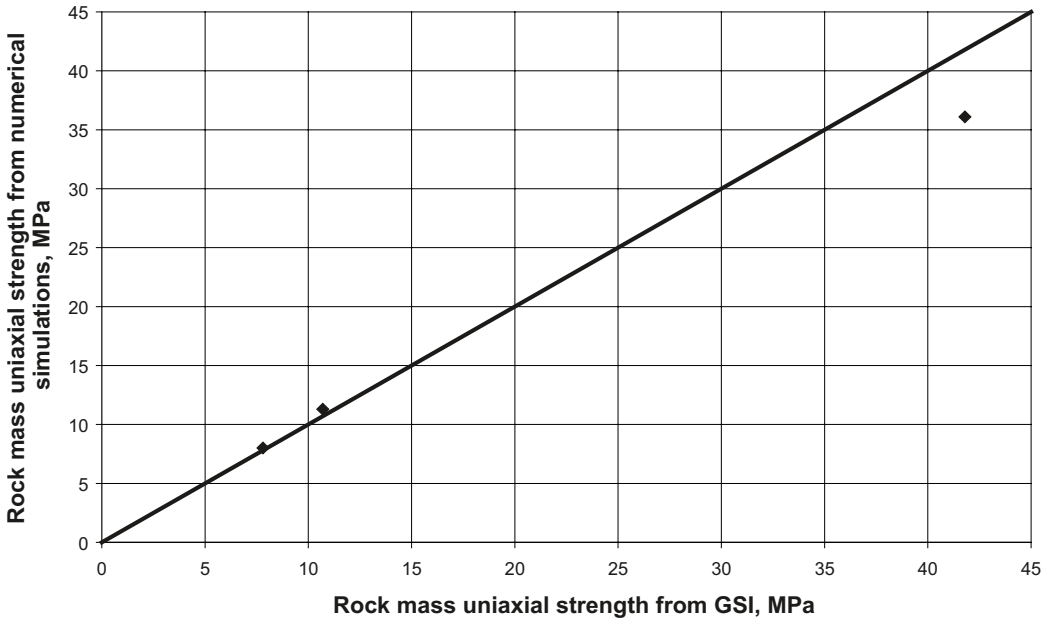

Figure 7-3. *Comparison between rock mass uniaxial strength estimated from GSI (line) and from numerical simulations (dots).*

7.3.2 Comparison with large-scale in situ load tests

The deformation modulus of the rock mass within the core of the zone has also been verified by comparison of the equivalent properties with records from in situ load tests. The plate load tests were performed in the bottom of the operational tunnel in section 1/254 to 1/257 /Jahanshahi and Vasseghi 1991/. The plate diametre was 0.5 m and the load from the hydraulic jack was transferred to the rock via a rock anchor in the centre of the plate. The mean value of the recorded deformation modulus of the rock mass was evaluated to 1.3 GPa from the in situ load tests. The corresponding value from the numerical simulations is 2.7 GPa. Thus, the numerical simulations result in a slightly higher modulus of the core than the in situ load tests.

8 Numerical modelling of deformations in the SFR-tunnel passage

The model presented here was used to estimate the rock mass response in the SFR-tunnel passage through the Singö fault. The numerical calculations were performed using a model created in 3DEC. The program is a three dimensional distinct element code based on the finite difference method /3DEC 2003/.

8.1 Description of the model

8.1.1 Geometry

Figure 8-1 shows the geometry of the model used. The size of the model is 250×250×100 m. The coordinate system is arranged in a manner such that the x-axis is perpendicular to the tunnel axis, the y-axis parallel to the tunnel axis and the z-axis upwards. The north direction in the model is directed approximately 50 degrees west from the y-axis.

The lower boundary of the model was located at level +395 and the ground surface or sea bottom at +495. The ground surface is assumed to be flat in the model. This simplification is feasible since results from refraction seismic in the area close to the tunnels indicate a level difference within 2 m /SKB 2005/ p. 161.

Based on the compiled geological information (Table 4-9, Section 4.5.2) the Singö fault is divided into five sectors, marked as color bands in the model view in Figure 8-1. The sectors are assumed to be parallel to each other. The angle between the tunnel axis and the strike of the sectors is 75 degrees in the model.

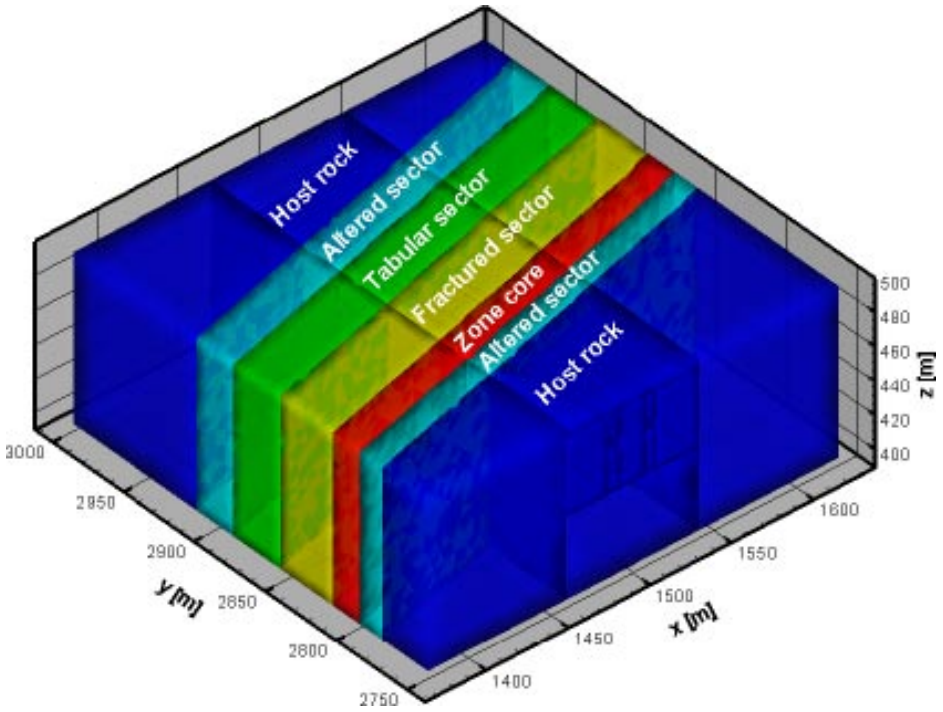

Figure 8-1. *Geometry of the numerical model.*

A more detailed picture of the fault sector division in a horizontal cross section is presented in Figure 8-2. Along the y-axis in a positive direction the fault is composed of an altered sector, a core, a fractured sector, a tabular sector and finally another altered sector. The length of each sector along the tunnel axis and the width normal to the fault strike direction is presented in Table 8-1. The total width of the fault is assumed to be approximately 130 m in the model.

The access tunnels are modeled with their theoretical cross-sectional areas of 65 m^2 for the operational tunnel and 49 m^2 for the construction tunnel. The cross-sectional area corresponds to a width of 8.7 m and height of 7.5 m for the operational tunnel and a width of 7.5 m and height of 7.0 m for the construction tunnel. The distance between the tunnels is 15 m.

A horizontal section through the generated mesh is presented in Figure 8-3. The mesh is based on tetrahedral zones. This type of zone element is not the most appropriate for plasticity problems as simulated here. High order zones with an extra grid point added to the centre of each zone edge or six-sided polyhedral zones normally give more accurate solutions for plasticity problems /3DEC 2003/. However, mesh generation with high order zones was not possible in this model due to shape restrictions.

Table 8-1. Length of each sector along the tunnel axis and width normal to the fault strike direction.

Sectors	Length along the tunnel axis (m)	Width normal to the fault strike direction (m)
Altered sector	16.0	15.5
Zone core	19.0	18.5
Fractured sector	37.0	36.0
Tabular sector	33.0	32.0
Altered sector	26.0	25.5
Total width	131.0	127.5

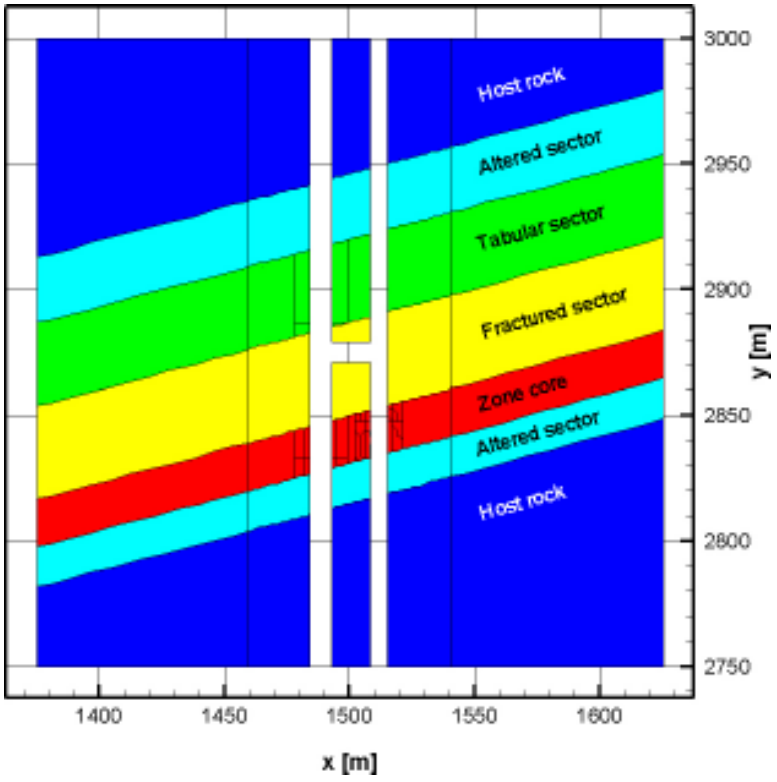

Figure 8-2. *Geometry of the Singö fault with assumed sector division.*

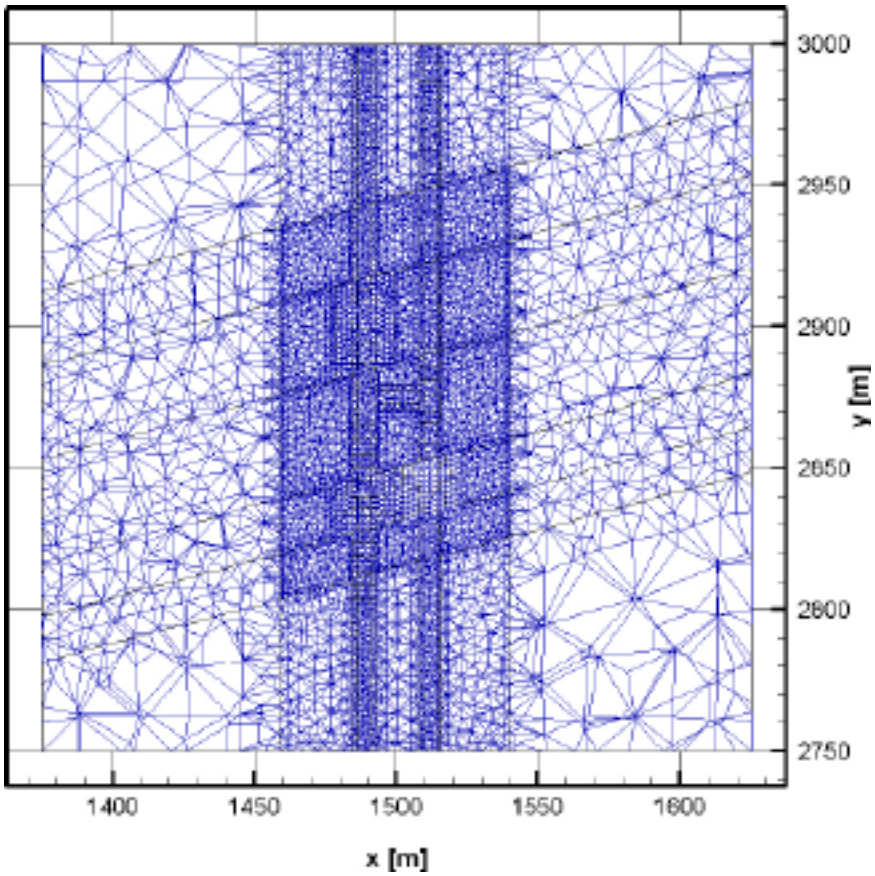

Figure 8-3. *Horizontal section through the generated mesh.*

8.1.2 In situ stress and boundary conditions

The in situ stress conditions adopted in the model are given in Table 8-2. The assigned in situ stresses in the model are based on SDM v1.1 /SKB 2004/. The stress components used should be valid also at the shallow depths, approximately 50 m below the seabed, where SFR is located. The stress components presented in SDM v1.2 /SKB 2005/ were not chosen for this model as they are valid for depths between 350 and 650 m. Calculated in situ stresses at the top, the mid height and the bottom of the model are presented in Table 8-3.

The stress field in the model is arranged such that the major horizontal stress is directed perpendicular to the tunnel axis and the minor horizontal stress parallel to it. This corresponds approximately to an orientation of the major horizontal stress of N140 degrees. The assumed orientation is in accordance with the average trend for the major stress component (σ_H) in SDM v1.2 /SKB 2005/.

The boundary conditions assumed in the model are given in Table 8-5. The lateral and lower boundaries are fixed in the normal direction. The ground surface is free to move.

Table 8-2. Adopted stress field in the model /SKB 2004/.

	Symbol	Value	Unit
Major horizontal stress component	σH	4+0.09z	MPa
Minor horizontal stress component	σh	1.4+0.028z	MPa
Vertical stress component	σV	0.027z	MPa

Table 8-3. Comparison between measured in situ stress magnitude and calculated magnitude in the model below the operational tunnel in section 1/177 /SKB 2005/.

	Measured magnitudes[1,2]	Calculated magnitudes	Unit
Major horizontal stress component	3.6–11.5 (7.7)	7.8	MPa
Minor horizontal stress component	0.1–7.3 (3.6)	2.6	MPa

[1)] The measured magnitudes are presented with a range and a mean value in brackets.

[2)] The measurements were performed at two levels 11 m and 16 m below the tunnel bottom.

Table 8-4. Calculated stress at the top, the mid level and the bottom of the model.

Depth (m)	Level	σH (MPa)	σh (MPa)	σV (MPa)
0	+495	4.0	1.4	0
50	+445	8.5	2.8	1.35
100	+395	13.0	4.2	2.7

Table 8-5. Boundary conditions.

Boundary	Condition
Ground surface	Free
Lateral boundaries	Fixed in normal direction
Lower boundary	Fixed in normal direction

8.1.3 Rock mass properties

The rock mass response was assumed to be ideally elasto-plastic. The yield function used in the model is the Mohr-Coulomb failure criterion. The joints included in the model are construction joints used for creation of the model geometry and for assignment of anchor position in modeled instrumented section. These joints are locked and do not influence the calculation.

The rock mass properties evaluated were based on the theoretical model (Section 7) and used in the initial calculation are listed in Table 8-6.

Table 8-6. Rock mass properties used in the initial calculation.

	Host rock	Altered sector	Tabular sector	Fractured sector	Zone core
Young's modulus (GPa)	45	16	16	16	2.7
Poisson's ratio[1]	0.36	0.43	0.43	0.43	0.43
Tensile strength (MPa)	–0.3	–0.1	–0.1	–0.1	–1.0
Cohesion (MPa)	4.0	2.0	2.0	2.0	2.0
Friction angle[1] (MPa)	65	51	51	51	37

[1)] The dilation angle is included in Poisson's ratio and the friction angle.

8.1.4 Steps in the modelling path

The sequence of the calculation steps in the modelling is given in Table 8-7. Initial equilibrium conditions in the model are established in the first step (A) and the resulting displacements are reset to zero following this step. In the second step (B) the tunnels are excavated from the model boundary to a position where the tunnel faces were located several excavation rounds before the monitoring section was reached in the construction tunnel. The next step (C) simulates tunnel excavation which passes monitoring sections. Step D simulates large excavation including several rounds. Step (E) is similar to Step (C) in that it simulates passage of monitoring sections. In the final step the tunnels are excavated to the boundary of the model to reach a definite deformation in the monitoring sections (F).

The excavation rounds included in the simulation are presented in Figure 8-4. The date and location of the tunnel face at initial readings in the monitoring sections are marked with arrows in the diagram.

Table 8-7. Steps in the modelling path.

Step	Comments
A In situ conditions	Setting of initial equilibrium conditions
B Initial excavations of the tunnel	Operational tunnel: length 54.0 m Construction tunnel: length 92.5 m
C Excavation of the tunnel in rounds	Operational tunnel: 1/238–1/295, 14 rounds Construction tunnel: 5/248–5/292.5, 11 rounds
D Large excavation including several rounds	Operational tunnel: length 29.0 m Construction tunnel: length 68.5 m
E Excavation of the tunnel in rounds	Operational tunnel: 1/324–1/343, 4 rounds Construction tunnel: 5/364–5/389, 4 rounds
F Final excavation of the tunnel	Operational tunnel: length 87.0 m Construction tunnel: length 13.5 m

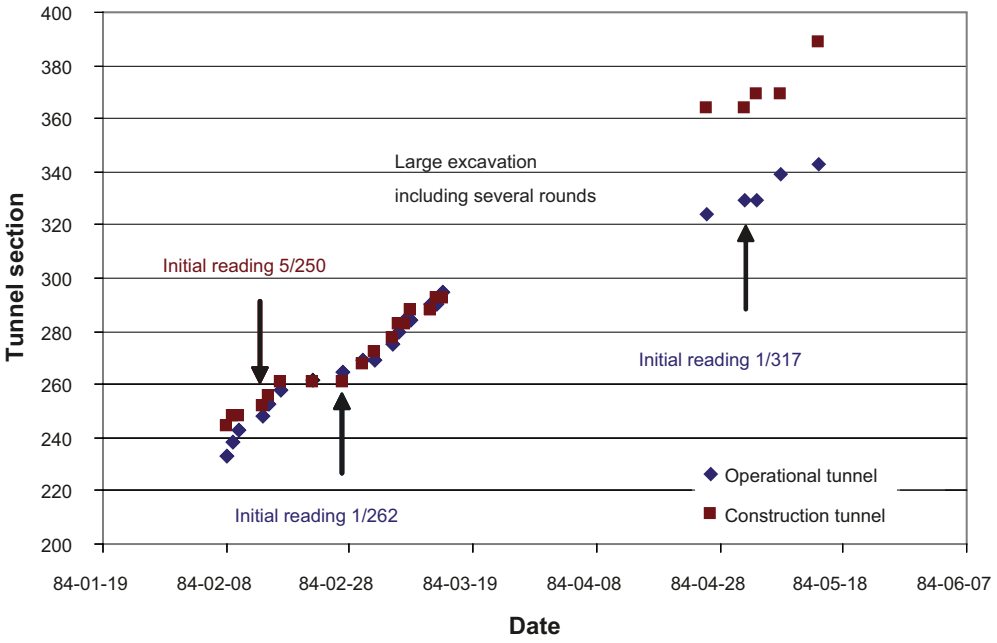

Figure 8-4. *Excavation rounds included in the simulation. The date and location of the tunnel face at initial reading in the monitoring sections are marked with arrows.*

The rock support in the tunnels, which consists of shotecrete and rock bolts, was not included in the modelling. Based on characteristics for different support systems in /Hoek et al. 1995/ and the information provided in Section 4.6 the supporting pressure that have been neglected in the analysis are in the range of approximately 0.2–0.4 MPa.

8.2 Results

In this section, the modelling results from the initial calculation are presented. The results, presented as stresses and displacements, are shown in a large-scale in a sloping plane with the same gradient as the access tunnels, and in a small-scale for each monitoring section.

8.2.1 Stresses in the rock mass

The magnitude of the major principal stress after final excavation of the access tunnel is presented in Figures 8-5 to 8-8.

A clear anomaly in the stress field around the tunnels can be observed in the core of the zone, see Figure 8-5. Compared to the stress magnitude within adjacent zone sectors, the magnitude in the core is somewhat lower. The reason is most likely due to the fact that more yielding has taken place in the core than in the nearby zone sectors. Both shear and tensile yielding are observed in the model, although yielding in shear is observed only close to the tunnel periphery.

The calculated magnitude of the major principal stress in the monitoring sections, Figure 8-6 to 8-8, is 1–2 MPa in the vicinity of the tunnel wall and 10–12 MPa close to the tunnel roof. Local stress concentrations occur in the corners of the tunnel floor.

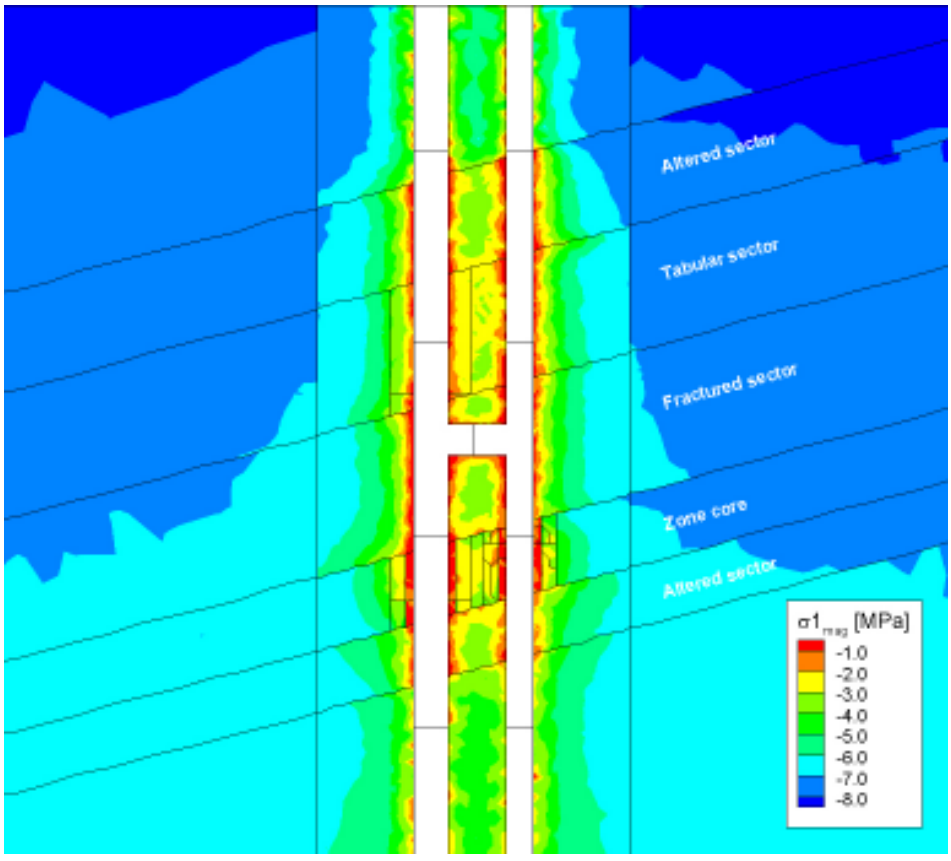

Figure 8-5. *Magnitude of the major principal stress in a sloping plane with the same gradient as the access tunnels.*

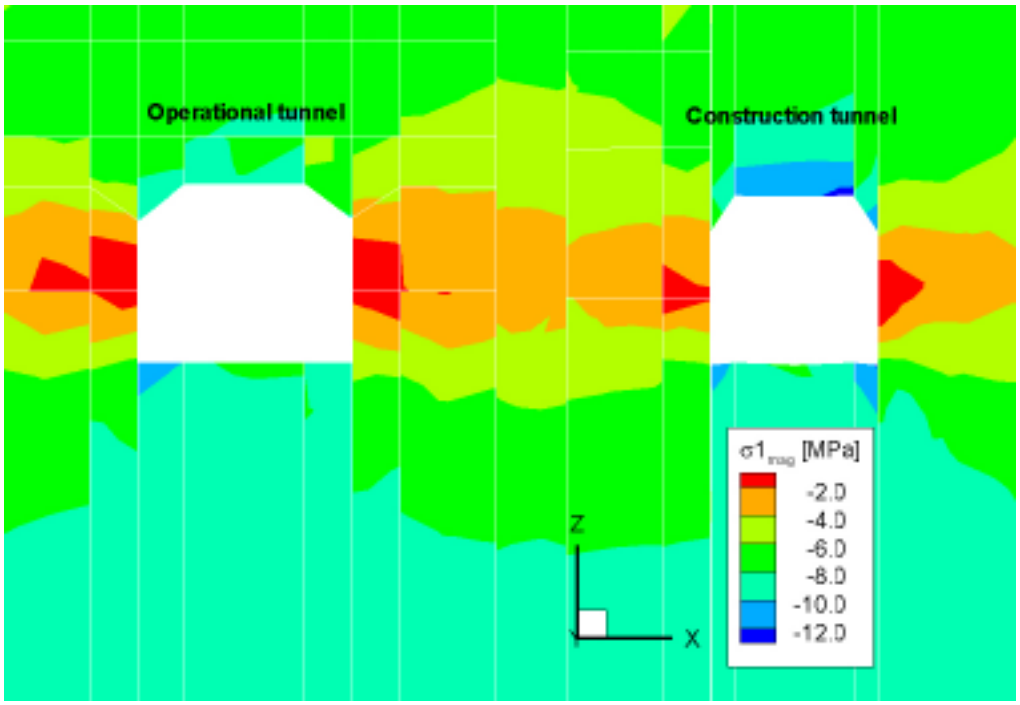

Figure 8-6. *Magnitude of the major principal stress in a vertical plane at section 1/262.5 of the operational tunnel.*

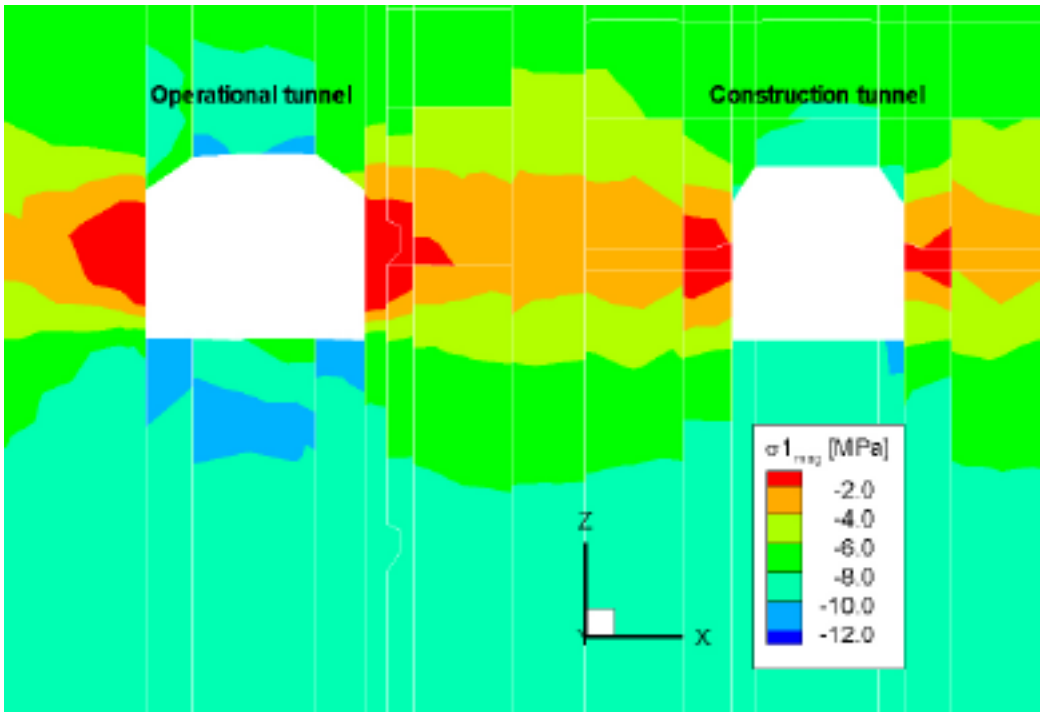

Figure 8-7. *Magnitude of the major principal stress in a vertical plane at section 5/250 of the construction tunnel.*

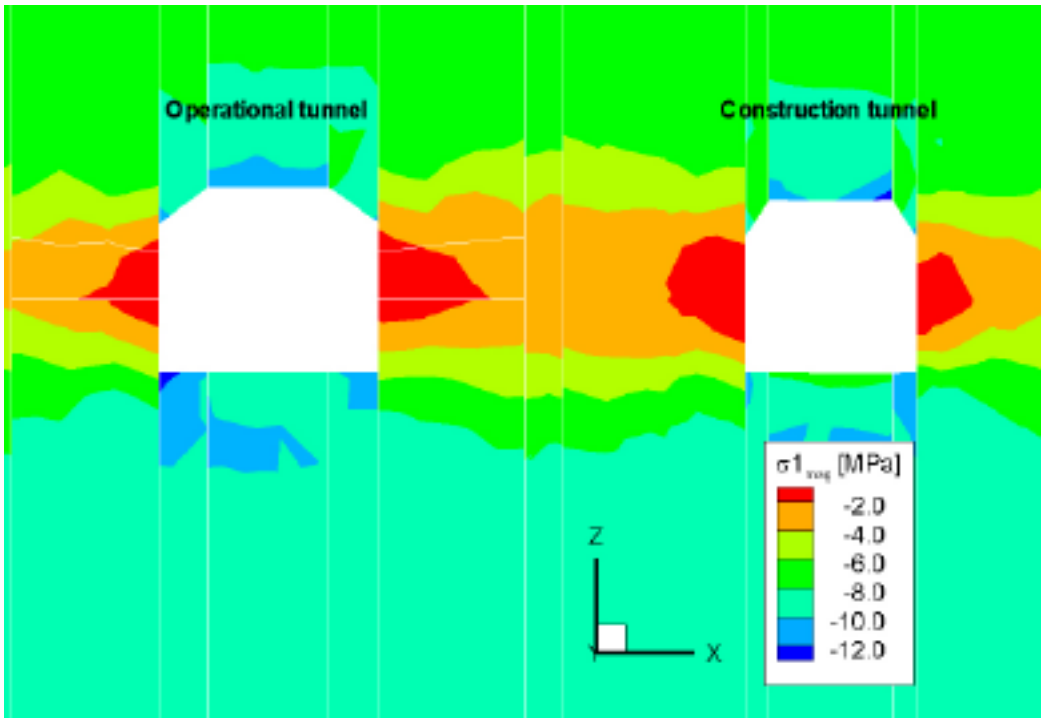

Figure 8-8. *Magnitude of the major principal stress in a vertical plane at section 1/317 of the operational tunnel.*

The in situ stress magnitudes in the model were compared with in situ stress measurements in the operational tunnel at section 1/177 in the vicinity of the Singö fault /SKB 2005/. The calculated in situ stresses in the model are comparable with the measured magnitudes at the corresponding locations at a depth of approximately 15 m below the tunnel floor. Furthermore, the model display that the tunnel excavation has an insignificant influence on the measured magnitudes. This is of importance since the measurements were performed at some distance behind the tunnel face.

8.2.2 Tunnel displacements

Plots showing the calculated displacements after final excavation of the access tunnels are presented in Figures 8-9 to 8-12. The calculated displacements at initial reading and final reading are presented in Table 8-8.

The displacements after final excavation of the access tunnels were approximately 30 mm in the core and 15 mm in the adjacent zone sectors, see Figure 8-9. The larger displacements calculated by the model do not coincide with the monitoring section.

The calculated displacements in the tunnel roof at the monitoring section are small in all three sections, see Figure 8-10 to 8-12. The calculated response in the roof during the monitoring period is less than 1 mm, see Table 8-8.

The calculated displacements in the walls are in the range of 15–20 mm at section 1/262.5, in the range of 10–15 mm at section 5/250 and in the range of 5 to 10 mm at section 1/317. The corresponding convergence of the walls during the monitoring period is for section 1/262.5 calculated to be 10.7 mm, for section 5/250 to 8.1 mm and for section 1/317 to 0.4 mm, see Table 8-8.

The displacements after the final excavation of the tunnels are generally less in the pillar wall than in the outer wall, see Figure 8-10 to 8-12. In section 5/250, the pillar wall remains essentially unaffected between initial and final reading.

Table 8-8. Calculated displacement on the tunnel perimeter at initial and final reading for each monitoring section.

	Left wall (mm)	Roof (mm)	Right wall (mm)
Section 1/262.5			
Initial reading (mm)	12.6	–1.6	–9.1
Final reading (mm)	18.8	–2.0	–13.6
Difference (mm)	6.2	–0.4	–4.5
Percentage initial/final reading	67.0	80.0	66.9
Section 5/250			
Initial reading (mm)	9.2	–0.9	–8.5
Final reading (mm)	10.8	–1.2	–15.0
Difference (mm)	1.6	–0.3	–6.5
Percentage initial/final reading	85.2	75.0	56.7
Section 1/317			
Initial reading (mm)	10.0	–0.10	–4.3
Final reading (mm)	10.3	–0.05	–4.4
Difference (mm)	0.3	0.05	–0.1
Percentage initial/final reading	97.1	–	97.7

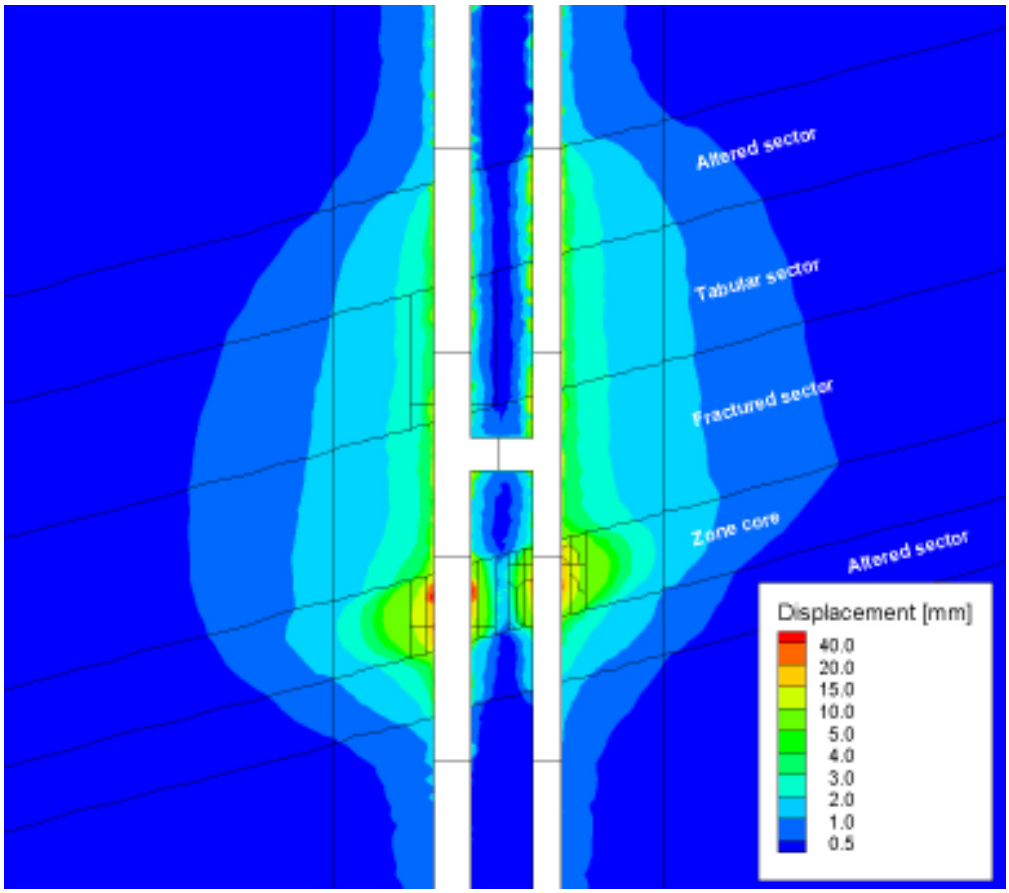

Figure 8-9. *Calculated displacements in a sloping plane with the same gradient as the access tunnels.*

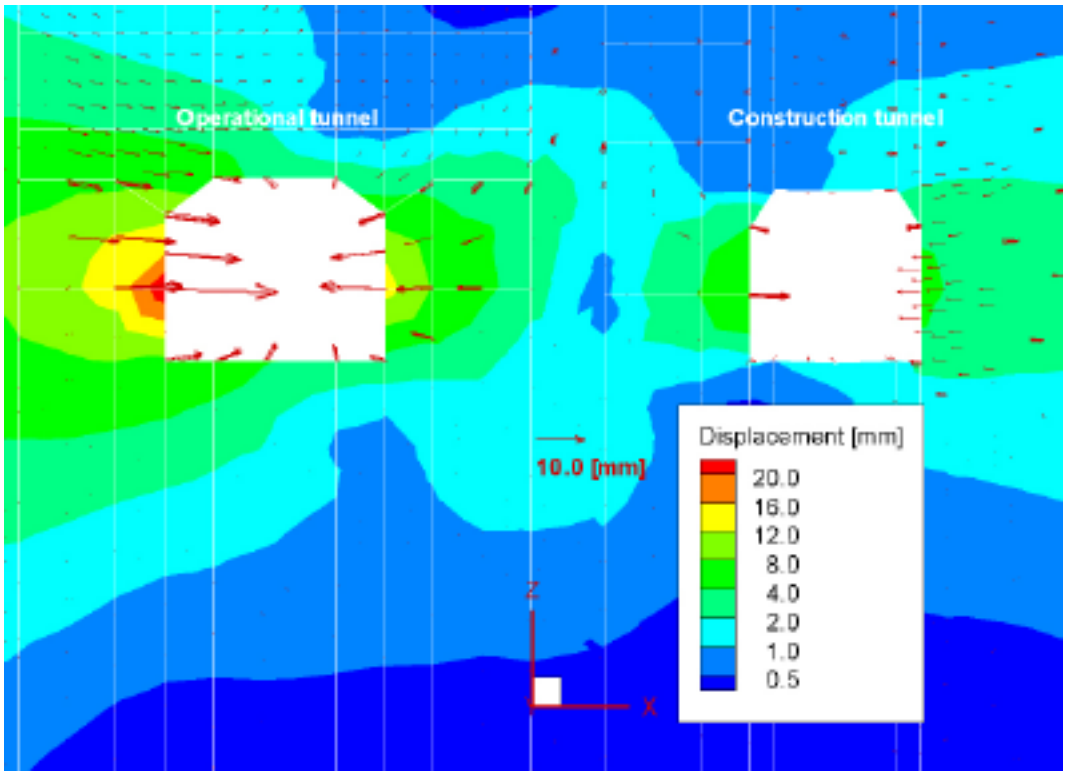

Figure 8-10. *Calculated displacements in a vertical plane at section 1/262.5 of the operational tunnel.*

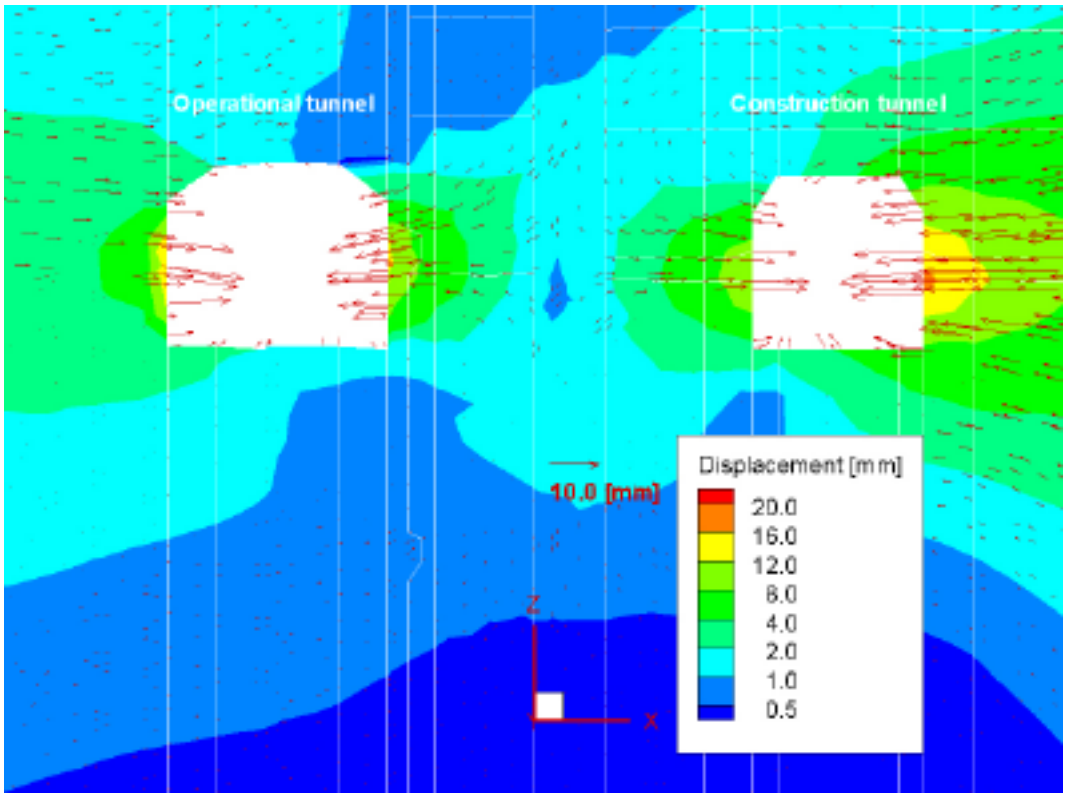

Figure 8-11. *Calculated displacements in a vertical plane at section 5/250 of the construction tunnel.*

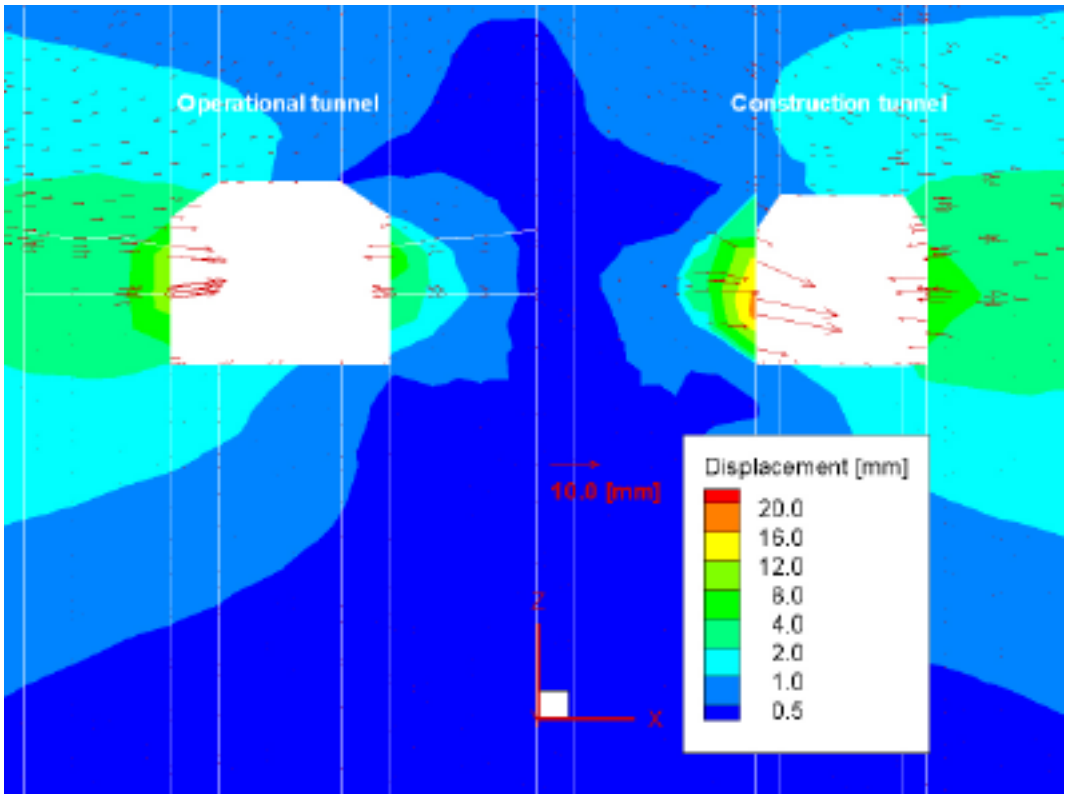

Figure 8-12. *Calculated displacements in a vertical plane at section 1/317 of the operational tunnel.*

The calculated displacements that had occurred at the time of the initial reading are in the range of 67% to 80% of the total displacement in section 1/262.5, in the range of 57% to 85% at section 5/250 and around 97% at section 1/317, see Table 8-8. Thus, the simulation indicates, as pointed out previously in Section 6.1, that the initial reading in monitoring section 1/317 in reality is performed too late for obtaining a good resolution in the measurements.

9 Comparison between calculated and measured rock mass response

To verify the numerical model, the calculated rock mass response and the measured deformations have been compared. A comparison between the results from the initial calculation and the measured deformations are presented in Table 9-1.

The comparison shows varying relationships between the calculated and measured rock mass response. The calculated response is smaller in some locations and larger in others. However, from a general point of view, the agreement between calculated and measured response is considered to be relatively good. This is particularly true in the roof where the difference is within 0.3 mm.

At monitoring section 1/262.5 the calculated deformation of the tunnel walls is consistently smaller than the measured deformation. The difference is about 1 mm with the exception of the long extensometer in the right wall (E5:6), where the difference is almost to 4.0 mm. The convergence measurements in section 1/262.5 show the opposite relation. The calculated response is between 1.5–2.5 mm greater than the measured.

At monitoring section 5/250 the calculated deformation in the tunnel walls is greater than the measured except for the short extensometer in the left wall (E1:2). The difference is between 0.5–2.5 mm. Of the three convergence measurements performed at section 5/250, the calculated convergence is smaller in one (C1) and larger in the two others. The difference is, in this case, approximately between 2.0–5.5 mm.

The monitoring section 1/317 in the operational tunnel without exception displays a calculated rock mass response that is smaller than the measured. However, since the response in this section is small, the comparison is considered to be uncertain.

Table 9-1. Calculated and measured rock mass response for each monitoring section after the final excavation of the tunnels.

Deformation	Section 1/262.5 (mm)			Section 5/250 (mm)			Section 1/317 (mm)		
Left wall	**E1:2**		**E1:6**	**E1:2**		**E1:6**			**E1:6**
Calculated	2.2		2.8	1.9		10.7			0.2
Measured	3.2		3.9	2.8		8.2			0.3
Difference	–1.0		–1.1	–0.9		2.5			–0.1
Roof	**E3:2**		**E3:4**	**E2:2**		**E2:6**			**E2:6**
Calculated	0.5		0.8	0.2		0.2			0.1
Measured	0.6		0.5	0.1		0.1			0.1
Difference	–0.1		0.3	0.1		0.1			0.0
Right wall	**E5:2**		**E5:6**	**E3:2**		**E3:6**			**E3:6**
Calculated	1.1		1.9	1.4		2.8			0.0
Measured	1.8		5.7	0.8		1.1			0.3
Difference	–0.7		–3.8	0.6		1.7			–0.3
Convergence	**C1**	**C2**	**C3**	**C1**	**C2**	**C3**	**C1**	**C2**	**C3**
Calculated	4.7	3.5	10.7	1.3	4.7	8.1	0.1	0.1	0.4
Measured	2.6	2.1	8.2	4.6	–0.7	6.3	0.6	0.5	0.6
Difference	2.1	1.4	2.5	–3.3	5.4	1.8	–0.5	–0.4	–0.2

In an attempt to improve the agreement between the calculated results and the measurements, back-calculations of the deformations were executed. The in situ stresses were kept constant in this analysis while the deformation modulus and the cohesion were adjusted according to Table 9-2.

The back-calculation included five cases, A–E, with comparison between the calculated and measured response of the tunnel walls at the three monitoring sections. In the first three cases (A–C) the Young's modulus is changed systematically in the transitions sectors surrounding the core. After that the Young's modulus is adjusted also in the core (D). In the final case (E) the cohesion is increased in one of the altered sectors that enclose the core while Young's modulus for the core is set back to its original value. The results are presented in Tables 9-3 to 9-5.

Table 9-2. Assigned values of Young's modulus (Em) and cohesion (Cm) in the back-calculation.

	Initial		A		B		C		D		E	
	Em (GPa)	Cm (MPa)	Em	Cm	Em	Cm	Em	Cm	Em	Cm	Em	Cm
Host rock	45	4	45	4	45	4	45	4	45	4	45	4
Altered sector	16	2	**32**	2	16	2	**32**	2	**32**	2	**32**	**4**
Tabular sector	16	2	16	2	16	2	16	2	16	2	16	2
Fractured sector	16	2	16	2	**8**	2	**8**	2	**8**	2	**8**	2
Zone core	2.7	2	2.7	2	2.7	2	2.7	2	**4**	2	2.7	2

Table 9-3. Comparison of calculated and measured wall convergence at section 1/262.5 for five cases studied in the back-calculation.

	Initial (mm)		A		B		C		D		E	
	L	R	L	R	L	R	L	R	L	R	L	R
Initial reading	12.6	–9.1	8.4	–6.8	8.0	–6.7	6.6	–5.5	9.0	–6.4	6.6	–5.6
Final reading	18.8	–13.6	23.2	–15.5	13.2	–10.5	17.6	–13.0	14.0	–10.8	12.6	–9.7
Difference	6.2	–4.5	14.8	–8.7	5.2	–3.8	11.0	–7.4	5.0	–4.4	6.0	–4.1
Calculated convergence	10.7		23.5		9.0		18.4		9.4		10.1	
Measured convergence	8.2											

Table 9-4. Comparison of calculated and measured wall convergence at section 5/250 for five cases studied in the back-calculation.

	Initial (mm)		A		B		C		D		E	
	L	R	L	R	L	R	L	R	L	R	L	R
Initial reading	9.2	–8.4	9.3	–8.4	7.5	–7.4	9.7	–8.6	6.3	–5.6	9.9	–8.6
Final reading	10.8	–15.0	11.2	–15.1	10.6	–15.9	10.8	–15.5	6.9	–11.1	10.5	–15.5
Difference	1.5	–6.6	1.9	–6.7	3.1	–8.5	1.1	–6.9	–0.6	–5.5	0.6	–6.9
Calculated convergence	8.1		8.6		11.6		8.0		6.1		7.5	
Measured convergence	6.3											

Table 9-5. Comparison of calculated and measured wall convergence at section 1/317 for five cases studied in the back-calculation.

	Initial (mm)		A		B		C		D		E	
	L	R	L	R	L	R	L	R	L	R	L	R
Initial reading	10.0	–4.3	5.8	–3.4	11.3	–7.6	11.9	–7.9	6.3	–4.9	3.6	–3.5
Final reading	10.3	–4.4	5.9	–3.5	11.9	–7.9	12.5	–8.3	6.5	–5.0	3.9	–3.7
Difference	0.3	–0.1	0.1	–0.1	0.6	–0.3	0.6	–0.4	0.2	–0.1	0.3	–0.2
Calculated convergence	0.4		0.2		0.9		1.0		0.3		0.5	
Measured convergence	0.6											

The difference in calculated convergence between the five cases is relatively larger in monitoring section 1/262.5, while the two other sections show a more modest difference in calculated convergence. It should be noted that for some of the cases the calculated convergence similar is although the calculated displacements at initial and final reading diverge a great deal.

In monitoring section 1/262.5 the agreement between calculated and measured convergence is best for case B. The best fit at monitoring section 5/250 is reached for case D. At monitoring section 1/317, finally, the best agreement is obtained for case E.

The calculation case that seems to correspond best to the measured wall convergence in all three monitoring sections at once, is case D. Another case that also corresponds relatively well throughout is case E. The latter case is also the one that has been chosen for a more detailed comparison between the calculated and measured rock mass response. This is because the overall correspondence for all observations in the monitoring sections is judged to be best for this case.

9.1 Comparison of the response at monitoring section 1/262.5

Figure 9-1 presents a comparison between calculated and measured convergence versus distance to tunnel face, and in Figure 9-2 a comparison between calculated and measured deformation versus distance to tunnel face is presented. The calculated response is based on calculation case E.

The calculated and measured convergence shows a similar proportion in the magnitude between the different convergence measurements. However, the calculated convergence is consistently about 2 mm larger than the measured convergence.

The extensometers located in the roof show similar magnitudes for calculated and measured deformation, while the calculated responses for the extensometers in the walls are always smaller than the measured. The calculated response, in this instance, is 1–4 mm less than the measured.

9.2 Comparison of the response at monitoring section 5/250

A comparison between calculated and measured rock mass response versus distance to tunnel face at monitoring section 5/250 is presented in Figure 9-3 regarding convergence measurements and in Figure 9-4 regarding extensometers. The calculated response is based on calculation case E.

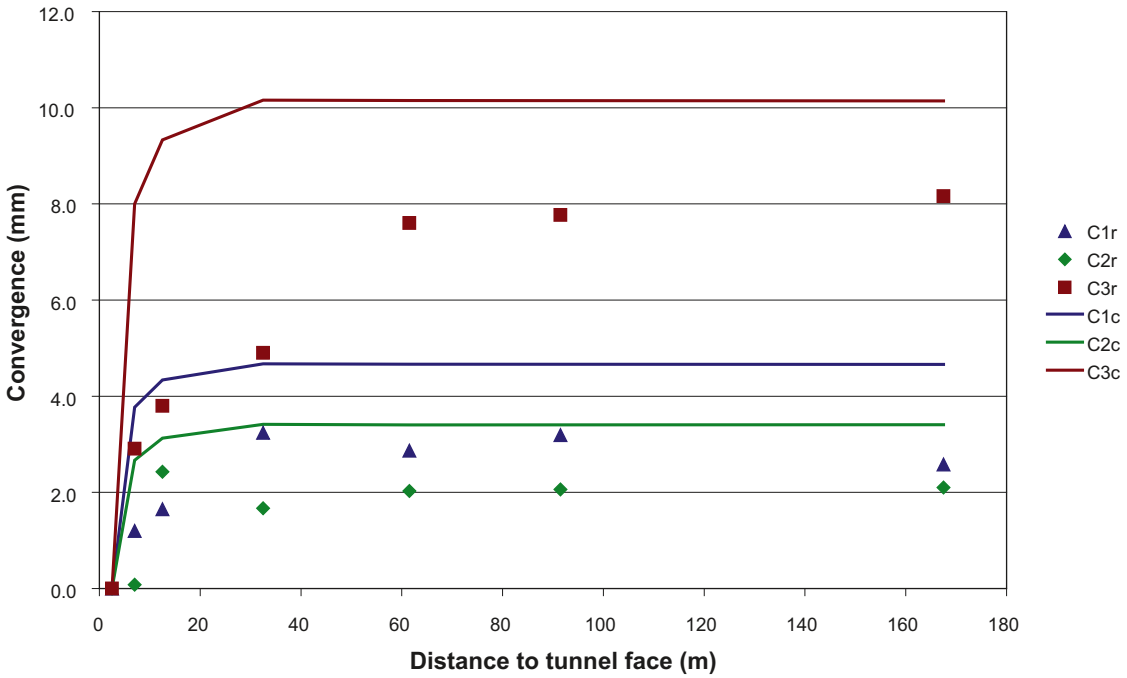

Figure 9-1. *Calculated and measured convergence versus distance to tunnel face at monitoring section 1/262.5 of the operational tunnel. The calculated response is based on case E.*

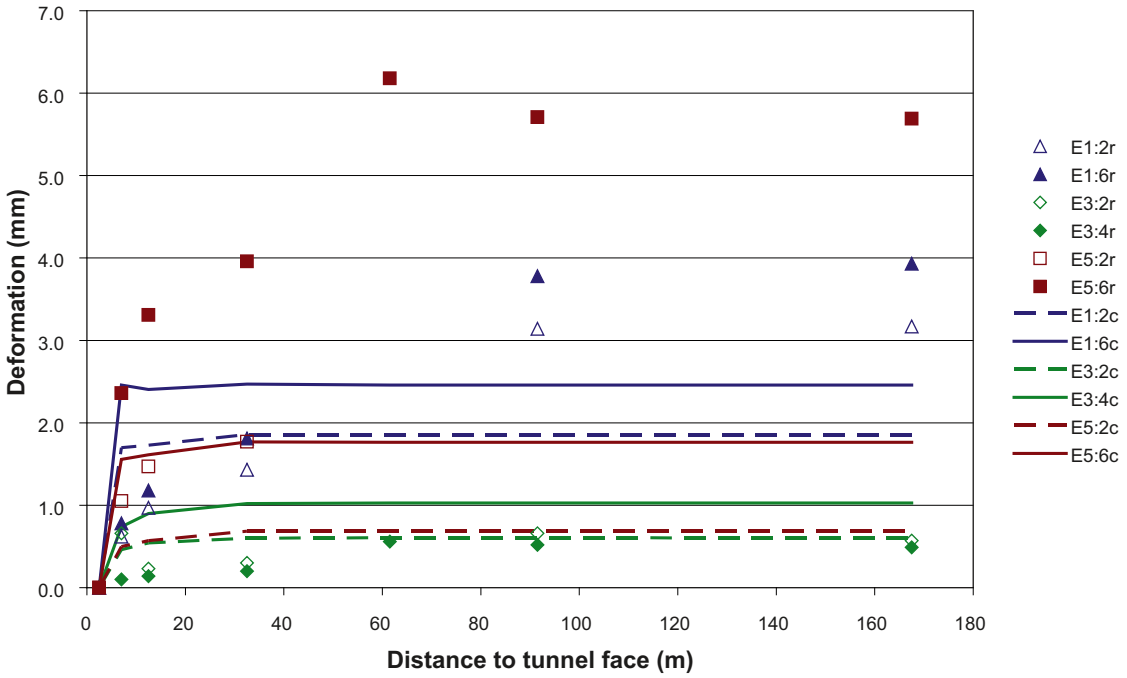

Figure 9-2. *Calculated and measured deformation versus distance to tunnel face at monitoring section 1/262.5 of the operational tunnel. The calculated response is based on case E.*

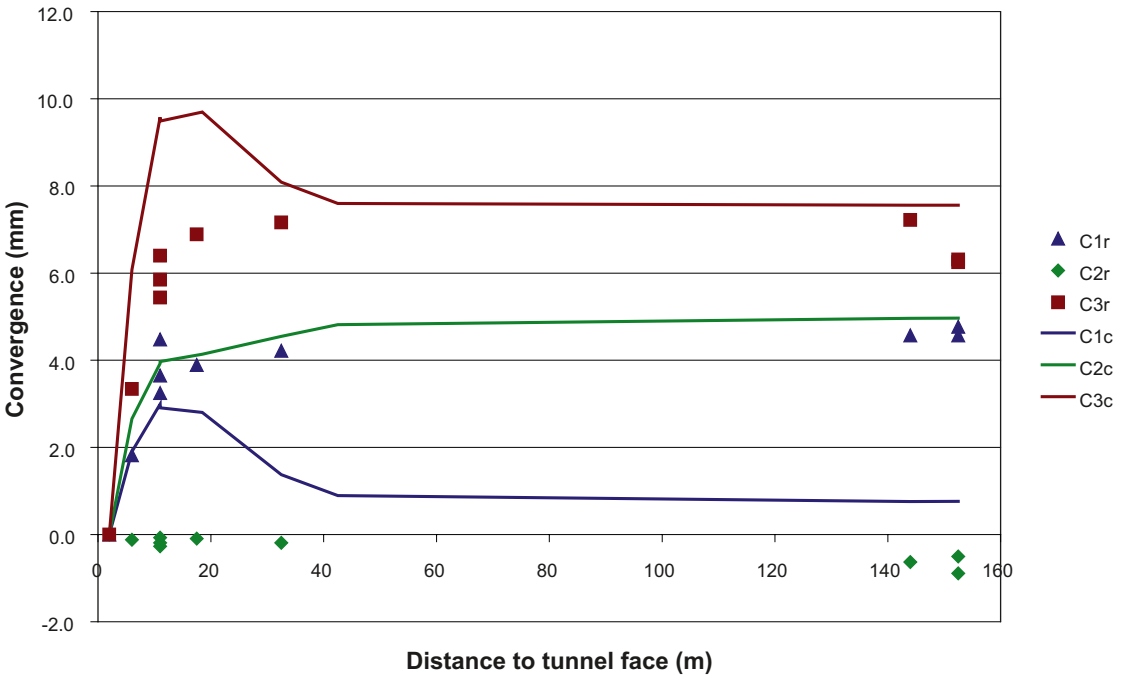

Figure 9-3. *Calculated and measured convergence versus distance to tunnel face at monitoring section 5/250 of the construction tunnel. The calculated response is based on case E.*

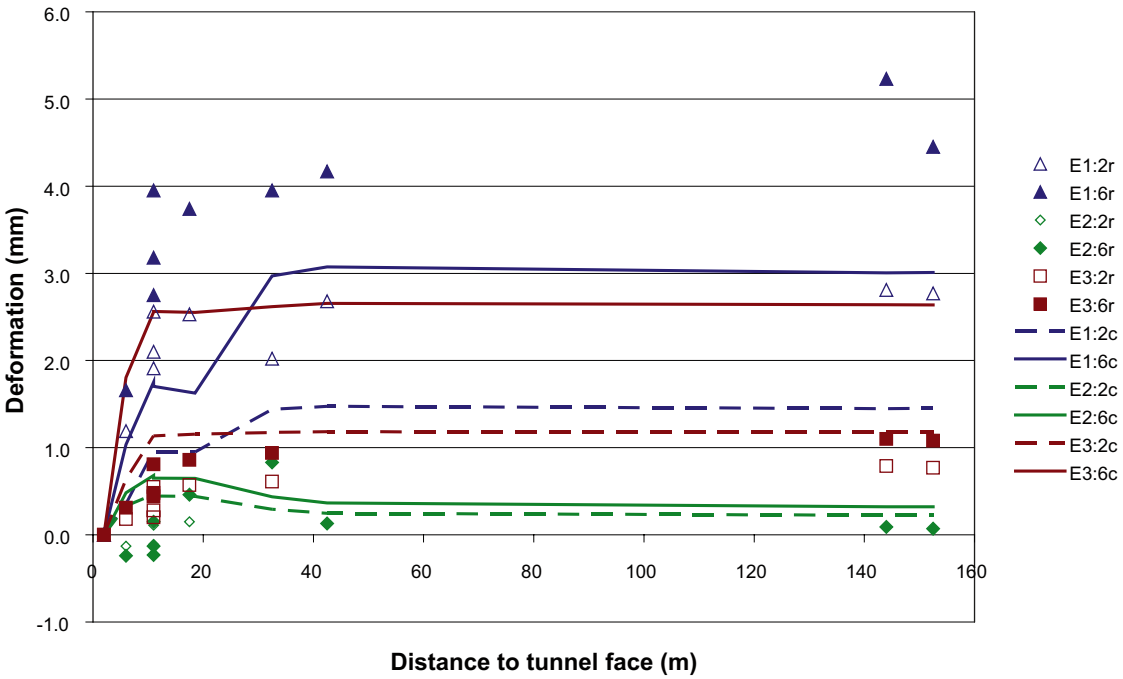

Figure 9-4. *Calculated and measured deformation versus distance to tunnel face at monitoring section 5/250 of the construction tunnel. The calculated response is based on case E.*

The calculated and measured wall convergence agrees relatively well, whereas the correspondence with the two other convergence measurements is poor. Convergence measurement C1 and C2 displays a reverse response in the model compared to what has been measured. This fact makes is natural to considered the possibility that the designation of the convergence measurements might have been reversed. A reversal of the designation should result in good agreement between calculated and measured convergence even for the actual convergence measurements.

It is worth noting that both the calculated and the measured wall convergence (C3) show a reduction in the final phase. However, the diminution of the convergence is larger and occurs earlier in the model than in the observation.

Concerning the extensometers located in the roof, the correspondence between calculated and measured deformation is good. For extensometers located in the walls the model displays alternating between less response or larger response than the measured deformation. The calculated deformation in the extensometers in the pillar wall (E1:2, E1:6) are approximately 0.5–2.0 mm less than the measured whereas the calculated deformation in the extensometers in the opposite wall (E3:2, E3:6) are just as much larger.

9.3 Comparison of the response at monitoring section 1/317

A comparison of the response in the model and the observations at monitoring section 1/317 is presented in Figure 9-5 regarding the convergence and in Figure 9-6 regarding the deformation. The calculated response is, as in previous sections, based on case E.

It should be noted that the comparison between the model and the observation is considered to be uncertain in this section. The reason is, as pointed out previously, that the initial reading was not performed until the tunnel face has passed far from the monitoring section. Thus, the calculated and measured rock mass response will be small throughout. Furthermore, the possible difference between the model and the observations will also be small.

The calculated and measured convergence of the walls again agrees relatively well, whereas the correspondence with the two other convergence measurements, which also includes the roof, is poor. Convergence measurement C1 and C2 displays less response in the model compared to what has been measured.

The extensometer measurements at this section display without exception a calculated rock mass response that is smaller than the measured. However, the difference between the model and the observation is, in fact, small.

9.4 Concluding remarks from the comparison

In this section some concluding remarks are drawn from the above comparison between calculated and measured rock mass response.

The calculated rock mass response agrees well with the response observed at the instruments located in the tunnel roof. This indicates that the in situ stress conditions assumed in the model generally represent the actual stresses in an accurate way. Based on these results the major principal stress within the core of the Singö deformation zone is with good confidence assumed to be horizontal as in the surrounding host rock.

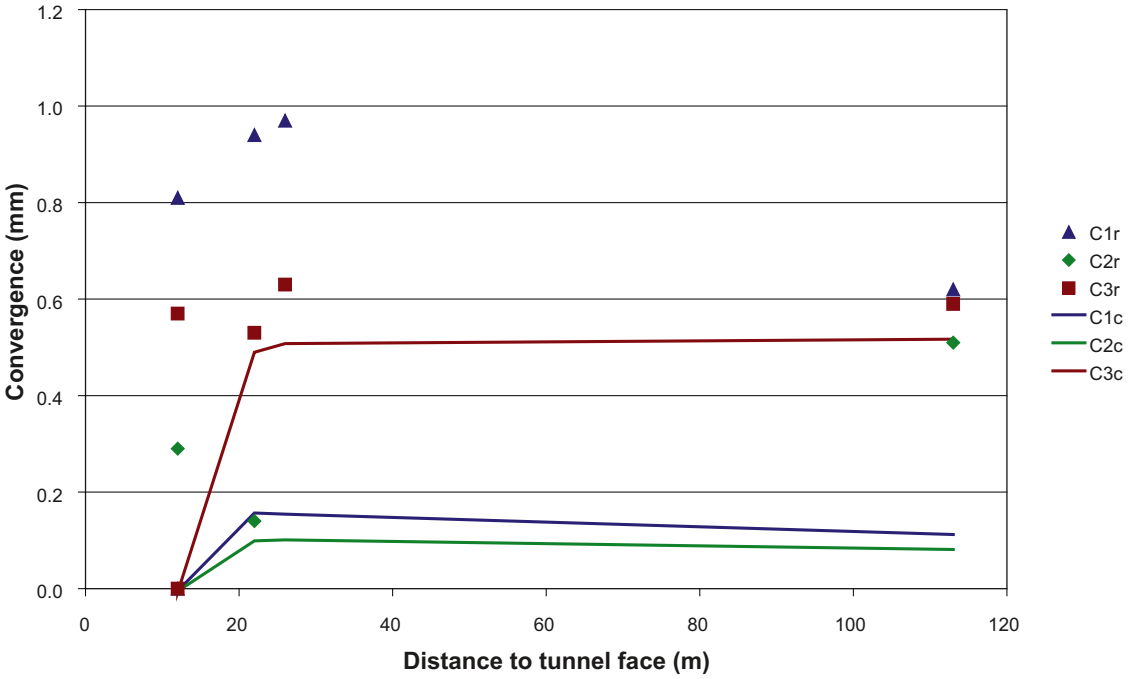

Figure 9-5. *Calculated and measured convergence versus distance to tunnel face at monitoring section 1/317 of the operational tunnel. The calculated response is based on case E.*

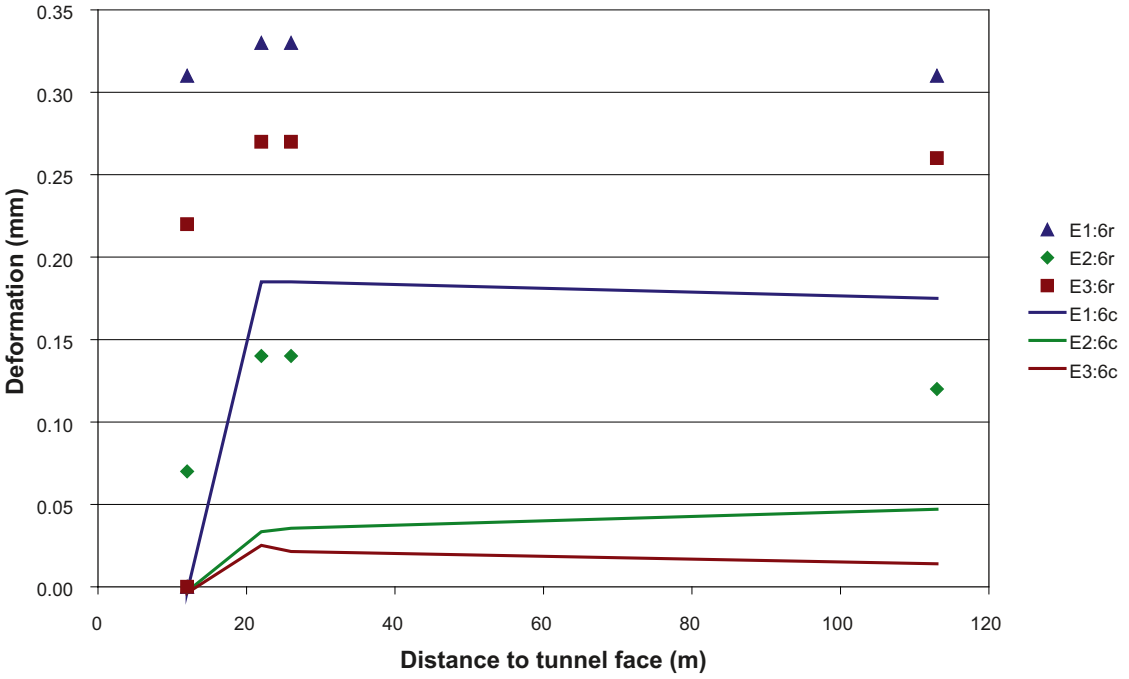

Figure 9-6. *Calculated and measured deformation versus distance to tunnel face at monitoring section 1/317 of the operational tunnel. The calculated response is based on case E.*

The agreement between the calculated and the measured tunnel wall response is better concerning the convergence measurements than the extensometer measurements. The calculated deformation normally is smaller than the measured deformation in the extensometers. The observed behavior of the rock mass may probably be achieved in the model by assuming an increase in the rock stiffness with the distance from the tunnel, or by reducing the cohesion in connection with an increase in the stiffness of the rock mass.

Most likely it had been possible to reach a better agreement by carrying on the back-calculation in an additional number of cases. It is also likely that other combinations of rock mass properties occur which should give as good correspondence as that of the selected calculation case. However, since the numerical model simplifies the actual conditions in some aspects and some of the conditions assumed in the model are uncertain, it has been judged as unproductive to pursue a full agreement between the calculated and measured response. Some simplifications and uncertainties in the performed simulation are for instance:

- The assumed strike and dip of the Singö deformation zone and subsequent sectors that are generalized in the model.
- The assumed tunnel geometry: The model is based on a theoretical cross-sectional area, while the real cross-sectional area is usually larger.
- The assumed position of the monitoring sections and the instrument anchor points in the model is somewhat uncertain.
- The location of the tunnel fronts relatively to the monitoring sections is partly uncertain, as well as the shape and inclination of the tunnel front.

One should also take into consideration that the measured deformations that have been used as reference in the back-calculation to some degree suffer from uncertainties, since every measurement involves error and uncertainty.

10 Numerical modelling of properties valid for the deformation zone as a whole

The rock mass properties for case E in the back-calculation were used for numerical modelling of equivalent properties that are valid for the deformation zone as a whole. The numerical calculation is, in this case, performed by a box shaped model that includes each typical sector of the zone and embraces the whole zone width, a size of 127.5 m.

10.1 Description of the model

10.1.1 Geometry

Figure 10-1 shows a view of the model used. The model is cube shaped with a side length of 127.5 m in three directions. The model represents a cut out normal to the strike of the Singö deformation zone.

The generated model mesh is performed with tetrahedral zones. This type of zone elements is not the most appropriate for plasticity problems as simulated here. Higher order zones with an extra grid point added to the centre of each zone, which are more appropriate for plasticity problems, were not possible in this model due to trouble with the code. The zones in the generated mesh have an average edge length of 5 m.

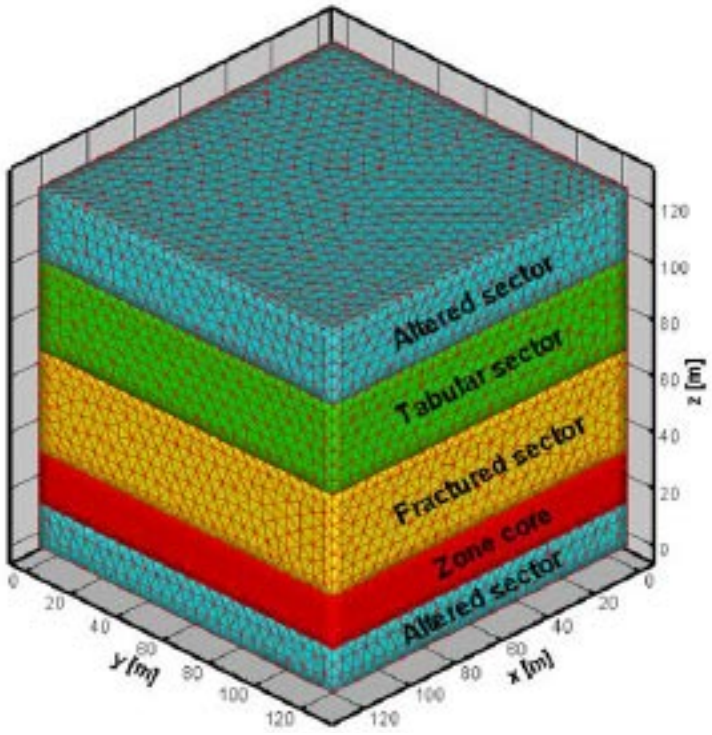

Figure 10-1. *Geometry of the model used.*

10.1.2 Rock mass properties

Table 10-1 presents the rock mass properties for case E in the back-calculation, see Section 9. The data has been used as in-data to the box shaped model. This data set was chosen because it was considered to give best agreement between simulated and observed deformation in the SFR-tunnel passage.

The yield function used in the model is the Mohr-Coulomb failure criterion. Joints included in the model are only used for creation of the model geometry and do not influence the calculation.

10.1.3 Modelling sequence

The modelling sequences, which contain three main steps, are given in Table 10-2. The displacements are reset after each step in the modelling sequence.

The normal stress on the upper xy-boundary comprises three stress levels: 0.5, 5.0 and 20 MPa. The shear stress comprises approximately ten stress levels for each level of the normal stress. The range of the normal stress amount approximately the evaluated magnitude of the minor horizontal stress in Forsmark at about 500 m depth.

10.1.4 Boundary conditions

The boundary conditions applied in the model are given in Table 10-3. The conditions are modified in each step of the modelling sequence. The shear stress on the lateral yz-planes is combined with stresses in normal direction due to the reactions from the normal stress applied on the upper boundary. The normal stress applied on the lateral yz-planes is 75% of the normal stress applied on the upper boundary.

Table 10-1. Rock mass properties used in the simulation. The adopted properties are based on case E in the back-calculation in previous section.

	Host rock	Altered sector	Tabular sector	Fractured sector	Zone core
Young's modulus (GPa)	45	32	16	8	2.7
Poisson's ratio[1]	0.36	0.43	0.43	0.43	0.43
Tensile strength (MPa)	–0.3	–0.1	–0.1	–0.1	–1.0
Cohesion (MPa)	4.0	4.0	2.0	2.0	2.0
Friction angle[1] (MPa)	65	51	51	51	37

[1)] The affect of the dilation angle are included in Poisson's ratio and the friction angle.

Table 10-2. Steps in the modelling sequence.

Step	Comments
A In situ conditions	Setting of initial equilibrium conditions
B Normal stress is applied to the model in steps on the upper xy-plane.	Comprises three stress levels: 0.5, 5.0 and 20 MPa.
C Shear stresses are applied to the model in steps on three planes, the upper xy-plane and the yz-planes.	Comprises approximately ten stress levels for each level of the normal stress.

Table 10-3. Boundary conditions.

Step	Boundary	Condition
A In situ-conditions	Upper xy-plane	Fixed in normal direction
	Lateral xz-planes	Fixed in normal direction
	Lateral yz-planes	Fixed in normal direction
	Lower xy-plane	Fixed in normal direction
B Normal stress applied	Upper xy-plane	Stress in normal direction
	Lateral xz-planes	Fixed in normal direction
	Lateral yz-planes	Fixed in normal direction
	Lower xy-plane	Fixed in normal direction
C Shear stress applied	Upper xy-plane	Shear stress
	Lateral xz-planes	Fixed in normal direction
	Lateral yz-planes	Shear stress and reaction forces from the normal stress applied on the upper boundary.
	Lower xy-plane	Fixed in x- and z-direction

10.2 Results

The modelling results are presented by plots and diagrams of the displacements during the simulated shear test. In addition to this, evaluated parameters that could be used in the regional stress modelling are also presented, i.e. normal stiffness, shear stiffness, cohesion and friction angle.

10.2.1 Displacements in the simulated shear test

A general picture of the displacements that arise during the simulated shear test is presented in Figure 10-2 and 10-3. The stress level in normal direction is 5 MPa in both plots and the shear stress 4.4 MPa in the latter plot. The shear stress touches up on the shear strength of the simulated block.

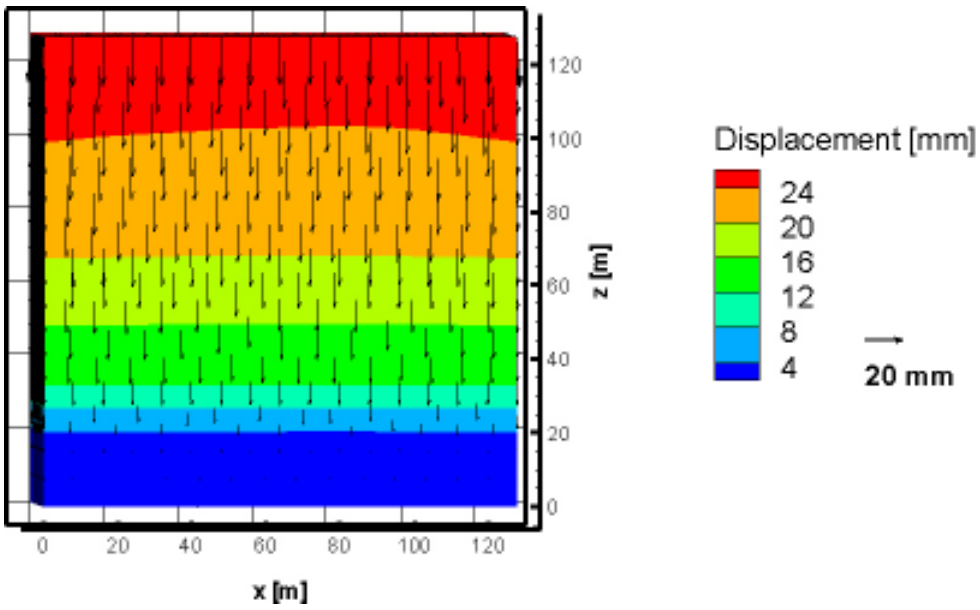

Figure 10-2. *Normal displacements that arise in the simulated test for a stress level of 5 MPa in a normal direction.*

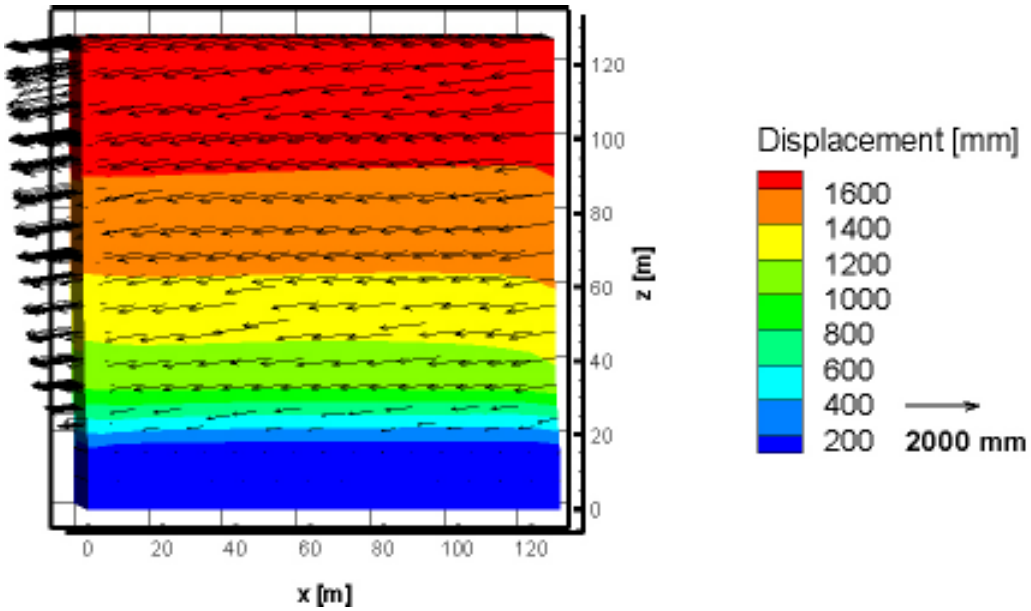

Figure 10-3. *Shear displacements that arise close to failure in the simulated test. The normal stress is 5MPa and the shear stress is 4.4 MPa.*

The displacement that arises at the upper boundary under the present loading is approximately 25 mm in normal direction and 1,700 mm in the shear direction. As expected the larger difference in the displacement field occurs at the border of the zone core and the altered sector at the bottom.

The normal displacement versus normal stress in the simulated test based on a monitoring point at the upper boundary is presented in Figure 10-4. The results that are rather linear correspond to a normal displacement of approximately 5 mm/MPa.

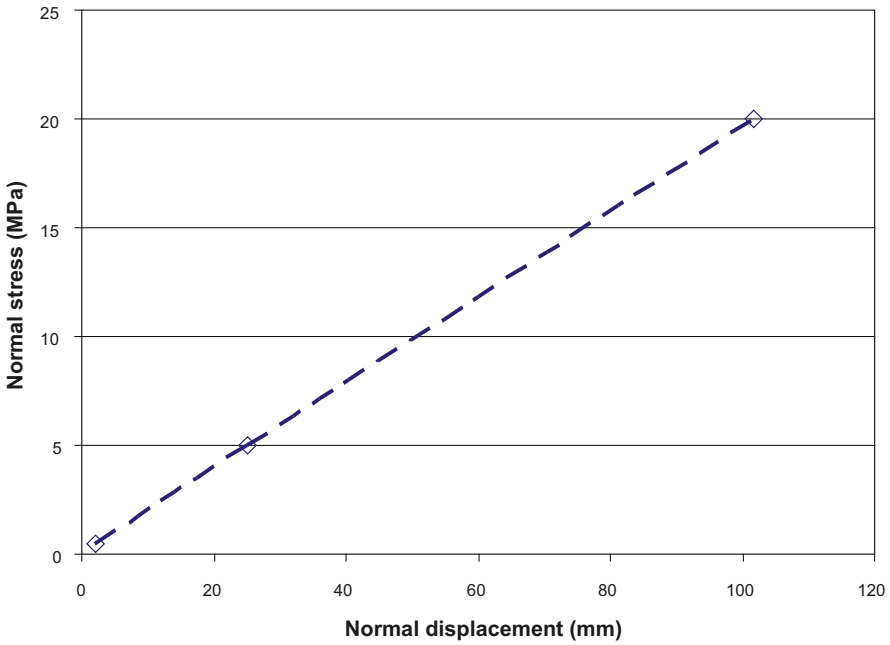

Figure 10-4. *Normal displacement versus normal stress in the simulated test based on a monitoring point located at the upper boundary.*

In Figure 10-5 the shear displacements versus shear stress are presented for a normal stress of 5 MPa. The results are based on the mean of three monitoring points located at the upper boundary in the simulated block. The results from 0.5 and 20 MPa in normal stress are not presented, since the performance for these stress levels are similar.

The constitutive model applied in the simulation does not result in an actual peak shear strength and subsequent residual shear strength. The shear failure in the simulation with corresponding shear peak strength is for that reason evaluated, at the stress level where the shear displacements increase considerably. This point which appears distinctly in the diagram in Figure 10-5, gives the estimated peak shear strength for 5 MPa normal stress of approximately 4.4 MPa.

10.2.2 Equivalent properties of the deformation zone

Equivalent properties that are valid for the deformation zone as a whole are presented in this section. The parameters that have been evaluated from the simulation are the normal stiffness, the shear stiffness, the cohesion and the friction angle.

The normal stiffness for stresses up to 20 MPa are presented in Figure 10-6. The results show a decreasing trend by an increasing normal stress. The normal stiffness is ranging from approximately 245–195 MPa/m within the stress interval.

Figure 10-7 presents the secant shear stiffness evaluated at 50% of the peak shear strength for the normal stress interval 0.5–20 MPa. As for the normal stiffness, the results show a decreasing trend by an increasing normal stress. The shear stiffness for the actual stress interval is ranging from 22–9 MPa/m.

In Figure 10-8 the peak shear strength is plotted for normal stresses up to 20 MPa. The results are rather linear and possible to represent by the Mohr-Coulomb equation. A graphical estimation of the equivalent cohesive strength and friction angle for the normal stresses in the interval 5–20 MPa gives c_m = 0.4 MPa and ϕ_m= 31.5 degrees.

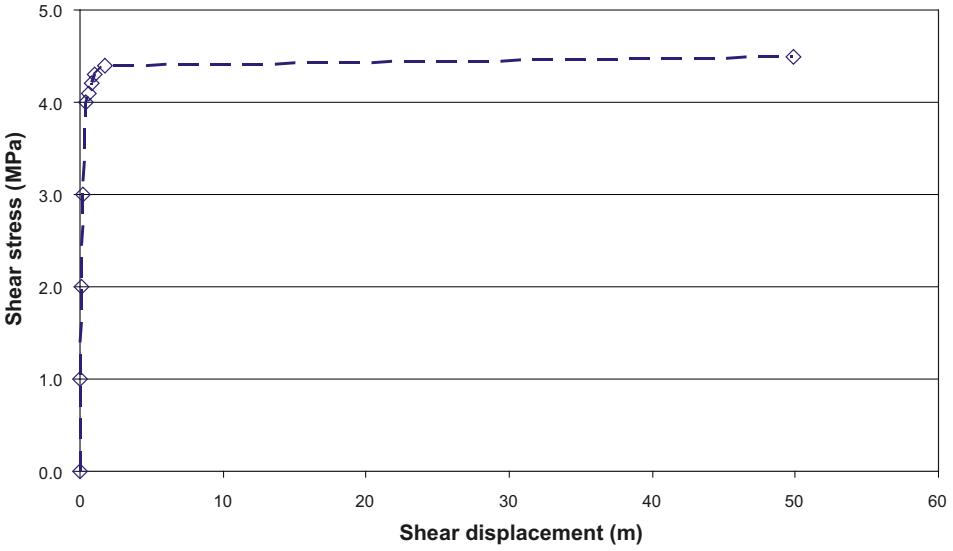

Figure 10-5. *Shear displacements versus shear stress in the simulated based on the mean of three monitoring points located at the upper boundary. The stress level in normal direction is 5 MPa.*

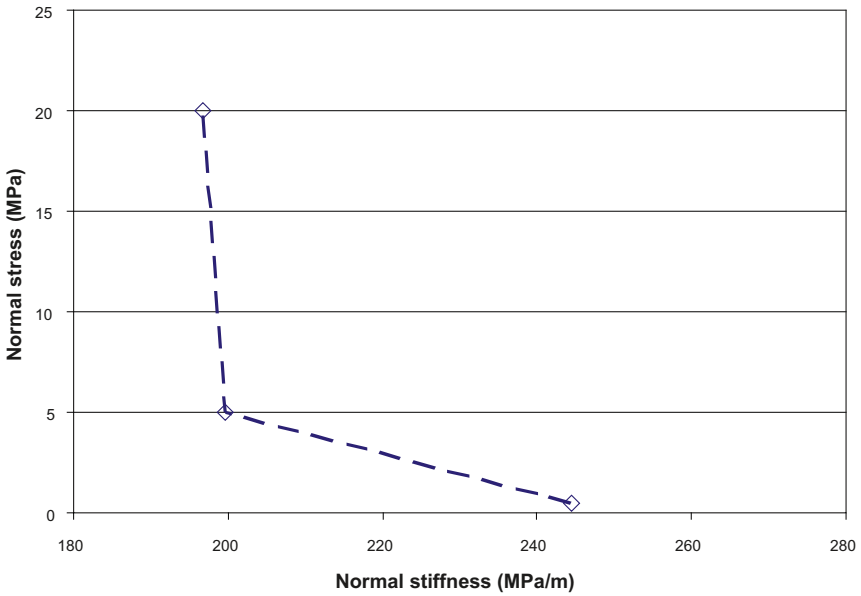

Figure 10-6. *Normal stiffness versus normal stress in the simulated test.*

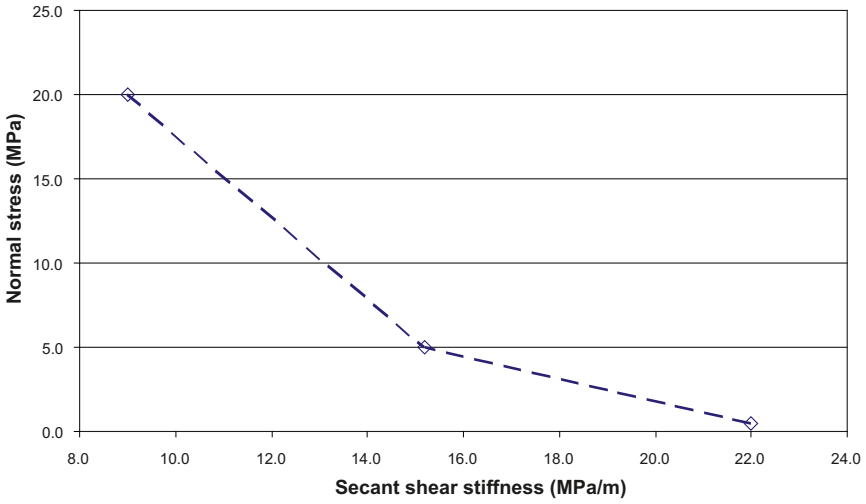

Figure 10-7. *Secant shear stiffness evaluated at 50% of the peak shear strength.*

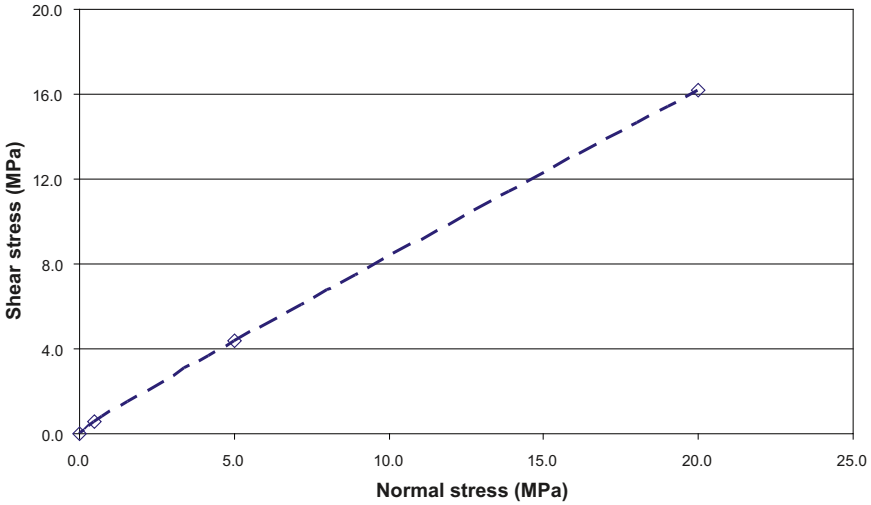

Figure 10-8. *Peak shear strength for normal stresses up to 20 MPa.*

11 Discussion

11.1 Geology

In Tunnel 3, a boundary has been mapped as separating grey metavolcanics from metasediment. The latter rock type is likely to be identical to the surface mapped muscovite altered metavolcanic.

Three rock samples exist from Tunnel 3, from the area of the boundary between what was mapped as aplitic metagranite and red metavolcanics. It may be discussed where the corresponding boundary in Tunnel 1-2 is located, as in that tunnel no metavolcanics have been mapped, only ”brecciated gneissic granite” (aplitic metagranite and possibly re metavolcanics) and ”sediment gneiss” (muscovite altered metavolcanic).

Over Tunnel 3 four seismic refraction profiles were carried out during the site investigations. Strong low velocity zones, coinciding with one another, are located some 30 m north of the zone observation in the tunnel and do also not fit with the drawing in which core drilling and seismic investigations are reported. Another less consistent set of anomalies are located south of the core in the tunnel. We recommend a check of the SICADA coordinates against original drawing and maps.

11.2 Numerical modelling

The agreement between the calculated and the measured tunnel wall response is better concerning the convergence measurements than the extensometer measurements. The calculated deformation is normally smaller than the measured deformation in the extensometers. The measured behavior probably may be achieved by assuming an increase in the rock stiffness with the distance from the tunnel, or by reducing the cohesion in connection with an increase in the stiffness of the rock mass.

Most likely it had been possible to reach a better agreement by carry on the back-calculation in an additional number of cases. It is also likely that other combinations of rock mass properties occur which should give as good correspondence as that of the selected calculation case. However, since the numerical model simplifies the actual conditions in some aspects and some of the conditions assumed in the model are uncertain, it has been judged as unproductive to pursue a full agreement between the calculated and recorded response. One should also take into consideration that the measured deformations that have been used as reference in the back-calculation to some degree suffer from uncertainties.

12 Conclusions

12.1 Geology

Compilation of occurrences of strongly crushed rock and gouge zones from the four tunnels coincide well with the magnetic anomaly centre line, except for at Tunnel 3, where the magnetic line is located 20–30 m to the south of the core in the tunnel. Including the transition zones, the tunnel observations fit fairly well with the estimated width derived from the anomaly.

In Tunnel 3, there are a lot of fracture zones on the SW side of the Singö deformation zone, while the rock NE of it is poor in fractures with the exception of a zone or two, while in SFR, the situation is just the reverse.

One of the NE located zones in Tunnel 3 fits fairly well with the splay on the geological map and with a zone in Tunnel 1-2.

The fracture system consists of three sets: one sub-horizontal, and two sub-vertical sets striking north-west and north-east, respectively. In Tunnel 3, in the north-west part of the area, the system appears to be rotated clockwise, as compared to SFR in the south-east. The fracture system does not change considerably across the Singö deformation zone.

Assessment of fracture intensity P20 defined as fractures per m^2, in Tunnel 3 coincides well with results from detail fracture mapping during site investigations for a repository for spent nuclear fuel.

Water-bearing fractures in the SFR and in Tunnel 1-2 at the Singö Zone, belong to a large extent to the north-west striking fracture set. Water inflow is generally lower in the Singö Zone due to clayey infillings, than in other fracture zones in the tunnels.

The boundaries between host rock and the two transition zones, defined as 4 fractures/m, is more clear in SFR and Tunnel 3, while in Tunnel 1-2, these boundaries have been estimated from applied temporary support measures.

12.2 Numerical modelling

The calculated and measured rock mass response within the SFR-tunnel passage agrees relatively well. The overall impression is that the results demonstrate that the methodology used for simulation of equivalent mechanical properties is an applicable and adequate method also in case of large deformation zones.

The numerical simulation of equivalent mechanical properties of the host rock and typical parts of the deformation zone, gave comparable estimations based on GSI of deformation modulus and strength properties for the zone core. However, for the host rock and the transition zone the deformation modulus estimated from the numerical simulations is considerably smaller than modulus estimated from GSI.

Comparison of the zone core deformation modulus based on estimations from numerical simulations with estimations based on large-scale in situ load tests show a slightly higher modulus from the simulations than from the in situ load tests.

Typical rock mechanical parameters of the Singö deformation zone that can be used in the regional stress model are presented in Table 12-1. The given deformation and strength parameters are valid considering the zone to be a single fracture in regional scale for normal stresses in the range of 5–20 MPa.

Table 12-1. Typical rock mechanical parameters of the Singö deformation zone for normal stresses in the range of 5–20 MPa.

Normal stiffness (MPa/m)	Shear stiffness (MPa/m)	Cohesion (MPa)	Friction angle (degrees)
200	10–15	0.4	31.5

13 References

13.1 Published sources

Barton N R, 1974. A review of the shear strength of filled discontinuities in rock. NGI publ. no. 105. Oslo.

Bieniawski Z T, 1976. Rock mass classification in rock engineering, Proc. Symposium on Exploration for Rock Engineering, Johannesburg, Volume 1, 1976, pages 97–106.

Boutard P and Groth T, 1975. Bergsprickors egenskaper, BeFo nr 21, Stockholm.

Carlsson A, Olsson T, 1977. Water leakage in the Forsmark tunnel. SGU Ser. C, 734.

Carlsson A, Olsson T and Stille H, 1985a. Submarine tunnelling in poor rock. Reprint. Tunnelling ’85. Brighton, England.

Carlsson A, Olsson T and Stille H, 1985b. Submarine tunnelling in poor rock. pp 21–25. Tunnels & Tunnelling.

Hanafy E E, 1980. Advancing face simulation of tunnel excavation and lining. Placement. In: Underground Rock Engineering, 13th Canadian Rock Mechanics Symposium, pp 119–125.

Hansen L M, Staub I, Vestgård J and Forssberg O, 2004. Description and assessment of glacial fractures at drill site 5, Forsmark. (In Leijon, B (ed.), 2005. Forsmark site investigation. Investigations of superficial fracturing and block displacements at drill site 5. SKB P-05-199. Svensk Kärnbränslehantering AB.

Hoek E, Kaiser P K and Bawden W F, 1995. Support of underground excavations in hard rock, Balkema.

Jahanshahi J and Vasseghi M, 1991. SFR-tunnlarnas passage genom Singölinjen. Stabilitetskontroll med FEM-beräkningar. Examensarbete Inst. för jord- och bergmekanik, KTH.

Munier R, Stenberg L, Stanfors R, Milnes A G, Hermanson J, Triumf C A, 2003. Geological site descriptive model, a strategy for model development during site investigations. SKB R-03-07. Svensk Kärnbränslehantering AB.

Olofsson I and Fredriksson A, 2005. Strategy for a numerical Rock Mechanics Site descriptive Model. SKB R-05-43. Svensk Kärnbränslehantering AB.

RocData. User´s Guide. Rocscience Inc. 2004.

RocLab. User´s Guide. Rocscience Inc. 2002.

SKB 2004. Preliminary site description. Forsmark area – version 1.1. Svensk Kärnbränslehantering AB.

SKB 2005. Preliminary site description. Forsmark area – version 1.2. Svensk Kärnbränslehantering AB.

SKB 2006. Site descriptive modelling Forsmark stage 2.1 Feedback for completion of the site investigation including input from safety assessment and repository engineering. SKB R-06-38. Svensk Kärnbränslehantering AB.

3DEC, 2003. 3 Dimensional Distinct Element Code, User´s Guide. Itasca consulting group, Inc., Minneapolis.

13.2 Unpublished sources

Carlsson A, Olsson T, 1976. Forsmarks Kraftstation. Block 1 and 2. Avloppstunnel. Geologisk kartering. 8 Ritningar numrerade 1 t.o.m 8. Vattenfall.

Christiansson R, Bolvede P, 1985. SFR. Geologisk kartering. Dagbok, ritningar och skisser. Svensk Kärnbränslehantering AB.

Hansen L M, 1982a. Forsmarks Kraftstation. Block 3. Avloppstunnel. Geologisk kartering. Rapport 10 skisser. Golder Associates, Uppsala.

Hansen L M, 1982b. Forsmarks Kraftstation. Block 3. Avloppstunnel. Geologisk kartering. Rapport daterad sept 1982. Vattenfall, Ludvika.

Larsson W, 1973. Forsmark Aggr 1 och 2. Avloppstunnel. Berggeologiska förhållanden utefter tunnelllinjen. Vattenfall.

Lundström L, Tenne M, 1976. Forsmarks Kraftstation. Avloppstunnel (Block 1 and 2). Förstärkningsförslag. Ritn 3291-2:10 and 3291-2:11. Hagconsult, Vattenfall.

Moberg M, 1973. Forsmarks Kraftstation. Aggr 1 and 2. Avloppstunneln. Geologisk-teknisk översikt 1973. Ritn nr 799542b. Vattenfall.

Moberg M, 1980. Forsmarks Kraftstation. Aggr 3. Avloppstunneln. Grundundersökningar 1971–1978. Ritn nr 970 802. Vattenfall.

Appendix A

RVS-modelling of the Singö deformation zone

FBE 250541-09-PM_001

RVS-model

An RVS model covering the area around the Singö deformation zone has been produced. The modeled volume consists of a model cube rotated 60 degrees anti-clockwise from the RT90 system north axis. The cube's southern corner lies in the RT90-RHB70 system at Easting = 1631900, Northing = 6699400. The area is 4,300(E) * 3,500 (N) metres in size and from –1,500 metres above sea level to ± 0 metres above sea level in elevation. The model coordinate system is RT90-RHB70 and the site is FORSMARK-SFR. For the selected site there is a transformation between the RT90-RHB70, FORSMARK T-U and SFR T-U coordinate systems.

Background data

The following background data has been included in the model.

Background model

The site investigation model *PFM_DZ_Local_v.2.1.rvs*.

Maps

Two maps are attached as external DGN:

- *Forsmark topo-underlag.dgn*, contains coastlines, buildings and roads.
- *FORSMARK_DTM.DGN*, contains topographic contours.

Source: Assen Simeonov, SKB.

Tunnels

An external DXF-file of SFR, *SFR.dxf*. However, the layout is not in complete agreement with the supplied tunnel coordinates and is therefore only used for illustration purposes.

Source: Rune Glamheden, Golder.

Tunnel line coordinates in Excel-format from sicada, delivered 2006-08-18. SICADA_06_171. *Tunnel_surveying TFK RT90-RHB70.xls* and *Tunnel_surveying TFR RT90-RHB70.xls*.

Tunnel lines for TFKB3 and TFKB12 have been plotted in RVS and saved as a DGN-file *Forsmark-TU-v8.dgn*. This has been attached to the model. The plotting was carried out in the FORSMARK T-U system and conversion to RT90-RHB70 was performed via SICADA's coordinate transformation in connection with the attachment of the file.

The tunnels have been plotted as centre lines based on the SICADA coordinates. This facilitates the visualization of parameters along the tunnel alignment.

Tunnel mapping

Structures

Mapped structures in TFRBT, TFRDT, TFKB12 and TFKB3 in Excel format, *Structures_SFR_geologicalmapping.xls*.

Source: Lars Berkvist and Lars Hansen, Golder.

The structures have been saved as circular *Fracture observations* along the tunnels, with a diametre of 25 m and a thickness equal to the observations length in the tunnel. The structures have been placed at the correct tunnel length position based on SICADA coordinates, with a centre point 3 m above the tunnel centre line.

The following colors have been used, the number in parentheses is from the RVS color table:

Red (2) = Fracture zone

Blue (1) = Crushed zone

Green (3) = Schistosity

Dark green (133) = Chlorite

Gray (32) = Weathered pegmatite

Fractures

Mapped mineral filled fractures in TFRBT, TFRDT and TFKB12 (TFKB3 missing) in Excel format, *Minfilled_fractures_SDZ.xls*.

Source: Lars Berkvist, Golder.

Fractures have been saved as circular *Fracture observations* along the tunnels, with a diametre of 15 m and without thickness. The fractures have been placed at the correct tunnel length position based on SICADA coordinates, with a centre point 3 m above the tunnel centre line.

The following colors have been used; the number in parentheses is from the RVS color table:

Dark green (133) = Chlorite

Gray(16) = Clay

Beige (56) = Sand

Black (0) = Calcite

Water-bearing structures

Mapped water-bearing structures in TFRBT, TFRDT, TFKB12 and TFKB3 in Excel format, *Water_Bearing_Structures_geological_mapping.xls*.

Source: Lars Hansen, Golder.

The structures have been saved as rectangular *Fracture observations* along the tunnels, with a diametre 40 m and a thickness corresponding to the observation length in the tunnel. The fractures have been placed at the correct tunnel length position based on SICADA coordinates, with a centre point 3 m above the tunnel centre line.

All the structures are light blue (aqua), number 7 in the RVS color table.

Rock types

Mapped rock types in TFRBT, TFRDT, TFKB12 and TFKB3 in Excel format, *Rock_type_distribution.xls*.

The rock type names and descriptions have been assigned rock type codes by Lars Hansen.

Source: Lars Berkvist and Lars Hansen, Golder.

The Excel files have been imported to create parameters that are associated with "borehole lines" corresponding to the tunnels. They have been visualized as cylinders around the tunnel lines with a diametre of 4 m and a color coding in accordance with SICADA check tables. sections with mylonite have been visualized with a diametre of 6 m.

Fracture frequency

Mapped fracture frequency in TFRDT and TFKB3 in Excel format, *Fractures_stat.xls*.

Source: Lars Hansen, Golder.

The Excel files have been imported to create parameters that are associated with "borehole lines" corresponding to the tunnels. They have been visualized as graduated cylinders around the tunnel lines with a diametre proportional to the measured value (20*).

Zone classification

Classified zones in TFRBT, TFRDT, TFKB12 and TFKB3 in Excel format, *Zones_06115_LMH.xls, flik zones_simplified*.

Source: Lars Hansen, Golder.

The Excel files have been imported to create parameters that are associated with "borehole lines" corresponding to the tunnels. They have been visualized as cylinders around the tunnel lines with a diametre of 4 m and a color coding in accordance with the following list:

The following colors have been used; the number in parentheses refers to the RVS color table:

Host Rock	=	Light blue (7)
Transition Zone	=	Green (2)
Zone core	=	Red (3) / Light red (121)
Schistose	=	Yellow (4)
Clay altered core	=	Lilac (5)

Boreholes

Source: SICADA via RVS Order Data (2006-09-13, *rock_proto-rock_type*).

The following 8 boreholes were selected for analysis: KFR71, KFR72, KFK084, KFK081, KFK083, KFK061, KFK058 and KFK059.

KFR71 and KFR72 have no data in the selected parameter tables.

KFK059, KFK058, KFK061, KFK081, KFK083 and KFK084 have limited associated data from the old mapping.

There is a SICADA-parameter with rock type code that also occurs as an RVS-parameter, *rock_proto-rock_type*. The parameter has been visualized as a line in the above named six boreholes.

Fracture frequency also exists but is not defined as a parameter in SICADA and is therefore not directly available as a parameter in RVS. *It is possible to arrange to obtain this data as a defined parameter or alternatively the data can be extracted and imported as external data directly into RVS. This has not been carried out.*

Geomagnetic lineament

The geomagnetic lineament is included in the site investigation model *PFM_DZ_Local_v.2.1.rvs*

Seismic

Seismic lines LFK and LFR from SICADA with mapped velocities.

Source: SICADA via Mats Elfström, FB Engineering.

The following seismic lines cross the Singö deformation zone:

- LFK000030, 037, 038, 044, 045, 053, 054, 055, 078, 079, 080, 082, 083, 125, 126, 139, 141 and 151.
- LFR000010, 012, 013, 014, 015, 025 and 026.

The lines have been plotted and saved as “boreholes”. The LFR lines have the prefix 910- which is the ID number of the RVS installation they are imported to.

Along every seismic line the seismic velocities have been visualized as green cylinders with a radius inversely proportional to the velocity value. LFR000025 and 026 have no associated seismic velocity records.

A velocity of 10 m/s gives a radius of 49,9 m whilst a velocity of 5,000 m/s gives a radius of 0 m. Velocities lower than 10 m/s and higher than 5,000 m/s have not been visualized.

Modelling

Zones

Based on the above background data the zone boundaries have been modeled as planar surfaces without thickness. The boundaries were named with a suffix -S or –N to indicate whether it is a southern or northern boundary of a zone that has been modeled.

Core

The Singö deformation zone core has been modeled and saved as two separate surfaces with the assigned type “deformation zone” that have been named “Core-S” and “Core-N”. The zone boundaries are largely based on the rock mass classification, in accordance with Section 2.4.6, for the class Zone Core in the TFKB3 tunnel in the north and the TFRBT tunnel in the south.

Core-S: Strike (RT90) = 121.5°, Dip = 90°

Core-N: Strike (RT90) = 121.9°, Dip = 90°

Zone TZ

Fracture zone TZ (Transition Zone) has been modeled and saved as two separate surfaces with the assigned type Deformation Zone and the names “TZ-S” and “TZ-N”. The zone boundaries are largely based on the rock mass classification, in accordance with Chapter 2.4.6, between the classes Transition and Host rock in TFKB3 in the north and TFRBT in the south.

TZ-S: Strike (RT90) = 120.6°, Dip = 90°

TZ-N: Strike (RT90) = 121.7°, Dip = 90°

Water bearing structures

Based on mapped water bearing structures a structure has been modeled between the TFK tunnels in the north and TFR tunnels in the south.

Structure WZ-1

The water bearing structure WZ-1 has been modeled and saved as a structure with a thickness of 6 m i.e. an object with two boundary surfaces. This represents the water bearing structures TFRBT_W_004 and TFRDT_W_004 in the SFR tunnels and follows the core zone *Core*. The structure has only been modeled in the vicinity of the SFR tunnels.

WZ-1: Strike (RT90) = 122.5°, Dip = 90°

Appendix B

Calculation of fracture frequency in host rock in Tunnel 3

From chainage	To chainage	length, m	width, m	Area, sq m	block shape in fracture zone	No of fractures	Fract/m², P20
1,010	1,050	40	20	800	cubic	291	0.36
1,050	1,100	50	20	1,000	cubic	41	0.04
1,100	1,150	50	20	1,000	no zones	60	0.06
1,150	1,200	50	20	1,000	no zones	55	0.06
1,200	1,250	50	20	1,000	cubic	340	0.34
1,250	1,300	50	20	1,000	cubic	322	0.32
1,300	1,350	50	20	1,000	cubic	870	0.87
1,350	1,400	50	20	1,000	cubic	320	0.32
1,400	1,450	50	20	1,000	no zones	49	0.05
1,450	1,500	50	20	1,000	no zones	56	0.06
1,500	1,585	85	20	1,700	no zones	63	0.04
1,585	1,602	17	20	340	cubic	175	0.51
1,602	1,642	40	20	800	cubic	93	0.12
1,642	1,672	30	20	600	cubic	294	0.49
1,672	1,810	138	20	2,760	cubic	654	0.24
1,810	1,860	50	20	1,000	cubic	283	0.28
1,860	1,900	40	20	800	cubic	288	0.36
1,900	1,950	50	20	1,000	no zones	34	0.03
1,950	2,000	50	20	1,000	cubic	228	0.23
2,000	2,050	50	20	1,000	no zones	24	0.02
2,050	2,100	50	20	1,000	no zones	29	0.03
2,100	2,150	50	20	1,000	no zones	41	0.04
2,150	2,190	40	20	800	cubic	191	0.24
2,190	2,240	50	20	1,000	cubic	315	0.32
2,240	2,290	50	20	1,000	cubic	516	0.52
2,290	2,340	50	20	1,000	cubic	339	0.34
2,340	2,385	45	20	900	cubic	164	0.18
Total SW of Singö DZ		1375		27,500		6,135	0.22
2,700	2,750	50	20	1,000	no zones	34	0.03
2,750	2,800	50	20	1,000	cubic	110	0.11
2,800	2,850	50	20	1,000	cubic	120	0.12
2,850	2,900	50	20	1,000	cubic	166	0.17
2,900	2,950	50	20	1,000	no zones	49	0.05
2,950	3,000	50	20	1,000	no zones	53	0.05
3,000	3,050	50	20	1,000	no zones	27	0.03
3,050	3,100	50	20	1,000	no zones	37	0.04
3,100	3,150	50	20	1,000	no zones	33	0.03
3,150	3,200	50	20	1,000	no zones	34	0.03
3,200	3,250	50	20	1,000	no zones	33	0.03
3,250	3,300	50	20	1,000	no zones	45	0.05
3,300	3,350	50	20	1,000	no zones	43	0.04
3,350	3,400	50	20	1,000	no zones	35	0.04
3,400	3,450	50	20	1,000	no zones	39	0.04
3,450	3,517	67	20	1,340	no zones	48	0.04
Total NE of Singö DZ		817		16,340		906	0.06
Grand total		2,192		43,840		7,041	0.16